AN ANALYSIS OF ENVIRONMENTAL INFLUENCES ON MORPHOLOGIES AND TORNADOGENESIS WITHIN QUASI-LINEAR CONVECTIVE SYSTEMS

A Thesis Presented to the Faculty of the Graduate School at the University of Missouri

In Partial Fulfillment of the Requirements for the Degree Masters of Science

by

BRADLEY WORKMAN

Dr. Patrick Market, Thesis Advisor

MAY 2013

The undersigned, appointed by the dean of the Graduate School, have examined the thesis entitled

AN ANALYSIS OF ENVIRONMENTAL INFLUENCES ON MORPHOLOGIES AND TORNADOGENESIS WITHIN QUASI-LINEAR CONVECTIVE SYSTEMS

Presented by Brad Workman,

a candidate for the degree of master of science,

and hereby certify that, in their opinion, it is worthy of acceptance.

_____

Associate Professor Patrick Market

_____

Associate Professor Neil Fox

_____

Assistant Professor Jason Hubbart

ACKNOWLEDGEMENTS

I would like to start off by thanking Dr. Anthony Lupo, Dr. Neil Fox, and especially Dr. Patrick Market for always pushing me forward and for all their help over the past four years, through undergraduate and graduate work. In this relatively short time, I have accomplished what I would have only dreamed possible and learned more than I ever could have imagined. I will always be grateful for the extra time you took out of your days to help me on my countless office drop-ins. I would like to thank Dr. Jason Hubbart for agreeing to be on my committee and supporting me through the thesis process. I would also like to thank Isabela Carlos for her help and advice through the data processing, especially as it pertained to MATLAB. Her hours of help really helped get this research off the ground. I would like to thank Katie Crandall for all of her help, as well. Through her advice on how to write this thesis, how to format it, and really just keeping me on track, I was able to finish this thesis on time. It would not have been possible without her, and the others listed above, help.

I would like to thank my parents for all the support they have provided, both in encouragement and monetary expenses. Without either of those, none of this would have been possible. They have always believed in me, no matter what the situation. I would like to thank my brother for putting up with me for the past four years, and for the help with countless questions in math and physics. I would also like to thank the rest of my family and friends for helping me get to this point. And last but not least, I would like to thank Christine Rapp for her support and encouragement throughout this process.

Table of Contents

Figures

Tables

Abstract

Mesoscale convective systems (MCSs) often take the form of quasi-linear convective systems (QLCSs) within the mid-latitudes of the United States. QLCSs have a quasi-linear convective precipitation structure either followed or led by stratiform precipitation, and often produce strong winds, hail, and tornadoes. Quasi-linear convective systems have been the subject of research for more than a half-century. Early work was performed to classify different morphologies and structures, whereas more recent work has been focused heavily on the dynamics associated with QLCS structures, and investigating forecasting problems that QLCSs pose, in particular the 3-12 hour time period. Thirty-two cases were selected for this investigation, comprised of 8 "tornado" events, 8 "hybrid" events, 8 "wind" events, and 8 "marginal" events. These thirty-two events were selected based on a general geographic location in the central United States. The purpose of this investigation was to better understand the atmospheric conditions resulting in the variety of observed event "types," to improve event predictability, and therefore forecasting, especially with regards to tornadic QLCS cases.

Chapter 1 Introduction

Mesoscale convective systems (MCSs) were defined by Parker and Johnson (2000) as collections of convective storms that are often organized on the mesoscale, behaving as long lived discrete entities. For a convective storm to be considered long lived, its lifespan must be greater than or equal to 3 hours. MCSs often take the form of quasi-linear convective systems (QLCSs) within the mid-latitudes of the United States. QLCSs are a type of "linear" MCS and are classified by Parker and Johnson (2000) based on their distribution of stratiform precipitation, which is largely determined by surrounding environmental thermodynamics and flow features. Furthermore, QLCSs often produce severe weather, making them important to understand from a forecasting perspective.

Field experiments were first used to analyze MCS populations and, soon after, operational radar data was used to create classification systems for QLCSs, of note being Bluestein and Jain (1985). Most recently, research work focused on the dynamics and structures of such systems, with the goal of solving the forecast problems that QLCSs pose. QLCSs occur with relative frequency and can be a threat to both property and lives; it is for these reasons that solving their associated forecast problems is important. This thesis work analyzed environmental data, layered with radar data, to begin to determine what values of certain atmospheric variables may be important to forecasting such widely varied events. The domain of events analyzed is shown in Figure 1.1.

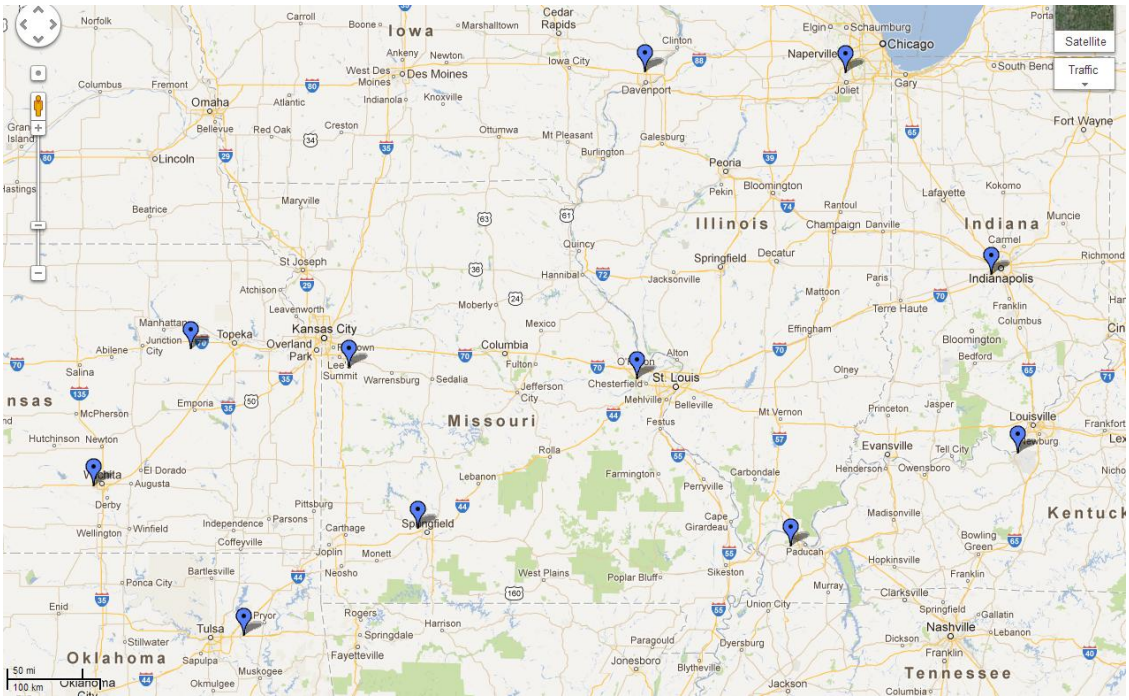

Figure 1.1 From Google Maps. This is the domain used for this research. Blue tags represent the radar locations utilized.

1.1 Purpose

The purpose of this research was to gain a better understanding of QLCS events, especially with regards to differences between tornadic and non-tornadic cases, to help increase forecast accuracy and reduce false alarms, while simultaneously reducing the number of missed events. An analysis of Near Storm Environment (NSE) parameter influences was performed on thirty-two QLCS cases (8 tornado events, 8 hybrid events, 8 wind events, and 8 marginal events) to determine which parameters may distinguish between event types (tornado, hybrid, wind, or marginal).Through this process, we will be able to determine that statistical differences do exist between some of the NSE parameters for the given event types.

1.2 Objectives

To achieve the purpose previously mentioned, the following objectives were identified:

- Collect and analyze environmental data from a representative time step of 32 QLCS events between 2005 and 2011. There shall be 8 QLCS event cases in each of the following categories; tornado events, hybrid events, wind events, and marginal events.
- Obtain radar data for a set of representative events and perform a plan-view and cross-sectional radar analysis, particularly focusing on base reflectivity and base velocity, and compare QLCS event structures to previous research.
- Create a hypothetical forecaster's chart from the statistical analysis for use when forecasting QLCS events, particularly focusing on forecasting tornado vs. wind events.

Chapter 2 Literature Review

To achieve the objectives of this research, an extensive literature review was performed to understand the causes of and physical processes responsible for QLCS development. Sections 2.1 through 2.4 of this literature review will detail MCSs and, in particular, linear MCSs, with regards to organizational modes, structures and dynamics of quasi-2D linear MCSs, and MCSs in general, and discriminating differing MCS environments through the use of sounding observations. From section 2.5 to section 2.7.6, the literature review will focus on bow echoes (a more specific QLCS structure), and the relationship between associated atmospheric variables and their influence on surface wind strength. Section 2.8 will detail more recent research concerning tornadic QLCSs, and section 2.9 will be a summary that leads into this current thesis research.

2.1 MCS organizational modes

Fankhauser et al. (1992) noted that the early work on convective lines of storms very often focused on systems with significant overturning updrafts and leading anvil cloudiness, and neglected other QLCS morphologies. He also showed that with the advent of MCS studies, there was an increased focus on the front-to-rear movement of hydrometeors. Coinciding with the work of Fankhauser et al. (1992), Moncrieff (1992) was able to show that mature thunderstorm lines could exhibit both of the following: an ascending front-to-rear flow (termed the *jump updraft*), and the well-noted *overturning updraft*, located directly above the leading edge of the surface outflow (Fig. 2.1).

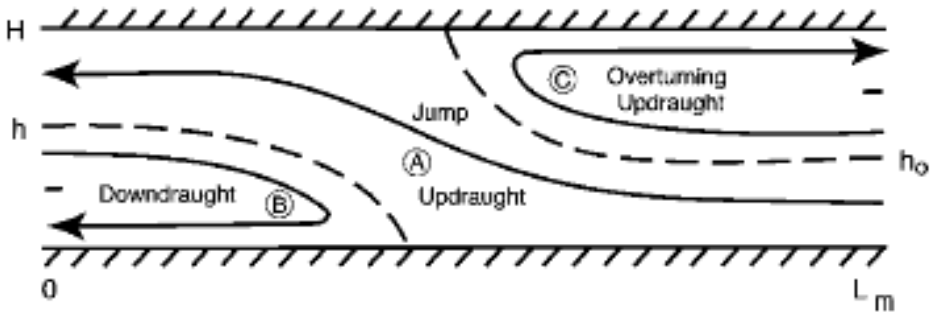

Figure 2.1 Fig. 3 from Parker and Johnson (2000) – Theoretical two-dimensional model of a convective line depicting both jump and overturning updrafts, redrafted from Moncrieff (1992).

Soon after these studies, Fovell and Dailey (1995) showed that "various modes of modeled multicell thunderstorms, regardless of regeneration periodicity, exhibited new convection near the leading edge of storm outflow, with subsequent upward and rearward motion within a canted updraft flow." This process leads to the structure known as *leading-line trailing-stratiform*, or TS in Parker and Johnson (2000). This structure is exhibited when there is a rearward deposition aloft of hydrometeors of the convective line. Furthermore, Houze et al. (1990) showed that the majority of mesoscale precipitation systems in Oklahoma, during the spring months of 1977-1982, exhibited this so-called TS structure.

In addition to the TS structure archetype, Schiesser et al. (1995) noted an additional archetype, known as LS, or *leading stratiform* (Fig. 2.2). Similarly, Parker (1999) was able to show that there are other recurrent modes of linear convection in addition to the TS archetype. A large number of cases within that study showed stratiform precipitation existing in advance of a moving convective line. While it had been noted previously that LS archetypes did exist, at the time of Parker and Johnson (2000) they had received very little attention. The lack of attention is suggested to be due

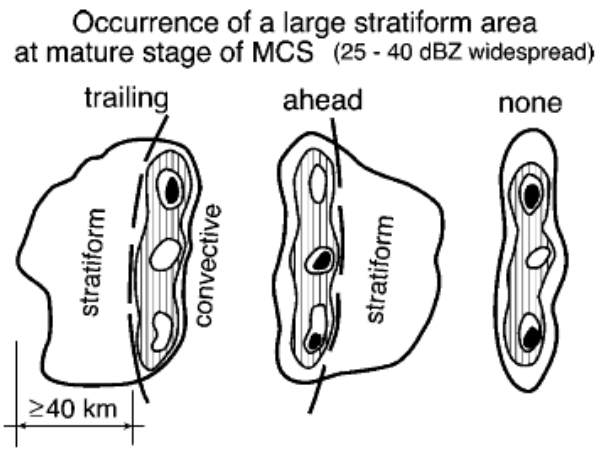

Figure 2.2 Fig. 2 from Parker and Johnson (2000) – Schematic reflectivity drawings of organizational archetypes for Swiss mesoscale convective systems, redrafted from Schiesser et al. (2005).

to the inherently complicated nature of LS systems that does not make them conducive to accurate numerical simulation.

A third mode of QLCS structure was also identified, known as the PS archetype, in which the stratiform precipitation moved parallel, in a storm-relative sense, to a MCSs convective line. The PS archetype has received even less attention than the LS archetype. Notably, both LS and PS modes were evident in their earlier presented squall line archetype (Newton and Fankhauser 1964).

To continue with the idea of MCS research based on organizational modes, Parker and Johnson (2000) performed a more detailed analysis of all three archetypes (TS, LS, and PS) in the United States, and were able to do so using the wind profiler network and the high frequency of MCSs that occur within the country. In addition, Parker and Johnson (2000) sought to address the aforementioned archetypes as a population, and in doing so, were able infer common reflectivity and environmental characteristics. More specifically, the aim of Parker and Johnson (2000) was to document the existence and

frequency of these convective modes, and outline conceptual models for the LS and PS archetypes that were consistent with observations, which "shed further light on the long-standing problem of MCS organization and its predictability."

According to Parker and Johnson's (2000) definition, MCSs are a "convective phenomenon for which the Coriolis acceleration is of the same order as the other terms in the Navier-Stokes equation."

$$\frac{d\vec{V}}{dt} = -\frac{1}{\rho}\nabla_p - 2\Omega \times \vec{V} + \vec{g} + \vec{F} \qquad (1)$$

Where V is velocity, ρ is fluid density, ∇_p is pressure gradient, $-2\,\Omega \times V$ represents Coriolis force, g is gravitational acceleration, and F represents frictional forces.

From this equation, and using the definition of MCSs, the appropriate MCS timescale is f^{-1}. The MCS timescale presented here is identical to the timescale identified by Emanuel (1986) for mesoscale circulations, and is sufficient for Parker and Johnson (2000) since the typical mid-latitude value for f yields a timescale (τ) of approximately 3 hours, or equal to the baseline timescale for the MCS definition presented by Parker and Johnson (2000). Furthermore, to define a length scale for their study, Parker and Johnson (2000) used an advective assumption that resulted in $L = U\,\tau$. Using the average mid-latitude wind speed (U) of 10 ms^{-1}, this yields an MCS length scale of 100 km, which is recommended by Houze (1993). Therefore, by utilizing the aforementioned length and time scales, only convective echoes greater than 100 km that last longer than 3 hours are included in Parker and Johnson (2000). Linear MCSs were also defined by Parker and

Johnson (2000), as those containing a convective line. A convective line is described as "a contiguous or nearly contiguous chain of convective echoes that share a nearly common leading edge and move approximately in tandem, whether they are arranged in nearly a straight line or a moderately curved arc". Conversely, nonlinear MCSs are defined as large convective systems with highly eccentric precipitation patterns, but do not include convective lines. And finally, Parker and Johnson (2000) defined warm sector MCSs (WS) and non-warm sector MCSs (non-WS). WS MCSs occur in the warm, moist, (typically) conditionally unstable air mass denoted by synoptic fronts. Non-WS MCSs occur on the cold side of a synoptic-scale warm or stationary front. All cases deemed to be non-WS were excluded from Parker and Johnson (2000) due to their frequent lack of surface-based convective available potential energy (CAPE), as well as the ambiguity of density current dynamics and inflow layer location.

Parker and Johnson (2000) utilized three sources for their study: national radar composite summaries, National Weather Service rawinsonde observations, and subjectively analyzed surface data and NCEP gridded reanalysis to describe synoptic set-up associated with the MCSs in question. With respect to national radar composite summaries, stratiform echoes are those with a reflectivity of 20-40 dBZ, convective echoes are greater than 40 dBZ, and echoes less than 20 dBZ were not considered. Furthermore, with respect to the rawinsonde observations, only one observation was used for each MCS. Moreover, following Houze et al. (1990), a sounding was only considered to represent the first MCS to traverse a region. Subsequent convective systems, prior to another sounding, were not included due to the high probability that the previous convection had altered the environment. Finally, the diagnosis of synoptic features or

NCEP gridded reanalysis was used to determine whether or not a convective system was associated with a surface synoptic feature. A convective system was deemed to be associated with a surface synoptic feature if more than half of its track coincided with the position of the analyzed feature.

Three modes of linear mesoscale convective systems were studied in Parker and Johnson (2000). Of the 88 linear MCSs studied, 24 were discarded due to being non-WS, leaving 59 "good quality" MCSs, of which 57 were classifiable. LS and PS cases accounted for 20% of the total each, and TS cases accounted for 55% of the total cases. Parker and Johnson (2000) noted that the omission of non-WS cases and bad observations did not preferentially affect any one subset of MCSs in their study.

2.1.1 Trailing stratiform

The trailing stratiform, TS, archetype (Fig. 2.3a) was described by Houze et al. (1990), and the definition was retained for Parker and Johnson (2000). The definition of a TS MCS is a convective line, "convex toward the leading edge," with "a series of intense reflectivity cells solidly connected by echo of more moderate intensity." Furthermore, the line should have a "very strong reflectivity gradient at [the] leading edge," and a large trailing stratiform precipitation region. This trailing stratiform precipitation region often exhibits a secondary reflectivity maximum, separated from the convective line by a narrow corridor of lower reflectivity. This narrow corridor was considered a "transition zone" by Parker and Johnson (2000). Notably, TS archetypes exhibit very little leading stratiform precipitation (Fig. 2.4), and three examples of TS structures are shown in (Fig. 2.5).

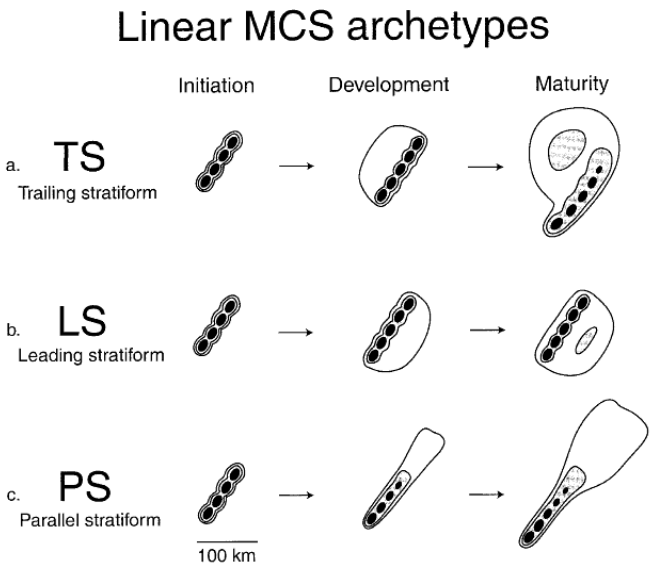

Figure 2.3 Fig. 4 from Parker and Johnson (2000) – Schematic reflectivity drawing of idealized life cycles for three linear MCS archetypes: (a) TS, (b) LS, (c) PS. Approximate time intervals between phases: for TS 3-4 h; for LS 2-3 h; for PS 2-3 h. Levels of shading roughly correspond to 20, 40, and 50 dBZ.

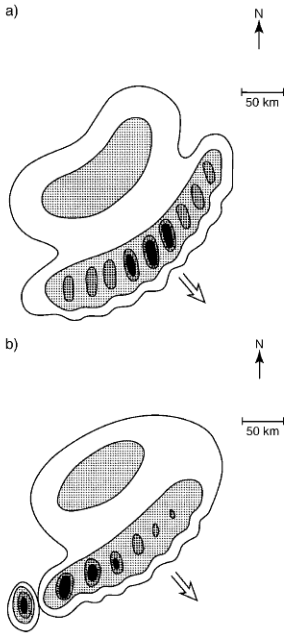

Figure 2.4 Fig. 1 from Parker and Johnson (2000) – Schematic reflectivity drawings of leading-line trailing-stratiform mesoscale precipitation systems, redrafted from Houze et al. (1990): (a) symmetric and (b) asymmetric archetypes.

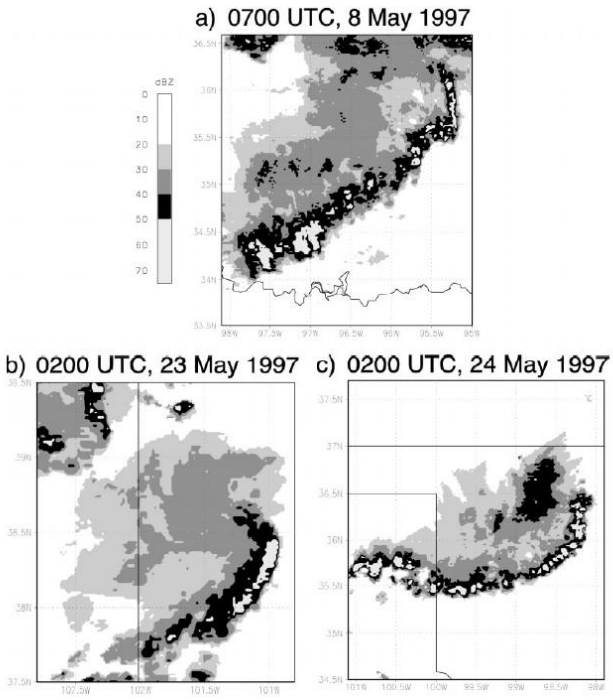

Figure 2.5 Fig. 5 from Parker and Johnson (2000) – Radar reflectivity – examples for TS archetype: (a) 0700 UTC 8 May 1997, (b) 0200 UTC 23 May 1997, and (c) 0200 UTC 24 May 1997.

Parker and Johnson (2000) described radar-observed traits of the TS population, including: length of time in which MCS criteria was met, distance covered, line orientation, evolution among archetypes, and a few others. First, Parker and Johnson (2000) noted that TS cases met the MCS length and reflectivity criteria, on average, for 12.2 hours, and traversed a greater distance than did the other members of the linear MCS spectrum. Furthermore, the line for all three archetypes were most often oriented northeast to southwest, and roughly along a 60° azimuth. However, TS cases had the strongest, on average, northeast-southwest orientation, partly due to TS MCSs' frequent association with synoptic cold fronts in Parker and Johnson (2000), rather than warm or stationary fronts that typically tend to be less consistently oriented. With respect to the evolution of linear MCSs among archetypes, nearly half of all linear MCSs initially

possessed TS characteristics (Fig. 2.6). In addition, relatively few MCSs in Parker and Johnson's (2000) population began as TS and then evolved into the other modes. It was more common that the other two modes evolved into a TS mode at some point in their lifetime. Parker and Johnson (2000) put forth the notion that it is possible, with time, that convective lines begin to accelerate forward, such that TS rain is favored in their later stages. Also, just as nocturnal maxima have been established by for thunderstorms (Wallace 1975), Parker and Johnson (2000) established that the nocturnal maximum occurred between 0100 and 0700 UTC, while a secondary maximum existed, but was relatively small for TS MCSs, near local sunrise, or 1100 UTC.

Parker and Johnson (2000) also documented a physical description of the different linear MCS archetypes, which included a description of wind fields and their relationship to stratiform precipitation distribution and durations of the different linear MCS classes. First, Parker and Johnson (2000) noted that TS cases' mean line-perpendicular storm-relative wind components were significantly different from LS and PS cases, and that the TS class average exhibited negative line-perpendicular storm-relative winds at every level. Furthermore, above 2 km, TS cases showed significantly greater storm-relative winds than those observed for LS and PS cases; this is consistent with rearward advection of hydrometeors by the mean flow. Finally, with respect to the duration of linear MCS cases, as presented by Parker and Johnson (2000), the average TS cases lasted nearly twice as long as the other two archetypes mentioned, and this appears to be correlated with the stability of the air masses into which the TS cases propagated. Greater values of mean convective available potential energy (CAPE), lifting condensation level (LCL), convective condensation level (CCL), and lifted index (LI) all point to the fact that TS

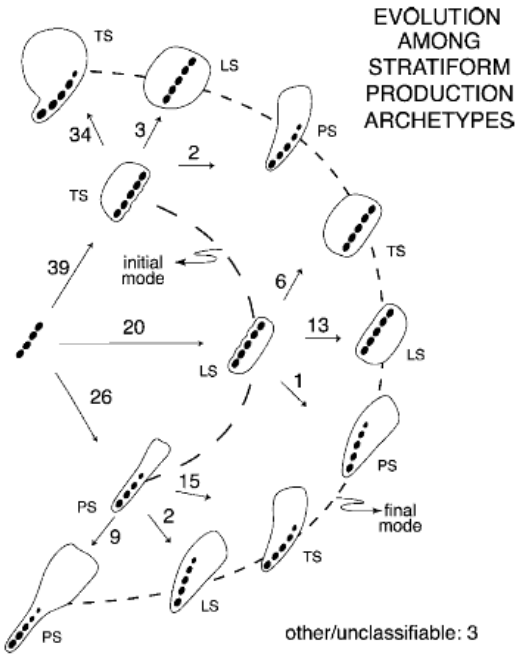

Figure 2.6 Fig. 9 from Parker and Johnson (2000) – Illustration of evolutionary pathways for MCSs in this study. Labels along each pathway denote the initial and final modes of stratiform precipitation production. The total number of cases following each step is indicated. Idealized composite positions of convective elements and stratiform precipitation are depicted schematically along each pathway. Note: some pairs of evolutionary pathways (e.g. TS → PS and PS → TS) resulted in generally similar reflectivity patterns. As discussed in the text, MCSs were classified based upon their predominant organizational mode, which could be either their initial or final organization.

Field	LS	PS	TS
CAPE	1009	813	1605
LCL	811	765	831
CCL	735	686	778
LI	−3.5	−2.2	−5.4
$T_{v_{dd}} - T_v$	−0.8	−2.1	−4.8
$T_{v_{dd}} - T_{v_{Tw}}$	5.3	4.1	0.7
PW	3.27	2.43	3.35

Table 2-1 Table 3 from Parker and Johnson (2000) – Summary of statistically significant (at 0.05) thermodynamic rawinsonde variables. Units: CAPE, J kg^{-1}; LCL and CCL, hPa; all temperatures and LI, K; PW, cm. Also, T_v is the surface virtual temperature; T_{vdd} is the surface virtual temperature of minimum θ_w downdraft; T_{vTw} is the surface virtual temperature when cooled to saturation.

MCSs occurred in air masses with the most conditional instability (Table 2-1). Furthermore, the mean TS environment could produce the strongest surface cold pool temperature perturbation (Table 2-1). Also, TS cases, on average, had higher precipitable water values, lower LCL and CCL than the other two classes. This would imply a greater potential for precipitation loading and a lower cloud base, as well as a relatively uninterrupted buoyant inflowing air (Parker and Johnson 2000).

2.1.2 Leading stratiform

The leading stratiform, LS, archetype describes linear MCSs whose stratiform precipitation is predominantly located in advance of the convective line (Fig. 2.3b). In the most extreme cases, LS archetypes, according to Parker and Johnson (2000), "exhibit a convective line preceded by a transition zone and secondary swath of stratiform precipitation with a reflectivity maximum" (Fig. 2.7a). More often, though, LS MCSs have moderate regions of leading stratiform precipitation, and do not have transition zones and secondary bands (Fig. 2.7b-d). To be classified as an LS MCS, the tendency of the MCS must be to generate predominantly pre-line precipitation, and it does not matter if post-line stratiform precipitation exists. Parker and Johnson (2000) explicated that cases that had extensive post- and pre-line precipitation were classified as LS, based on greater similarity to the LS extreme rather than the TS extreme.

Just as with TS cases, Parker and Johnson (2000) described radar-observed traits of the LS population, including: Length of time in which MCS criteria was met, distance covered, line orientation, evolution among archetypes, among others. First, Parker and Johnson (2000) noted that LS cases met the MCS length and reflectivity criteria, on

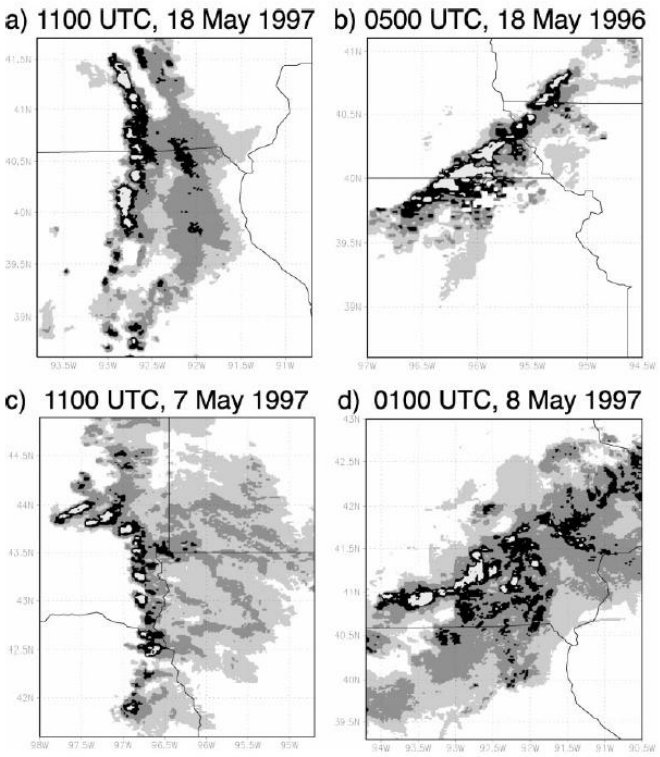

Figure 2.7 Fig. 6 from Parker and Johnson (2000) – Radar reflectivity – examples for LS archetype: (a) 1100 UTC 18 May 1997, (b) 0500 UTC 18 May 1996, (c) 1100 UTC 7 May 1997, and (d) 0100 UTC 8 May 1997. Reflectivities shaded as in Fig. 5.

average, for 6.5 hours, which is about half as long as the TS cases, and just a bit longer than PS cases. Similarly, LS cases were quicker moving than TS cases, yet didn't traverse as great of distances, due to their significantly shorter duration. Just as the TS archetype, LS MCSs are most often oriented northeast to southwest, roughly along the same 60° azimuth as TS MCSs. Also, within the population, 30% of all cases that began as LS cases evolved into the TS archetype. As previously established that TS cases have a nocturnal maximum, so do LS cases; the majority of them occurred between 2300 and 0500 UTC. A secondary maximum was also noted near local sunrise for LS cases, and appeared to be the dominant mode for those cases, yet the reasons for that are not fully understood (Parker and Johnson 2000).

Just as with the TS archetype, Parker and Johnson (2000) documented a physical description for the LS archetype. As stated previously, LS cases exhibit weak middle-tropospheric storm-relative winds and modest rear-to-front storm-relative winds at upper levels. Also, line-perpendicular storm-relative winds within LS cases are not very distinct from those in PS cases; however, the line-parallel winds are stronger in LS cases as compared to PS cases. Therefore, on average, there is a greater rear-to-front component of the storm-relative flow aloft for LS cases, and the "downgradient mixing of low-level rear-to-front storm-relative momentum or slantwise solenoidal overturning" may both play a role in the forward advection of precipitation. Furthermore, upper-tropospheric shear for LS cases was not remarkably different from that of PS and TS MCSs, thus suggesting that shear aloft may not universally explain pre-line precipitation (Parker and Johnson 2000). In fact, according to Parker and Johnson (2000), the 5-8- and 3-10-km mean line-perpendicular storm-relative winds were the most statistically significant differentiators among the three classes in their study. That suggests that middle- and upper-tropospheric storm-relative flow fields are of utmost importance in determining the organizational mode of linear MCSs (Parker and Johnson 2000). Furthermore, lower-tropospheric storm-relative flow suggests that inflow toward LS cases passed through the stratiform precipitation region, on average. Parker and Johnson (2000) stated that perhaps this inflow air, cooled to its wet-bulb temperature, remains positively buoyant and therefore fuels the LS updraft towers in some MCSs. However, Parker and Johnson (2000) were quick to point out that this scenario is not depicted in the mean post-MCS wind profiles and, therefore, may be anomalous. Also thought to contribute to an LS lines' longevity is the observed quasi-supercellular characteristics within their convective

lines, even though supercellular lines, according to Parker and Johnson (2000), are generally regarded as rare. Therefore, it is possible that a variety of LS modes exist, and each may be sustained in their own unique way (Parker and Johnson 2000).

2.1.3 Parallel stratiform

A linear MCS, according to Parker and Johnson (2000), was categorized as a PS MCS if "most or all of the stratiform precipitation region associated with the convective line moves parallel to the line itself (in a storm-relative framework) and to the left of the line's motion vector throughout its life cycle" (Fig. 2.3c). Notably, very little stratiform precipitation surrounds the convective lines of PS cases (Fig. 2.8). More specifically, the reflectivity gradient is relatively large on both sides of the convective line, and the movement of the stratiform region usually deviates less than 30° from the convective lines' orientation. In some PS cases, the convective lines backbuild to the right of their motion vectors. This behavior, as noted by Parker and Johnson (2000), "may be accompanied by the general decay of convective cells to the left of a line's motion vector, yielding a progressively larger region of lower reflectivity echoes to the left of and parallel to the convective line." In other cases still, PS lines do not appear to backbuild substantially. Instead, a location of persistent deep convection appears to give rise to the PS echoes through line-parallel advection. Furthermore, it is probably best to assume that both processes are at work to some degree in most PS MCSs (Parker and Johnson 2000).

Just as with TS and LS cases, Parker and Johnson (2000) described radar-observed traits of the PS population, including: Length of time in which MCS criteria was met, distance covered, line orientation, evolution among archetypes, among others.

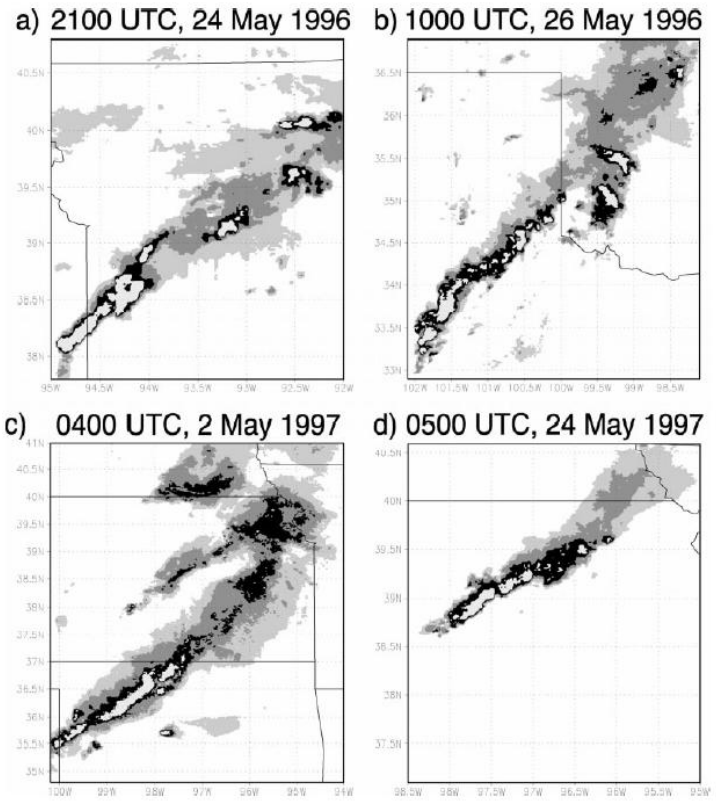

Figure 2.8 Fig. 7 from Parker and Johnson (2000) – Radar reflectivity – examples for PS archetype: (a) 2100 UTC 24 May 1996, (b) 1000 UTC 26 May 1996, (c) 0400 UTC 2 May 1997, and (d) 0500 UTC 24 May 1997. Reflectivities shaded as in Fig. 5.

Parker and Johnson (2000) noted that PS cases met the MCS length and reflectivity criteria, on average, for 6.3 hours, which is just slightly shorter than LS cases. Additionally, just as LS cases were quicker moving than TS cases, so were PS cases and PS cases traversed less distances than did TS cases. Just as the other two archetypes, PS cases were roughly oriented northeast to southwest, along a roughly 60° azimuth. Furthermore, more so than LS cases, cases that began as PS evolved to TS cases. They did so roughly 58% of the time. Notably, very few MCSs evolved toward the PS archetype. Parker and Johnson (2000) suggested that "a unique juxtaposition of low-level convergence boundaries and upper-level winds is important to some PS cases; it may be

that such arrangements may not be generally produced during ongoing convective events." Finally, just as TS and LS cases have a nocturnal maximum, PS cases do as well, between 2200 and 0500 UTC. A secondary maximum also existed near local sunrise (1100 UTC) for PS cases, but just as for TS MCSs, was relatively small (Parker and Johnson 2000).

A physical description of PS MCSs was also provided by Parker and Johnson (2000). As stated previously, PS cases are nearly identical to LS cases in regards to most of the line-perpendicular fields: PS cases, just as LS cases, exhibit weak middle-tropospheric storm-relative winds and modest rear-to-front storm-relative winds at upper-levels. However, one exception was found to this generalization, and that is that "within the 0-1 km layer, in which the magnitude of line-perpendicular flow for the PS cases was, on average, greater than that of the TS cases" (Parker and Johnson 2000). Furthermore, the line-perpendicular winds in the lower-troposphere near PS MCSs were very strong within a shallow layer, and above 2 km PS cases exhibited deep line-parallel storm-relative flow. This causes the middle-tropospheric advection of hydrometeors to be mainly along the line. Also, in the 5-8 km layer PS cases exhibit nearly purely line-parallel storm-relative winds. Notably, though, is that the line-parallel winds were much weaker in the PS cases, as compared to the other two archetypes. With regard to the duration of linear MCSs, the PS cases occurred in air masses with the least conditional instability as compared to the LS and TS cases (Table 2-1). Furthermore, unlike LS cases, PS MCSs do not contaminate their inflow through their stratiform region; therefore their persistence is much less mysterious. Even though PS cases exhibit possibly weaker cold pools, Parker and Johnson (2000) noted that they should have encountered relatively

uninterrupted buoyant inflowing air on a continual basis, just as TS MCSs do. This fact makes it somewhat surprising that PS cases did not, on average, last longer than LS MCSs. It has been suggested, however, that perhaps the PS arrangement of precipitation is less favorable to self-sustenance due to gravity wave dynamics (Parker and Johnson 2000).

It is reasonable to suggest that differing lifetimes among the three different MCS classes may be determined by, to some extent, environmental stability, presence or absence of rainfall into inflowing air streams, strength of surface cold pools (which will be discussed in section 2.7.3 as it relates to bow echoes), and the distribution of gravity wave energy from convective and stratiform heating. Furthermore, the relative speeds of the three different classes may result, to some degree, from cold pool dynamics (Parker and Johnson 2000). As a final note, the results of Parker and Johnson (2000) suggest that the arrangement of stratiform precipitation in linear MCSs is largely related to the storm-relative flow in and near the level of maximum hydrometeor transport [approximately 5-8 km according to Rutledge and Houze (1987)].

2.2 Structure and Dynamics of Quasi-2D MCSs

Following from Parker and Johnson (2000), Parker and Johnson (2004) noted that LS and PS MCS cases had received very little attention; aside from defining and characterizing the three classes (TS, LS, PS). This led Parker and Johnson (2004) to incorporate numerical simulations in order to perform detailed analyses and test sensitivities of the various MCS cases. The Parker and Johnson (2004) study was done as a first approach to the problem of understanding the dynamics and possibly unique

internal structures of LS and PS modes. However, the PS mode was left for a later study due to its three-dimensional complexity. Hence, the focus of Parker and Johnson (2004) was on the structure and dynamics of quasi-two-dimensional mesoscale convective systems, otherwise referred to as TS and LS modes. More specifically, Parker and Johnson (2004) described three common quasi-2D flow and precipitation structures among linear MCSs; front-fed TS systems, front-fed LS systems, and rear-fed LS systems. Front-fed systems are sustained by front-to-rear storm relative inflow, whereas rear-fed systems are sustained by rear-to-front storm-relative inflow.

2.2.1 Front-fed TS systems

Parker and Johnson (2004) noted that the basic flow structures for the TS archetype had already been relatively well documented. Front-fed TS, or FFTS, systems "possess deep convective cells that are fed by front-to-rear storm-relative inflow in the lower troposphere, which partly ascends and weakly overturns, but which mostly exits the convective region with some part of its front-to-rear momentum remaining." This is outlined in (Fig. 2.9), originally from Houze et al. (1989). After leaving the convective region, humid air and hydrometeors move rearward, and comprise a zone into which both liquid and ice particles are advected. In the stratiform region, continued condensational and depositional growth occurs, and becomes known as the trailing precipitation region. Modest ascent occurs in the front-to-rear flow stream, due to small upward accelerations as a result of remaining buoyancy from the convective region and contributions from in situ latent heating (Fig. 2.9).

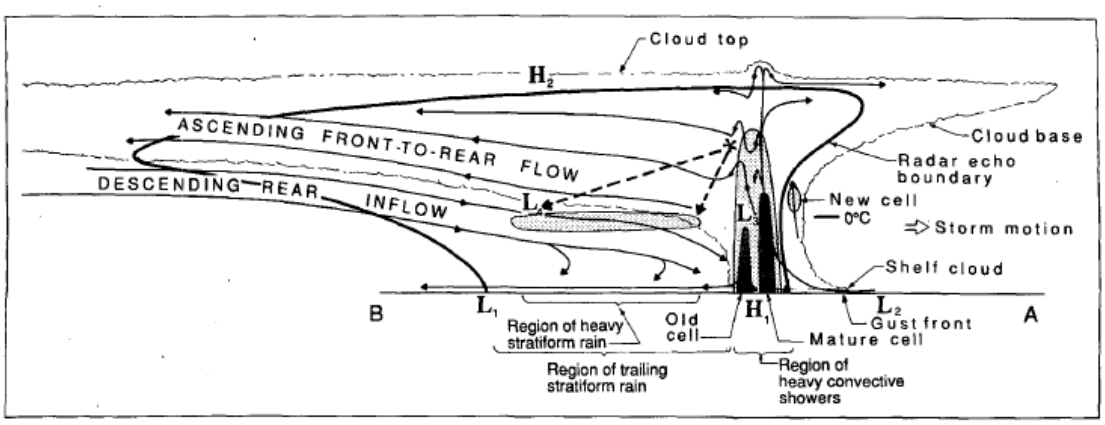

Figure 2.9 Fig. 4 from Parker and Johnson (2004) – Conceptual model from Houze et al. (1989) of front-fed convective line with trailing (stratiform) precipitation, viewed in a vertical cross section oriented perpendicular to the convective line and parallel to its motion.

Furthermore, beneath the region of middle- and upper-tropospheric positive buoyancy, a quasi-static pressure minimum develops and as a result, environmental air from behind the system may be accelerated inward. The accelerated air will begin to constitute a rear inflow jet. Due mostly to melting, evaporation, and sublimation of the precipitation that falls into this rear inflow jet, as well as water loading, downward accelerations amass in this region and commonly add a descending slope to the flow of this airstream (Parker and Johnson 2004).

2.2.2 Rear-fed LS systems

Parker and Johnson (2004) noted that the observations of rear-fed leading-stratiform (RFLS) systems are much less common in past studies than those of FFTS systems. This is not surprising since FFTS systems are a more commonly observed linear MCS type. A schematic composite depiction of the RFLS structure is provided in Figure 2.10.

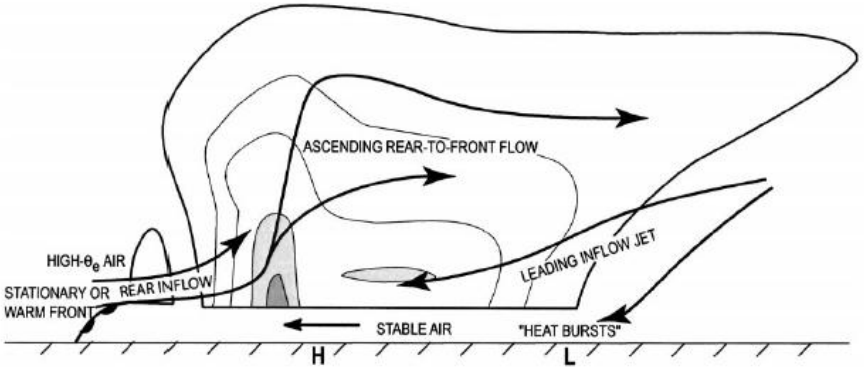

Figure 2.10 Fig. 5 from Parker and Johnson (2004) – Conceptual model, from Pettet and Johnson (2003), of a rear-fed convective line with leading precipitation, viewed in a vertical cross section oriented perpendicular to the convective line and parallel to its motion.

The predominant flow branches, although "mirrored" with respect to line orientation, are remarkably similar to those of FFTS systems (Fig. 2.9). Rather than the front-to-rear airstream that feeds the trailing precipitation region of the FFTS system, a rear-to-front airstream exists in RFLS systems. This airstream feeds the convective line, and then slopes upwards and forward to create the leading-stratiform precipitation (Fig. 2.10). Much like the FFTS system, only "mirrored," a descending jet of front-to-rear flow exists in the RFLS system owing to similar microphysical and dynamical processes (Parker and Johnson 2004).

2.2.3 Front-fed LS systems

Due to the fact that front-fed leading-stratiform (FFLS) systems have appeared in previous studies yet have not been given a thorough description, Parker and Johnson (2004) presented vertical cross sections depicting the quasi-two-dimensional reflectivity

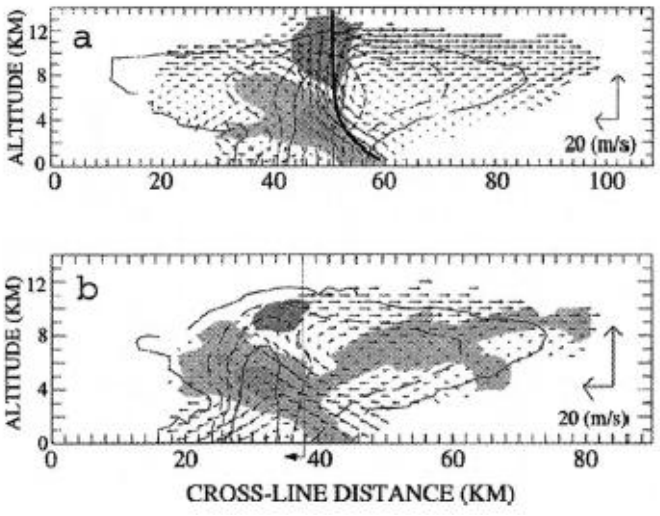

Figure 2.11 Fig. 6 from Parker and Johnson (2004) – Along-line averaged cross sections at two times for squall line from Grady and Verlinde (1997), at (a) 2102 UTC and (b) 2131 UTC 21 Jun 1993. Reflectivity contours are in 10-dBZ increments beginning with 10 dBZ. Vectors depict line-relative flow. Light shading indicates convergence, dark shading indicates divergence.

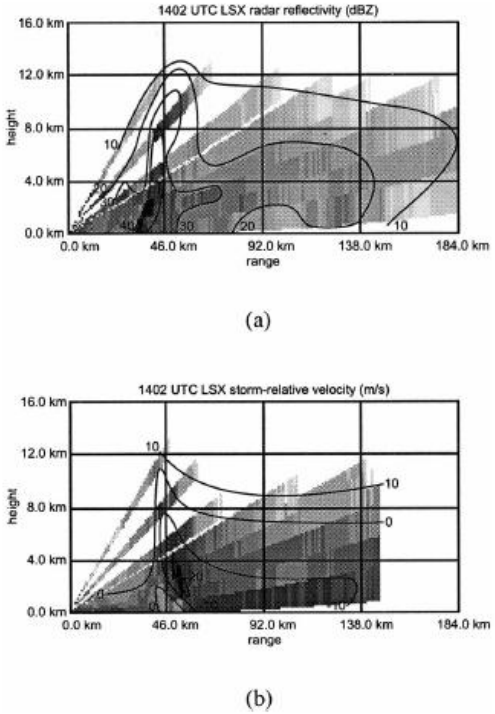

Figure 2.12 Fig. 7 from Parker and Johnson (2004) – Vertical range-height cross sections of a front-fed convective line with leading precipitation from St. Louis (LSX) radar at 1402 UTC 4 May 1996, azimuth 110° (a) Reflectivity (dBZ), (b) storm-relative velocity (ms^{-1}) using a storm motion of 20 ms^{-1} parallel to the cross section. Measured data are plotted, with subjectively analyzed contours added manually.

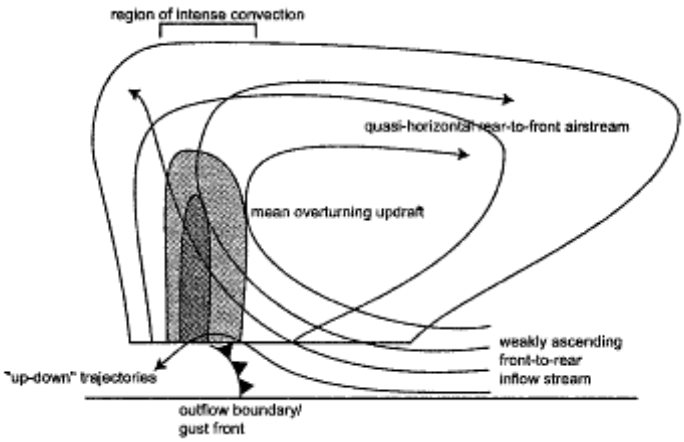

Figure 2.13 Fig. 8 from Parker and Johnson (2004) – Conceptual model, based on compiled radar observations, of a front-fed convective line with leading precipitation, viewed in a vertical cross section oriented perpendicular to the convective line and parallel to its motion.

and wind structures from two FFLS systems. The first (Fig. 2.11) is a system from 21 June 1993, and the second is an archetypal system from the Parker and Johnson (2000) study that occurred on 4 May 1996 (Fig. 2.12). In both cases, a deep convective line was preceded by a large overhanging region of line-leading precipitation.

The 4 May 1996 system was more archetypal given that line-leading precipitation had appreciable reflectivity very near the surface (Fig. 2.12a). Both examples exhibited deep front-to-rear storm-relative inflow (at least 0-5 km AGL) that passed through their line-leading precipitation. Furthermore, Parker and Johnson (2004) noted that the vectors in Figure 2.11 and contours in Figure 2.12b suggest that inflowing airstreams within those cases cases ascended slightly as they traveled through the pre-line precipitation. Also depicted in Figure 2.11 is a deep overturning updraft, revealed through wind vectors, but can also be inferred from the reflectivity and storm-relative flow fields in Figure 2.12 (Parker and Johnson 2004). Furthermore, both examples suggest that some air in the front-to-rear airstream ascended near the surface gust front, only to descend and

join the surface cold pool. Finally, both examples presented exhibited a strong, roughly horizontal stream of rear-to-front flow in the middle- and upper-troposphere; this appears to be the predominant source of moisture and hydrometeors for the line-leading precipitation region. The ascending rear-to-front flow in FFLS systems is much like the ascending front-to-rear flow branch in FFTS systems and the ascending rear-to-front flow branch in RFLS systems. With these characteristics in mind, a third, simple schematic diagram for FFLS systems is shown in Figure 2.13 (Parker and Johnson 2004).

2.2.4 Results of numerical simulations of quasi-2D MCSs

Parker and Johnson (2004) showed that idealized two-dimensional simulations can realistically reproduce the prominent features of the hydrometeor and wind fields of the three quasi-2D linear MCS archetypes (FFTS, RFLS, and FFLS). The results Parker and Johnson (2004) gathered suggest that the mesoscale organizational mode can be anticipated by considering the preferred direction of the acceleration owing to the combined effects of local buoyancy and the gradient in the buoyant pressure field (ACCB) and the acceleration owing to the gradient in the linear dynamic pressure field (ACCDL) (Parker and Johnson 2004).

Near the boundary of a surface cold pool, the buoyant pressure field slows the inflowing air and accelerates it upward for a period of time. Then, the inflowing air is accelerated "rapidly rearward over the cold pool and thereafter downward (Parker and Johnson 2004)." In the case of an FFTS system, on the downshear side of the cold pool the linear dynamic pressure field associated with an updraft within mean environmental shear creates a downshear-directed ACCDL that opposes the rearward ACCB. This acts

to create a more upright and vigorous updraft. On the other hand, in the case of the RFLS system, on the upshear side of the cold pool the ACCDL instead contributes an additional downshear, forward acceleration. The downshear, forward acceleration acts to create trajectories that have very shallow slopes, and indeed, in many basic RFLS systems, does not allow deep convection to develop. Therefore, RFLS systems are not the dynamical equivalent of a "reversed FFTS system," despite their apparent similarities in reflectivity and flow features. The addition of reverse shear above a low-level jet in the RFLS setting can allow for slightly more upright and vigorous updrafts than otherwise observed (a result of the rearward ACCDL in the middle troposphere), and is especially true when combined with an elevated, high θ_e inflow source (Parker and Johnson 2004).

In the common setting of development on the downshear side of the surface cold pool, the addition of deep-layer shear causes an overturning updraft structure; this occurs as a result of the downshear-directed ACCDL in the middle- and upper-troposphere. Due to this addition, this can lead to an FFLS convective system in which air leaves the region with rear-to-front momentum, and this momentum will act to carry the hydrometeors into the leading precipitation region. As important as the deep-layer shear may be, however, idealized simulations by Parker and Johnson (2004) suggest that lower-tropospheric shear has a greater effect. Parker and Johnson (2004) also noted that the idealized simulation results suggest predictability of quasi-2D linear MCS modes. For any particular simulation, "awareness of whether fresh convection is forming on the upshear or downshear side of a cold pool or baroclinic boundary, along with an assessment of the depth and strength of that shear, should enable one to anticipate whether the FFTS, RFLS, or FFLS organizational structure is most likely." Furthermore, from an

acceleration perspective, Parker and Johnson (2004) stated that it must be differences in vertical wind shear that accounts for the different structures, and this occurs as a result of the "direct impact of the magnitude of the environmental shear upon the linear part of the dynamic pressure perturbation."

2.3 MCS structure and dynamics

2.3.1 Layer lifting, overturning, and gravity wave response within MCSs

A review of MCSs presented by Houze (2004) highlighted new insights with regards to MCS structure and dynamics. One of the more important insights provided is that maybe it's not best to view the organized vertical structure in a large, mature MCS with parcel theory. It may be best, in the view of Houze (2004), to describe the vertical structure using layer lifting concepts. "The upward air motion in an MCS may begin in the form of buoyant convective-scale parcels rooted in the boundary layer and rising high into the upper troposphere; however, after the MCS matures, a layer of air much deeper than the boundary layer enters and rises on a slantwise path through the system" (Houze 2004). Furthermore, this rising layer is often potentially unstable and overturns, yet remains a coherent unit as it rises through the system.

The overturning within the layer allows the highest θ_e air to ascend to the top of the system. Even though the cause of the overturning within the layer remains a topic of research, evidence provided by modeling suggests that "buoyant elements triggered at the

nose of the cold pool of an MCS develop characteristics of trapped gravity waves as they propagate rearward into the stratiform region," and also may develop a lateral component of overturning in the form of longitudinal rolls. Furthermore, slantwise layer ascent appears to be a part of a gravity wave response to the mean latent heat release in the convective region, and this layer lifting allows for the formation of the broad saturated upper stratiform cloud region of the MCS (Houze 2004).

Another result of the gravity wave response is that the middle-level inflow enters the stratiform region and passes under the stratiform cloud deck. This middle-level inflow initially enters the stratiform region from a direction mandated by the large-scale environmental wind, and is accelerated inward by pressure gradient forces within the MCS. This effectively feeds the mesoscale downdraft of the system (Houze 2004).

2.3.2 Mesoscale Convective Vortices within MCSs

The "Mesoscale Convective Vortex," or MCV, was described by Houze (2004) who noted that an MCV tends to form in the mid-levels at the base of the stratiform cloud deck of an MCS, and will, in some cases, be initiated as a "bookend" vortex. Since the general focus of this literature review is within the mid-latitudes, it is important to note that the Coriolis force will enhance the cyclonic bookend vortex. This enhancement by the Coriolis force accounts for the asymmetric squall line structure often seen in the mid-latitudes, but rarely seen in the tropics. Within longer-lived MCSs, the MCV is more prominent. The MCV will tend to become inertially stable; this is due to the value of static stability being reduced by the saturated conditions within the stratiform upper-level cloud deck. These conditions effectively reduce the Rossby radius of deformation of the

system. Furthermore, the inertial stability of the vortex becomes a quasi-balanced flow maintained by a secondary vertical circulation. In turn, the secondary vertical circulation will prolong the life of the MCS by triggering new convection (Houze 2004).

2.3.3 MCS propagation

MCS propagation is also an important factor within the study of MCSs as a whole. In addition to the direct lifting of unstable air by an advancing cold pool, wave dynamics may also affect a system's propagation. For instance, the heating profile of a MCS produces mass divergence that acts to generate bores moving at gravity wave speed. The slower, shorter-wavelength bores produced may give the MCS an aspect of discrete propagation, due to the bores triggering new convective cells at a distance from the cold pool. The new convective cells could be incorporated by the existent convective region, or form an entirely new convective region while the older convective region weakens and becomes stratiform (Houze 2004). Furthermore, waves generated external to the MCS may become phase locked with the MCS as they continue to propagate downstream. The movement of some larger MCSs studied by Houze (2004) showed cooperation between the wave and the MCS, and this effect has been likened to wave-CISK concepts. More specifically, in this case, the velocity of movement of the MCS becomes exactly that of the wave, and this velocity may be different than the preferred direction of cold pool propagation. It is in instances of different directional preferences, between the wave and the cold pool, that the MCS may bifurcate and have one portion directed by wave propagation and the other directed by cold pool propagation (Houze 2004).

2.3.4 Spatial size of MCSs

Spatial size of the MCS is determined by the development and regeneration of the stratiform region. The stratiform region consists of material left behind from previously active convective cells as a result of the convective cells weakening, or as the result of the tops of active cells being sheared off. Therefore, the size of the stratiform region is determined by the ability of the MCS to regenerate new convection. For the stratiform region to grow in size, including the spatial extent of the MCS, the stratiform elements must have a dissipation time that is greater than the active lifetime. Over time, a balance can be reached between the dissipation time and active lifetime (Houze 2004).

The number of convective cells possible at any given time limits the maximum size of the MCS. Only if the environment is able to sustain the maximum number of convective cells over a long period of time will the MCS reach its maximum size – an environment like this is said to have "sustainability" (Houze 2004). Furthermore, a boundary layer that has favorable thermodynamic structure, that remains over a long period of time, in the same area as the MCS would enhance sustainability of the MCS. Over land, the development of the stratiform region is limited and, according to Houze (2004), is due to the warm, moist boundary layer becoming stable at night. An exception to instances when the development of the stratiform region is limited due to boundary layer conditions is when there is the presence of the low level jet to replenish the boundary layer through the night. This acts to create a continually replenished boundary layer capable of sustaining the MCS. In summary, the maximum MCS size is determined by a balance stage in which the MCS old stratiform region is disappearing with age at the

same rate that a new convective region is being created and that old convection is converting to stratiform cloud and precipitation (Houze 2004).

2.3.5 Vertical redistribution of momentum within MCSs

Houze (2004) outlined two processes by which MCSs vertically redistribute momentum: through horizontal accelerations by pressure gradient forces that develop within the system and vertical eddy fluxes associated with their internal circulations. Two-dimensional steady state idealizations are sufficient to describe the momentum redistribution by squall line MCSs, but have a difficult time describing the momentum redistribution in all of the various MCS structures that exist. To mitigate these problems, Houze (2004) showed that dividing the QLCS systems into their convective and stratiform components allows for one to separate the momentum redistribution into fundamental components that are allowed to vary from on MCS to the next. Furthermore, the net change in the environmental momentum profile can be strongly affected by the stratiform component, while the final vertical profile of the environmental momentum is a function of the size of the stratiform region relative to the convective region (Houze 2004).

2.3.6 Vertical profile of heating within MCSs

Just as the momentum varies systematically between the convective and stratiform regions of MCSs, so does the vertical profile of heating, which does so without regard to whether the MCS is a leading-stratiform or trailing-stratiform structure type.

The heating profiles of the convective and stratiform regions are distinctly all their own, and constitute "two distinct wavelengths of forcing" (Houze 2004). The stratiform heating wavelength is *H*, whereas the convective heating wavelength is 2*H*, where *H* represents the depth of the troposphere. "These two wavelengths of forcing produce distinct effects on the large-scale environment of the MCS; as the stratiform component of the heating becomes greater, the more the net heating by an MCS intensifies and shifts to upper levels" (Houze 2004). These two modes, as noted by Houze (2004), dominate the divergent response of the environment to the MCS. This fact can be verified through analysis of wind data within and surrounding MCSs. It is therefore unnecessary to examine radar echo structure to understand the heating impact of MCSs on the large-scale wind field (Houze 2004).

2.4 Discrimination of MCS environments using sounding observations

Forecasting the strength of MCSs is a major concern to operational meteorologists and the public, and is probably more vital than just forecasting the appearance of an MCS. To address this issue, Cohen et al. (2007) set forth a study to examine meteorological variables derived from sounding observations taken in the environment of quasi-linear MCSs. Within this study, Cohen et al. (2007) used a set of 186 soundings in which the beginning and mature stages of MCSs were sampled. The MCSs were categorized by production of severe surface winds into weak, severe, and derecho-producing MCSs. It was determined that knowledge of a few specific variables and their distributions among the different categories of MCS intensity can be used to improve forecasts, as well as convective watches for organized wind events (Cohen et al. 2007).

2.4.1 Background on derechos

Derechos are on the most intense end of the MCS spectrum and can be as destructive to life and property as tornadoes and hurricanes (Miller and Johns 2000). Derechos have received attention due to their ability to produce damage and human fatalities (Cohen et al. 2007). Johns and Hirt (1987), for example, studied 70 warm season (May-August) derechos and found that large convective instability and the presence of mid-level dry air above low-level moisture are common characteristics to many derecho environments. Furthermore, Cohen et al. (2007) noted that this dry-over-moist profile is of utmost importance; it allows for the development of air parcels with large negative buoyancy in the lower levels. It is this that allows for the development of organized, very cold "cold pools," and severe winds at the surface (Wakimoto 2001).

Evans and Doswell (2001) suggested that strong system-relative winds at mid-levels may be important to derecho development, owing to their effects on the formation of the cold pool and the subsequent speed of the MCS. Furthermore, Evans and Doswell (2001) noted that CAPE and vertical wind shear vary widely in their dataset, and that this likely reflects the large number of forcing mechanisms that may produce derechos. Environmental shear associated with derechos often extends through a deep layer as derechos strengthen, and this same deep-layer shear weakens as derechos decay (Coniglio et al. 2004).

2.4.2 QLCS quick-notes

Cohen et al. (2007) pointed out that the potential for an MCS to produce an organized severe windstorm is enhanced as it organizes into a quasi-linear convective

system, or QLCS. The structure that a QLCS exhibits is a reflection of the organization of the downdrafts and cold convective outflows, or cold pools. Certain modes of QLCSs, such as bow echoes (which will be discussed in detail in Part 2), and certain kinematic features like line-end vortices and rear inflow jets, are especially associated with the production of severe surface winds (Klimowski et al. 2003; Wheatley et al. 2006). Cohen et al. (2007) notes that although the real-time use of Doppler radars has increased the skill of very short-term forecasts for QLCSs significantly, the forecast for severity of an MCS on longer time scales remains difficult. Therefore, the focus of Cohen et al. (2007) was to identify those environmental variables that may reduce the difficulty of the aforementioned forecast problem, on the time scale of 3-12 hours.

2.4.3 Classification methodology for WCS, SCS, and DCS MCSs

Cohen et al. (2007) provided three classifications for severity of surface winds: Weak MCS (WCS), severe but non-derecho-producing MCS (SCS), and derecho-producing MCS (DCS). To be classified as severe, the winds must have reached a threshold of wind gusts greater than, or equal to, 26 ms^{-1}, or in some cases, there needed to be at least six severe wind reports produced. The wind report guideline reflects the National Weather Service Storm Prediction Center's (Norman, OK) guidelines for issuing severe thunderstorm watches. To determine if an MCS qualified as a DCS MCS, three criteria were used: 1) there were at least six severe wind reports produced by the MCS, 2) successive severe wind reports occurred within 3 hours or 250 km of each other in a chronological progression and in a concentrated area, and 3) the major axis of the line

connecting the initial and final severe wind reports was at least 400 km long. If either the second or third criteria were not met, it was then classified as an SCS.

Furthermore, Cohen et al. (2007) stated that it is important to know the stage of the MCS in its life-cycle, owing to the fact that environments associated with weakening MCSs are largely different than the environments during earlier stages. With the knowledge of environmental differences between stages in mind, Cohen et al. (2007) presented three life-cycle stages: 1) Initial cells prior to MCS development, 2) A mature MCS with strengthening or quasi-steady high reflectivity echoes (50 dBZ or higher), and 3) A decaying MCS with significantly weakened or shrinking areas of high reflectivity or a loss of system organization without any later reintensification. Systems that were decaying around the time of the sounding were removed from the Cohen et al. (2007) dataset to allow for focus on systems during the more intense stages.

2.4.4 CAPE and lapse rates

Cohen et al. (2007) noted that none of the various CAPE variables discriminated well between SCS and DCS environments. However, all of the CAPE variables discriminate at very high levels between WCS MCSs and the other two categories (Fig. 2.14). The ability to discriminate between categories, according to Cohen et al. (2007), suggests that single values of CAPE can provide some useful information as to whether or not an MCS will produce severe wind, regardless of the longevity of the convective windstorm.

The differences between WCS and SCS/DCS environments is largest for MLCAPE: Median MLCAPE for WCSs is around 1400 J kg^{-1}, and around 2400 J kg^{-1} for

SCSs and 2100 J kg^{-1} for DCSs. Cohen et al. (2007) noted that it may be that the higher CAPE values are more elongated along fronts for DCS events. The elongated nature of CAPE values for DCS events is similar to the findings of Coniglio et al. (2004), who showed that higher low-level dewpoint air tends to "pool" along boundaries ahead of derechos. Cohen et al. (2007) noted that pooling may actually be the deciding factor with regards to longevity of severe MCSs. Furthermore, the diagnosis of a unidirectional wind profile, with mean wind and mean shear being large and in the same direction, may allow for the proper diagnosis of pooling along the boundary and subsequent longevity. This wind profile is a feature of DCS environments, and may be a reflection of the larger-scale processes that create strong, elongated frontal features with regions of enhanced instability and wind shear (Cohen et al. 2007).

Mid-level environmental lapse rates are found to be greatest for DCSs, despite the fact that CAPE was largest for SCSs than for DCSs and WCSs (Fig. 2.15). Additionally, the 2-6- and 3-8-km lapse rates were found to discriminate very well among all three MCS environments (Cohen et al. 2007). Analysis of the 2-6-km lapse rate reveals that values >7°C km^{-1} (Fig. 2.15a) likely lead to severe MCSs. This observation could be a way to use environmental instability to discriminate between weak and longer-lived severe MCSs, although its practical utility could be questioned due to relatively small difference between the mean values among the three different categories (Cohen et al. 2007). Notably, the utility of lapse rates diminishes as a discriminator with the surface-based layers. The results of Cohen et al. (2007) indicate that 0-2- and 0-3-km lapse rates do not discriminate very well among the different MCS categories, and can be highly variable owing to diurnal effects and the frequent placement of sounding on the cool side

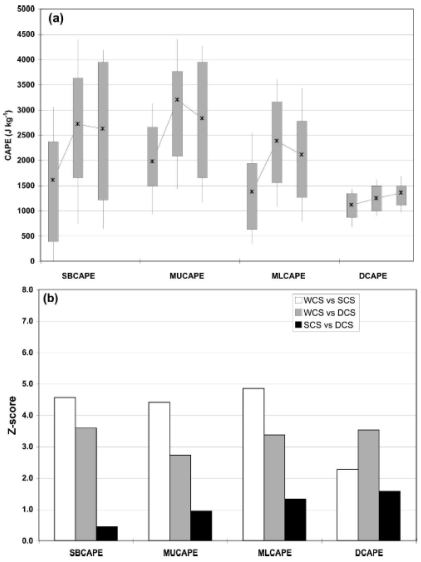

Figure 2.14 Fig. 8 from Cohen et al. (2007) – (a) Box-and-whiskers plot for SBCAPE, MUCAPE, MLCAPE, and DCAPE. Each set of three categories indicates the results for the WCSs, SCSs, and DCSs, from left to right. The whiskers stretch to the 10th and 90th percentiles and boxes enclose the 25th and 75th percentiles. The lines connect the medians (asterisks) for the distributions for each variable. (b) Absolute values of Z scores resulting from the Mann-Whitney test between WCSs and SCSs, SCSs and DCSs, and WCSs and DCSs for SBCAPE, MUCAPE, MLCAPE, and DCAPE.

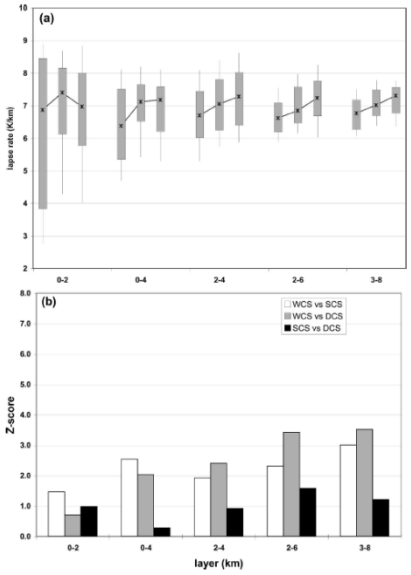

Figure 2.15 Fig. 9 from Cohen et al. (2007) – (a) Box-and-whiskers plots for 0-2-, 0-4-, 2-4-, 2-6-, and 3-8-km lapse rates (K km^{-1}). Each set of three categories indicates the results for the WCSs, SCSs, and DCSs, from left to right. The whiskers stretch to the 10th and 90th percentiles and the boxes enclose the 25th and 75th percentiles. The lines connect the medians (asterisks) for the distributions for each variable. (b) Absolute values of Z scores resulting from the Mann-Whitney test between WCSs and SCSs, SCSs and DCSs, and WCSs and DCSs for 0-2-, 0-4-, 2-4-, 2-6-, and 3-8 km lapse rates (K km^{-1}).

of stationary or warm fronts. This fact suggests that the processes responsible for the organization of cold pools and instability over deeper layers, which leads to deeper overturning, are more important in determining the severity of a MCS (Cohen et al. 2007).

2.4.5 DCAPE and θ_e

DCAPE and $\Delta\theta_e$ between low- and mid-levels are two measures used by Cohen et al. (2007) to assess the potential for organized cold downdrafts. Cohen et al. (2007) found that DCAPE increases with increasing MCS intensity (Fig. 2.14a). Furthermore, if a warm season MCS develops in an environment with DCAPE < 900-1000 J kg^{-1}, it is likely to be weak or non-severe. Therefore, DCAPE may also be used as an exclusionary factor. The use of DCAPE should be cautioned, however, because just as with using lapse rates, it is important to remember that this value is often estimated within the MCS due to the observations being collected near the MCS, and not directly within it. Objective analyses are likely to be less accurate than direct observations, which may cause a problem with using DCAPE as the sole severity forecast tool (Cohen et al. 2007).

Regarding $\Delta\theta_e$, it should be noted that relatively dry conditions below cloud base can be supportive of downdrafts due to the continued initiation of negatively buoyant parcels. However, strong downdrafts already underway can be enhanced by very moist low-level environments, due to the fact that the parcels will encounter relatively high virtual potential temperatures at low-levels (Wakimoto 2001). In support of the findings from Wakimoto (2001), Cohen et al. (2007) found that $\Delta\theta_e$ between the surface and mid-

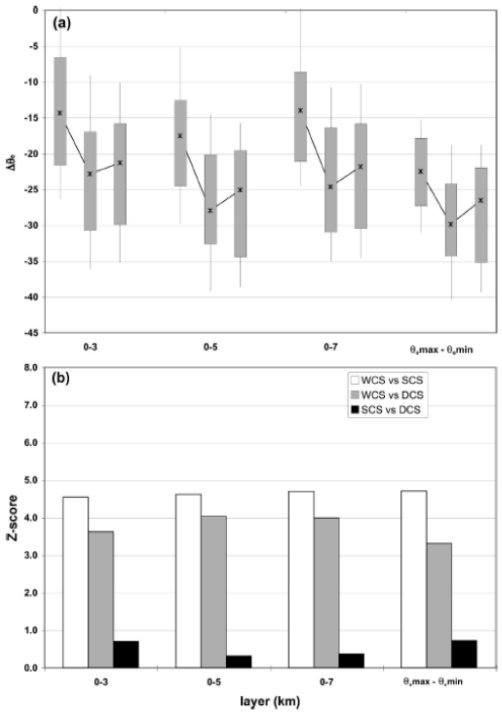

Figure 2.16 Fig. 10 from Cohen et al. (2007) – Same as in Fig. 9 and Fig. 10 from Cohen et al. (2008) but for the vertical difference in θ_e between 0-3, 0-5, and 0-7 km, and the levels of the maximum and minimum θ_e (θ_{emax} - θ_{emin}).

levels (0-3, 0-5, and 0-7 km) can be a very good discriminator between WCS and both SCS and DCS environments (Fig. 2.16). Furthermore, Cohen et al. (2007) determined that DCAPE doesn't do as well of a job discriminating between WCS and SCS environments as does using the 0-7-km $\Delta\theta_e$ and the $\Delta\theta_e$ between the maximum and minimum θ_e between low- and mid-levels ($\theta_{emin} - \theta_{emax}$) (Fig. 2.16). The median of $\theta_{emin} - \theta_{emax}$ is around -23 K for WCSs, and around -30 K for SCSs. This fact alone suggests that the use of $\Delta\theta_e$ may be a better predictor for severe wind potential than DCAPE, especially considering practical utility of each (Cohen et al. 2007).

2.5 Bow Echo Introduction

A continuation of the literature review on QLCSs is presented, and the following section will be focused specifically on bow echoes, and the influencing factors on their damaging surface winds. First to be presented is background information on bow echoes, followed by the development and history of their research. Following that is a current knowledge section starting with initialization modes of bow echoes, to the maturation of bow echoes and the atmospheric characteristics that influence the strength of surface winds. Last, under the current knowledge section, specific case studies of bow echoes analyzed during BAMEX are presented.

2.5.1 Background information on bow echoes

The term "bow echo" was first coined by Tetsuya Theodore "Ted" Fujita in 1978. He used the term in reference to a "bow or crescent" shaped radar echo that was associated with downbursts. Over the years, the understanding of bow echoes has changed and the definition has been broadened. A bow echo is now defined as a "bow or crescent-shaped radar echo with a tight reflectivity gradient on the leading edge, the evolution and horizontal structure of which is consistent with outflow dominated systems" (Klimowski et al. 2000). Essentially this means that a bow echo should have an increasing radius over time, have associated strong winds, and/or exhibit a persistent arc that deviates from the mean tropospheric wind in direction or magnitude. A common radar feature that will be described in section 2.7.2 is a signature known as the rear inflow notch. Rear inflow notches are associated with a strong rear inflow jet (RIJ), and they give knowledge into the severity of the winds, however, are not required by the

definition. Furthermore, bow echoes are the result of downburst activity, and therefore are not a predictor for severe weather. Rather, they are an indicator that severe weather is already occurring.

Bow echoes are complex storm systems and can evolve from a diverse set of morphologies (Fujita 1978) and develop into 4 different acknowledged classifications: Cell Bow Echo (CBE), Squall Line Bow Echo (SLBE), Bow Echo (BE), and Bow Echo Complex (BEC). Furthermore complexity is added to the situation by the fact that bow echoes form over a wide variety of time scales, and persist for various amounts of time. Collectively, the many characteristics and potentially dangerous severe weather associated with bow echoes have created an interest in this topic for nearly a half-century.

Different initiation modes of bow echoes have been studied over the years, first by Fujita (1978), then Johns and Hirt (1987), Lee et al. (1992), Przybylinksi (1995), and Klimowski et al. (2003), with each successive study improving on the previous. Klimowski et al. (2000, 2003) looked to further describe the varied nature of bow echoes by introducing a classification system. Once initial evolution modes and classifications were set, attention turned to influences on the surface winds of bow echoes, as well as the processes that drive them. For example, James et al. (2006) detailed bow echo sensitivity to ambient moisture and the strength of the cold pool. Atkins and St. Laurent (2009) and Wakimoto et al. (2006) described the relationship between mesovortices within bow echoes and damaging straight-line winds. Also, observational studies have been employed to take a physical approach to understanding the damaging capabilities of bow echoes and other squall lines, whether it be from tornadoes (Trapp et al. 2005) or from straight-line winds (Wheatley et al. 2006).

2.5.2 Development (history) of bow echoes and their research

Observational research had dominated the landscape of Bow Echo studies until recently when numerical simulations could be processed well enough to use them for research purposes. Over time, bow echo research has tried to accomplish many things, from labeling/describing structures and initial modes of development, to narrowing down what influences the strength of their straight-line winds.

One of the earliest studies of note by Nolen (1959) contributed the knowledge of severe weather potential from bulging radar-echo configurations. Fujita (1978) presented the first conceptual model of the structure and evolution of bow echoes, including a discussion on their diverse morphologies, and showed that a strong, tall echo would transition to a bow echo because of intense downdrafts near the apex of the bow echo itself. Further work by Johns and Hirt (1987), Lee et al. (1992), and Przybylinski (1995) began to explain the morphologies themselves. Fujita (1978) also recorded that bow echoes spawned tornadoes occasionally, and this has been well documented in many studies since, including Forbes and Wakimoto (1983) and Wakimoto (1983). Przybylinski (1995), Funk et al. (1999) and Atkins et al. (2004, 2005) all expanded on this further by using Doppler radar studies to show that mesovortices are often the parent of tornadic circulation. Trapp et al. (2005) concluded that tornadoes often form near the bow echo apex and often produce F0-F2 surface wind damage, however can sometimes produce, albeit rarely, F3-F4 classified tornadoes.

Observational studies from the 1980's were mostly encompassed by the **Pre-Storm Project.** Most notably, this project led to the development of the conceptual model of a mature squall line (Houze et al. 1989). The **Pre-Storm Project** categorized

key storm reflectivity features, including the multicellular evolution of bow echoes and mature squall lines, signatures of mature convective cells, and dissipating cells immediately behind the mature cells. Also shown were differing zones of weather reflectivity, which are referred to as transition zones. Transition zones were shown to separate the leading convective line from the trailing stratiform region (Houze et al. 1989). The **Pre-Storm Project** also began to introduce different mesoscale airflow streams, including the rear inflow jet (RIJ).

Przybylinksi and Decaire (1985) investigated reflectivity patterns in order to categorize echo patterns. The four types of bow echo patterns that they suggested are the pre-cursor to the classifications used currently. Presently, bow echoes are classified by reflectivity patterns and their initialization modes. Przybylinski and Decaire (1985) showed that the rear inflow jet created a rear inflow notch in the radar reflectivity, and these notches were a good indication as to where the strongest winds would occur.

Leary and Houze (1979) studied the stages of linear mesoscale convective system (MCS) evolution. By using reflectivity from GARP Atlantic Tropical Experiment (GATE), they showed that linear MCS's evolved through four different stages. These four different stages were then expanded upon by Rasmussen and Rutledge (1993), as they showed that certain characteristics of the squall line helped to determine what stage that the system was in.

One of the biggest misconceptions of early bow echo research was the thought that squall lines were considered to be the biggest producer of tornadoes. The introduction of Browning's (1964) description of the supercell model acted to dissolve that notion. Since, it has been understood that even though they aren't the largest

producers of tornadoes they still pose the threat, and even through the risk of strong, and violent, tornadoes is more likely in supercells, it is not exclusively the case.

2.6 Current Knowledge

2.6.1 Bow echo classifications and initial modes

To further understand bow echoes and adequately describe their varied nature, a classification system exists: Bow echo (BE), bow-echo complex (BEC), cell bow echo (CBE), and squall line bow echo (SLBE). A bow echo (BE) is one that is described to be (i) larger than a single thunderstorm, (ii) not associated with a large linear complex, and (iii) is mostly isolated from other organized convection. The classification bow-echo complex (BEC) is used to describe mesoscale convective systems in which the bow echo is the primary, but not only, form of organized convective structure. Supercell thunderstorms are often a part of a BEC. A cell bow echo (CBE) is used describe bow echoes that occur on a very small spatial scale (10-25 km) and are not associated with any larger-scale convective system. Finally, the classification squall line bow echo (SLBE) describes bow echoes that are a part of a large-scale, elongated (quasi-linear) convective system.

Due to the variable nature of bow echoes, different initial modes of bow echo evolution have been established in order to add further understanding. The three different initial modes of evolution as described by Klimowski et al. (2000) are (i) isolated (non-interacting) cells, or group of storms, (ii) squall lines, and (iii) supercells. All three are

formed over a wide variety of time scales and basically all were associated with severe surface winds. And even though large hail is not common from most bow echoes, some of those that evolved from supercells did produce large hail. This situation creates a dangerous combination of both severe winds and large hail.

The isolated, or group of cells initial mode of evolution, is typically comprised of 4 to 10 unorganized members. A merger of these cells is initiated when one or more of the cells exhibit deviant motion as compared to the others. The combining of these different cells is what causes the formation of the bow echo itself. However, a brief convective line of storms may form prior to bow echo initiation, and in that case is treated as a transitional feature if the line itself lasts for less than 20 minutes. During the study performed by Klimowski et al. (2000), seventy percent of bow echoes observed formed from this type of initial mode. These resulting bow echoes can develop very rapidly, in as little as 5-10 minutes, and moved most frequently in the direction of the fastest moving and often strongest cell.

The squall line initial mode of evolution results when the bow echo evolves from a preexisting squall line. These bow echoes later evolved into a medium to large solitary bow echo, or became a part of a larger-scale linear convective structure. In this type of evolution, bow echoes develop 2-4 hours into the lifetime of the squall system. Observations from the work of Klimowski et al. (2000) note that mergers with preexisting cells can significantly accelerate the creation of bow echoes from the squall line.

The final of the four initial evolution modes to be discussed is the supercell evolution mode. In most cases, the parent supercell from which the bow echo formed was

classified as a high precipitation (HP) supercell. In a transition of this nature, it is noted to be more of a gradual and predictable process. Also, bow echoes formed by this evolutionary mode were observed to be isolated, imbedded within squall lines or as part of bow echo complexes (BECs). These bow echoes were observed to show a preference to move along surface boundaries and were associated with both severe winds and very large hail. Furthermore, bow echoes formed of the supercell evolution mode frequently developed in a series of 2 or 3 storms, with the newest developing storms forming along the outflow from the previous storms (Klimowski et al. 2000).

2.6.2 Pre-storm environments: Warm and Cool season

As stated before, bow echoes are complex systems that involve many different classifications to help determine the nature of a particular bow echo. The complexity extends to determining pre-storm environments that are conducive to bow echo formation. These pre-storm environments of concern are broken into two main subsets; warm season environments and cool season environments. The two main subsets will further be broken down into surface and upper-level patterns, as well as thermodynamic and vertical wind shear profiles. The rest of this section (section 2.6.2) consists of findings by the National Weather Service Weather Forecast Office in Louisville, KY.

Warm season events are those described to be occurring during the summer months and are involved with weak synoptic forcing. Surface patterns observed to be of importance toward the creation and evolution of bow echoes are an east-west oriented frontal boundary, with strong surface convergence near the storm's genesis location. Also needed at the surface are pools of high dewpoints near the front and/or genesis area, with

maximum dewpoint values just to be south of the front. Bow echoes have also been observed to move parallel to the front, with a slight component towards the warm sector.

Moving into the upper-levels, certain patterns have also been associated with the creation of bow echoes. Straight or anticyclonically curved mid- and upper-level flow near a ridge axis is ideal, along with a weak shortwave trough located near or just upstream from the genesis region. Another very important environmental component is moderate-to-strong warm air advection (WAA) at 850-mb and 700-mb present near the genesis region, with weaker advections located downwind. Neutral or weak cold air advection (CAA) has also been noted in mid- to upper-levels over and just downwind of the genesis area. Moisture profiles are a very important component of the creation and intensification of bow echoes. The moisture profile that is most conducive for bow echoes is very high saturation levels at the 850-mb level, and pooled just south of the bow echo track. Damaging wind potential can be increased by drier air present at the 700-mb and 500-mb levels. Upper-level patterns have also have a correlation with the track over which a bow echo propagates, and that is along the thermal gradient of the 850-mb and 700-mb levels.

Thermodynamic and vertical wind shear profiles play a large part in the creation and development of bow echoes. A very unstable air mass is associated with long-lived, warm season bow echoes. The average maximum CAPE values, located in the genesis area, are approximately 2400 J kg^{-1} with even greater instability downwind where the average maximum CAPE is on the order of about 3500-4000 J kg^{-1}. This extreme instability is due to a pooling of moisture near the front.

Cool season events are associated with late winter/early spring months, and need strong dynamic forcing to be initiated. Surface patterns that are associated with the creation of bow echoes include a strong, progressive low and associated warm and cold fronts. The squall line and embedded bowing line segments will often be located along or north of the warm front, and stretches southward across warm sector along or ahead of the cold front. Due to usually limited moisture and instability associated with cool season months, significant divergence/convergence fields as well as dynamical forcing to produce strong lift associated with convective development is needed. As well, wind fields are preferred to be stronger than those in warm season bow echoes. 850 mb wind speeds on the order of 30-60 knots are common with upper-level jet stream axis nearby.

Thermodynamic and vertical wind shear profiles are largely different from those associated with warm season events, owing to the fact that they are associated with less instability than are warm season bow echoes. The actual degree of instability can vary widely between cold season bow echoes, and range from 500 J kg^{-1} to upwards of 2000 J kg^{-1}. Strong forcing and vertical shear compensates for the usually limited instability in cool season events. A layer of dry, and usually cold air, or backing winds, is often present in the mid-level downdraft entrainment area, which moves in on the squall line from the upstream side. This component often acts to enhance the damaging surface wind potential. Also of note, optimal conditions for a bow echo to form are a linear shear profile, with strong speed shear (limited directional shear) of 50 knots within the lowest 2.5 km layer of the atmosphere, with minimal shear present aloft.

A brief discussion about the pattern classification of bow echoes is necessary for completeness, and can also help to forecast possible duration of these highly destructive

storm systems. The two types of patterns are progressive and serial. A progressive pattern is associated with shorter length and curved echoes that are oriented perpendicular to the mean environmental wind. These convective lines bulge/bow downwind, which is associated with high instability and an east-west surface front. Serial pattern bow echoes are oriented more parallel to mean environmental wind than that of progressive patterns. Dynamically induced cold season events often exhibit the serial pattern, while warm season events often exhibit the progressive pattern.

2.7 Mature bow echo characteristics and observations

First to be discussed will be the atmospheric characteristics that act to strengthen and/or weaken bow echo surface winds. The following review will focus on three main factors; mesovortices, the rear inflow jet, and the effects of ambient moisture and cold pool strength.

2.7.1 Mesovortices and their influence on bow echo surface winds

Recent increases in reliability of numerical models have allowed for comparisons between numerical simulations and actual observations to determine the influences of mesovortices, with regards to both time and space. Trapp and Weisman (2003) noted that the strongest ground-relative winds were observed to the north of the bow echo apex, and were associated with a mesovortex. These strong, near-surface winds are generated by the horizontal pressure gradient that is created by the mesolow associated with a mesovortex. A mesolow is produced by intense mesovortices via the fluid shear terms in the

diagnostic perturbation pressure equation, and the horizontal pressure gradients that develop have been proposed to be the primary forcing mechanism for the generation of strong surface winds. Furthermore, recent numerical and observational studies have shown that these low-level, meso-γ-scale (Orlanski 1975) mesovortices formed on the bow echo gust front are also capable of producing expansive regions of straight-line wind damage. Furthermore, according to Wakimoto et al. (2006), intense mesovortices largely determine the locations of the strongest winds by modifying the low-level outflow from the system. It was found that the strongest winds occur on the side of the vortex where both translation and rotation effects are oriented in the same direction, not necessarily where the maximum horizontal pressure gradient is located in correlation with the mesolow. This finding by Wakimoto et al. (2006) also supports the research done by Atkins et al. (2005), in which they numerically simulated a bow echo event and removed the mesovortex circulation from the system. The removal of the mesovortex circulation resulted in a displacement of the high winds to another location and along a wider area. It was also found that in contrast to Trapp and Weisman (2003), the dual-Doppler radar data collected suggested that damaging surface winds were created by a linear superposition of the vortex flow, which is associated with the descending rear inflow jet (RIJ).

It is important to note, however, that not all mesovortices are damaging. It is important to distinguish between stronger mesovortices and those that are weaker and non-damaging. Tornadic mesovortices, the stronger of the two types discussed here, are usually longer-lived, deepened, and intensify rapidly just prior to tornadogenesis. Tornadic mesovortices also form concurrently with or after the creation of the rear inflow

jet, and along the portion of the gust front strengthened by the RIJ (Atkins et al. 2005). Non-tornadic mesovortices, the weaker of the two types, tend to be much shallower and shorter-lived than their tornadic counterparts. These non-tornadic mesovortices have been observed to form along the gust front both north and south of the RIJ (Atkins et al. 2005).

2.7.2 Rear inflow jet influence on strength of bow echo surface winds

In research reported by Atkins and St. Laurent (2009), the strongest near-surface ground-relative winds were found on the southern flank of a strengthening mesovortex, and one that was located just north or near of the RIJ core that descended to the surface. It was also noted that weaker maxima in the near-surface ground-relative winds were the result of mesovortices formed prior to RIJ genesis, or north and south of the RIJ position These results are consistent with those reported by Atkins et al. (2005), who suggested a combination of both the RIJ and mesovortex flows may be important in creating strong local maxima in the near-surface ground-relative winds. Wakimoto et al. (2006) observed a similar pattern and concluded that strengthening mesovortices that are collocated with a descending rear inflow jet produced the strongest near-surface ground-relative winds. Unlike the other physical processes that influence the strength of the surface winds, such as mesovortices, the RIJ may be the most unique by the fact it has a signature that can be found in radar reflectivity, while others cannot. The rear inflow notch, as it is known, is frequently noted behind leading, intense convection, and signifies the presence of the rear inflow jet along the gust front.

The National Weather Service Forecast Office (NWSWFO) of Louisville, KY noted that the local enhancements in the RIJ tend to develop along and behind the axes of

bowing line segments, and this is especially true with those associated with significant, trailing-stratiform precipitation. Furthermore, if the ambient wind shear is moderate-to-strong, the RIJ tends to remain elevated up to near the leading edge of the bow echo. The suspension of the RIJ, up to near the leading edge of the bow echo, causes the RIJ to then rapidly descend along the updraft/downdraft interface of the gust front, and cause significant wind damage. Systems with elevated rear inflow jets tend to be long-lived and exhibit rapid multicell growth along the leading edge of the system. On the other hand, if the ambient shear is weak, the RIJ tends to descend and spread out along and behind the leading line, and is associated with a potential for surface wind damage, but is usually less intense and shorter-lived.

2.7.3 Ambient moisture and cold pool strength influences on bow echo surface winds

During research performed by James et al. (2006), it was shown that relatively dry conditions at lower and mid-levels favored intense cold air production and very strong cold pool development. The very strong cold pool leads to upshear-tilted convection, which varies for different magnitudes of convective available potential energy (CAPE) and low level shear. However, high relative humidity values in the environment tend to reduce the production of cold air, and this leads to weak cold pools and downshear-tilted convective systems. When moisture contents reached intermediate levels, long-lived and noticeable bowing segments were generated within the convective line. James et al. (2006) noted that the growth of bow echo structures within a linear convective system depend critically on local strengthening of the cold pool, and to the extent that convection

associated became locally upshear-tilted. The local upshear-tilting creates a positive feedback process, and allows for continued intensification of the bow echo.

It is important for the cold pool to be only enhanced locally, as with intermediate levels of moisture, and not enhanced across the entirety of the system; this allows for the cold pool to overwhelm the low-level shear, locally. If the cold pool is locally strong enough, the convection tilts upshear in the specific area and initiates the positive feedback process that allows for the intensification of the bow echo. If the rate of production of the cold air is great, everywhere along the line, then the convection will become upshear-tilted across the length of the system. Furthermore, owing to the similarity of the cold pools along the entire line, local cold pool heterogeneity wouldn't last long enough to allow for significant bowing to occur. Finally, James et al. (2006) noted that cold pool strength depends on many other environmental factors than just ambient moisture values, thus bow echo sensitivity likely exists for many other atmospheric parameters.

2.7.4 Radar signatures of mature bow echoes

Just as there is radar signatures associated with initial modes, there are also those to describe mature bow echoes, as well as physical characteristics that can be seen on radar reflectivity. Fujita (1978) introduced the first conceptual representation of the structure and evolution of bow echoes and showed that a strong, tall echo transitions to a bow echo due to intense downdrafts near the apex of the bow echo. It is now known due to further research that the intense winds at the apex are formed by more than just downdrafts. A figure from Atkins et al. (2005) ties previous discussion of mesovortices

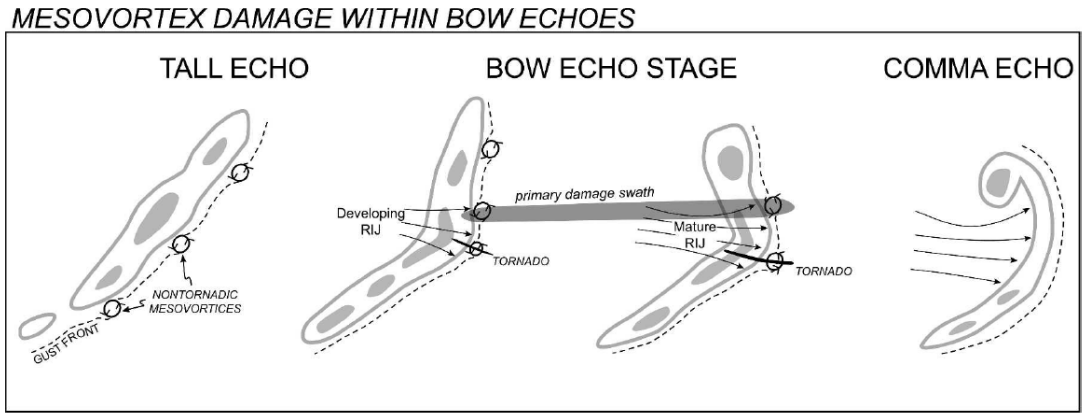

Figure 2.17 Fig. 16 from Atkins et al. (2005) – Schematic model of damage produced by the bow echo observed on 10 Jun 2003 east of St. Louis.

and rear inflow jets to bow echo evolution as noticed in radar reflectivity. Figure 2.17 describes how the bow echo develops from a tall echo to bow echo, as Fujita (1978) suggested, as well as showing associated mesovortices that become tornadic, along with the developing RIJ and the primary damage swatch. Atkins et al. (2005) took it one step further and demonstrated the bow echo finally transitioning out of the bow echo stage and into a comma echo stage. The comma echo stage is described as such due to its apparent shape.

The motion of the bow echo is important to understand if any effort for forecasting these unique storms is to be put forth. The three different evolution classifications previously mentioned in this paper (isolated, or group of cells, squall line, and supercell) are important to recognize when trying to forecast the probable motion of the bow echo. The isolated, or group of cells evolution mode, initiates a bow echo when the deviant motion of one convective cell initiates a merger between other cells. These bow echoes that form simultaneously with storm mergers can develop within 5-10 minutes, and frequently move in the direction of the fastest and often strongest cell. The

squall line evolution mode is formed as either a broken line of convection encounters a north-south oriented, quasi-stationary boundary, or as a gradual transition from a squall to a bow echo. The storm motion of this evolution mode moves as a result of dynamic forcing associated with progressive surface fronts. The last evolution mode to be discussed when considering storm motion is the supercell evolution mode. With this evolutionary mode, the supercell frequently developed in a series of 2 or 3 storms, with the later storms moving along the outflow of the previous storms, and this convective line became a bow echo. Bow echoes of this type show a preference to move along surface boundaries, such as fronts, drylines, and outflow boundaries.

2.7.5 Bow echo observations and associated damage

Bow echoes can result in extensive damage with their often damaging surface winds and hail, and occasional tornadoes. Damage from bow echo surface winds alone has been observed to most often be on the scale of EF-0 damage, with localized damage swaths that have areas of EF-1 damage.

Tornadoes have also been observed in association with bow echo convective systems. A study performed by Trapp et al. (2005), in which tornadic events from bow echoes between the years of 1998 and 2000 were researched, showed that 18% of all tornadoes occurred annually as a result of quasi-linear convective systems (QLCS), which includes bow echoes. Climatological distribution was also discussed (Fig. 2.18), and it was found that states along a curved axis from Pennsylvania to Louisiana had greater than 25% of their tornadoes form from QLCS system, while Indiana had the largest percentage at around 50%. The intensity of such tornadoes were found to mostly

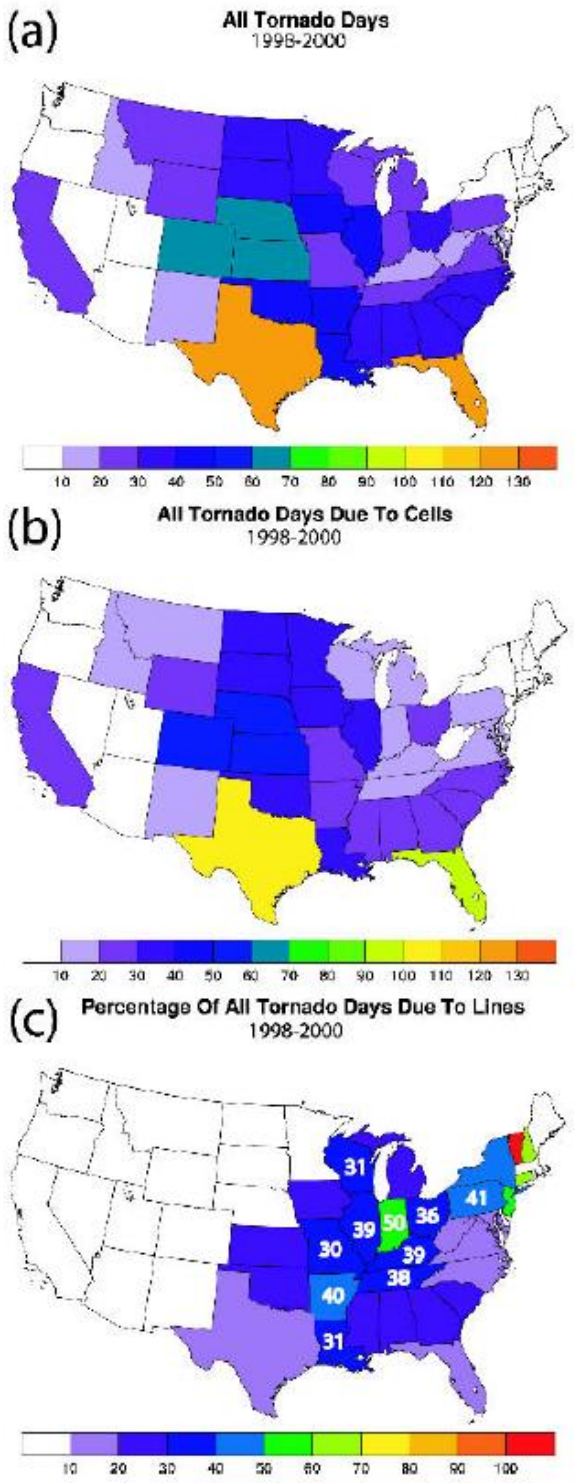

Figure 2.18 Fig. 2 from Trapp et al. (2005) – Geographical distribution of (a) all tornado days, (b) all tornado days due to cells, and (c) the percentage of all tornado days due to QLCSs, for 1998-2000.

be EF-1, however the threat for violent tornadoes still exists, as stronger tornadoes have been observed with intensity on the order of EF-2 to EF-3. Another concern associated with QLCS tornadoes is the fact that the large, horizontal length of the system creates an extended region upon which tornadoes can occur. The extended region of possible tornadogenesis creates an increased hazard with unpredictability that doesn't necessarily exist with supercell tornadoes.

2.7.6 BAMEX observations

Analysis from the *Bow Echo and MCV Experiment* (BAMEX) showed that bow echo durations could differ depending on the environment through which the bow echo is propagating. Many factors can act to strengthen, or weaken, a bow echo. The atmospheric characteristics previously discussed in this portion of the literature review are important to create the right conditions to extend the life of a bow echo, and if they do not exist can cause the bow echo to dissipate rapidly. Therefore, there is not an apparent way to assign common duration lengths. BAMEX noted bow echoes that lasted anywhere from thirty minutes after initiation to eleven hours.

On the 10 June 2003, a mature and extensive bow echo propagated through eastern Nebraska. This particular bow echo evolved from two cell bow echoes (CBE's), which had previously evolved from a merger of tornadic supercells. The first supercell to bow echo evolution occurred around 0100 UTC and the other at around 0300 UTC, over east-central Nebraska. The damaging wind production was observed to occur during the early formation of the bow echo, and so attention was focused on the two smaller scale bow echoes before the last merger to create the larger-scale bow echo. Emerson,

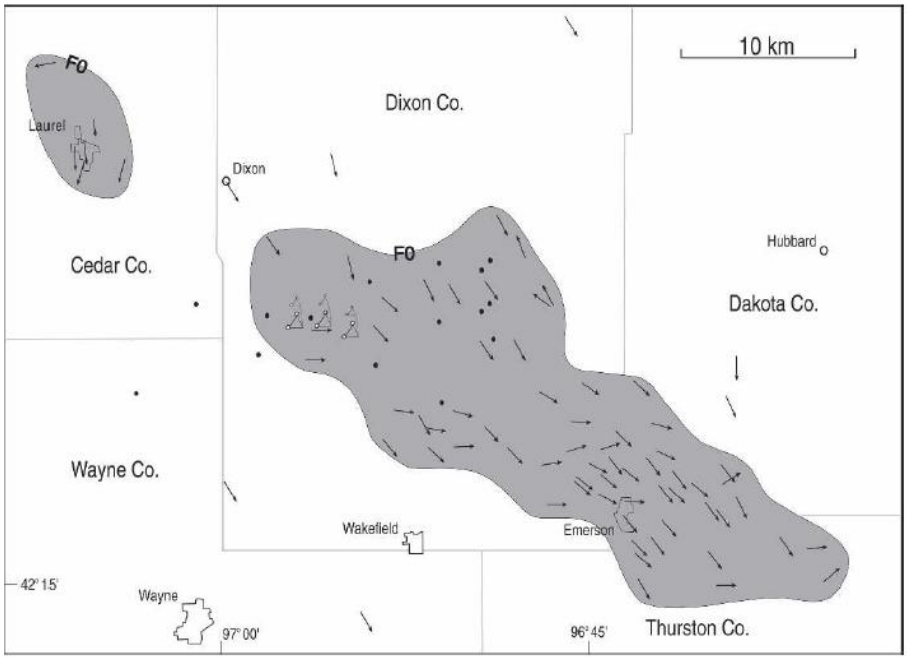

Figure 2.19 Fig. 7 from Wheatley et al. (2006) – Analysis of wind damage for the "Emerson" bow echo on 10 Jun 2003 over northeast Nebraska. Contours of F0 damage are lightly shaded in gray. Arrows represent "damage vectors," and dots represent damage from which wind direction could not be inferred. Triangular symbols represent damaged irrigation systems.

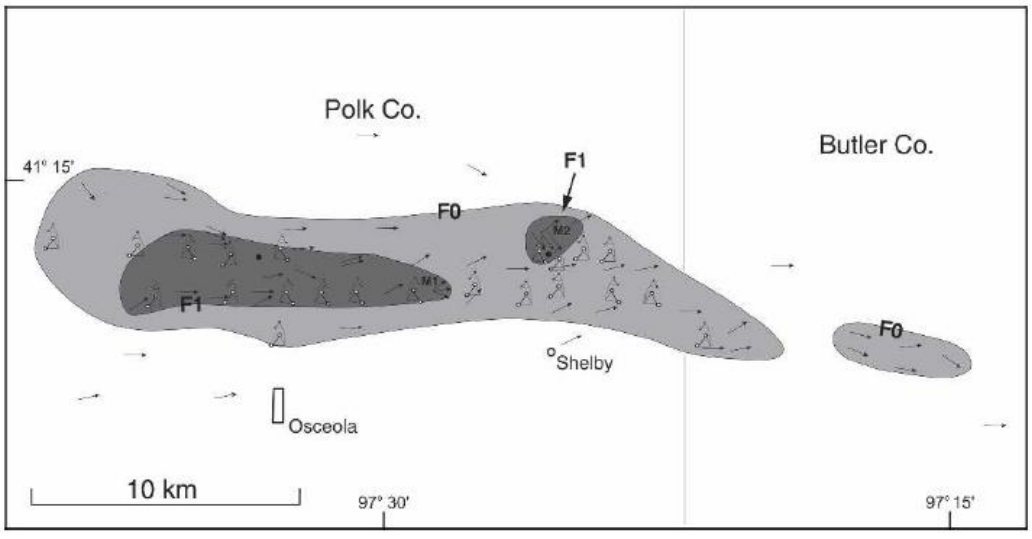

Figure 2.20 Fig. 8 from Wheatley et al. (2006) – As in Fig. 7 from Wheatley et al. (2006), except for the "Shelby" bow echo on 10 Jun 2003 over east-central Nebraska. Contours of F1 damage are heavily shaded in gray. (M1 and M2 denote localized areas of damage caused by microbursts.)

Nebraska encountered a swath of EF-0 intensity wind damage about 40 km in length (Fig. 2.19). Widespread tree and power line damage was recorded, as well as minor structural damage. In total, Emerson, NE property damage totaled $100,000. The other small-scale bow echo moved through Shelby, NE and the surrounding areas in east-central Nebraska (Fig. 2.20). Surveys revealed a narrow swath of EF-1 intensity wind damage about 10 km in length, which was embedded within a broader damage swath of EF-0 intensity about 30 km in length. A secondary area of EF-1 wind damage was found, and appeared to be the result of microburst winds. Property damage in Shelby, NE was estimated at a staggering $1 million and included damage to twenty-two irrigation systems, which were overturned in the surrounding farmland. Some of the irrigation systems had appeared to be rolled over twice. These two examples were chosen to show the extensive damage that bow echoes can inflict on a region. Straight-line surface winds are often as damaging as tornadoes, and across wider swaths, thus lending further motivation to the study of QLCSs.

2.8 Recent Research Concerning Tornadic QLCSs

On the foundation built by the numerous studies reviewed, from the early work of Fujita (1978) to more recent studies performed by Atkins and Laurent (2009), comes the work of Smith et al. (2012) and Thompson et al. (2012). Throughout the history of MCS research, attempts have been made to classify organizational modes, various structures, and the dynamics of such systems. More recently, the focus has turned towards increasing forecast accuracy, and resolving one of the largest forecast problems associated with QLCSs; tornadogenesis embedded within the QLCS. At the forefront of

this forecast problem, stands research performed by Smith et al. (2012) and Thompson et al. (2012).

Smith et al. (2012) was Part I of III of research performed entitled "Convective Modes for Significant Severe Thunderstorms in the Contiguous United States." Smith et al. (2012) looked to enhance the results from past convective mode investigations by increasing the number of storm classifications recognizable by radar (Fig. 2.21). For each event, Smith et al. (2012) utilized archived level II WSR-88D data from the National Climatic Data Center (NCDC) from the closest radar site to an event, up to 230 km away, to assign events to the convective mode classes. A subjective reflectivity threshold of 35 dBZ was also used for storm identification. The reasoning for the reflectivity threshold is that cells of discrete areas of above-threshold reflectivity generally contain a single dominant updraft (Smith et al. 2012).

Smith et al. (2012) detailed the statistical distributions of event by mode, and noted a few things. First, as one would expect, tornadoes are much more common with discrete and cluster right-moving supercells compared to QLCSs and disorganized modes. Right-moving (RM) supercells accounted for more than 71% of the total number of tornadoes during the time of their study (2003- 2011). Similar to Trapp et al. (2005), Smith et al. (2012) results indicate that EF1+ tornadoes are reported more frequently with QLCS convective modes compared to the total sample of tornado events. Also, it is likely that QLCS EF0 tornadoes are underreported.

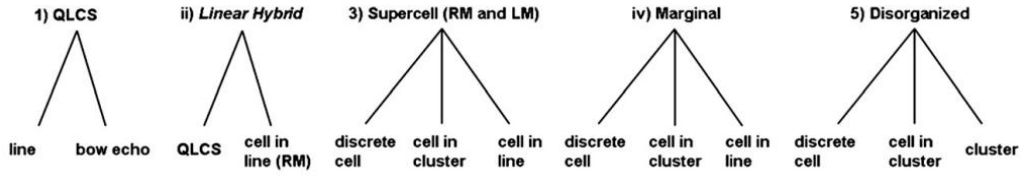

Figure 2.21 Fig. 2 from Smith et al. (2012) – Convective mode decision tree.

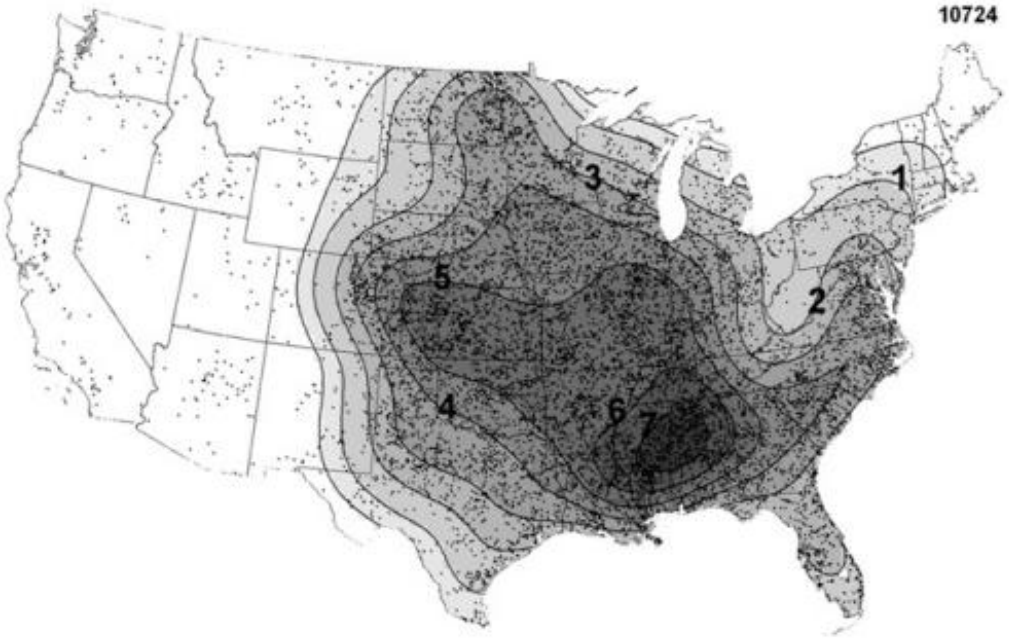

Figure 2.22 Fig. 6 from Smith et al. (2012) – Kernel density estimate on a 40 km x 40 km grid of all tornado events (EF0-EF5) assigned a convective mode. The minimum contour is 0.5 events per 10-yr estimate based on 2003-11 data. Labeled contours begin at 1 event per 10 yr. Black dots represent tornado events (10 274, labeled in the top right) that formed the basis of the kernel density estimate, and the color-fill scheme is gray scaled with heavier gray representing a higher tornado event estimate.

2.8.1 Tornado Occurrence and Relative Frequency by Mode

Kernel density estimation was performed on the data sample within Smith et al. (2012). For example, an estimate for tornado event occurrence linearly extrapolated to 10 years based on the 2003-2011 dataset shows much of the country east of the Rockies, but excluding the northeastern states, exceeded one tornado event per 10 years (Fig. 2.22).

For the years 2003-2011, one can notice that the highest kernel density exists across much of the central United States, from the central Great Plains eastward to the middle Mississippi Valley and south to Mississippi and Alabama. In this region, one tornado event is estimated every other year within a 1600 km^2 area, or about the size of a typical county in southeastern Kansas (Smith et al. 2012). QLCSs, in particular, had an estimated tornado event rate of occurrence east of the Great Plains, from Mississippi and Alabama northward in the Mississippi Valley and lower Ohio Valley (Fig. 2.23). Figure 2.24a-d shows a kernel density estimation for tornado event rate of occurrence associated with the following four convective mode classifications: Discrete + Cluster RM, QLCS + Line RM + Line Marginal, All RM, and Disorganized. Particular interest should be paid to Figure 2.24b, which highlights the tornado rate of occurrence for linear modes of convection, or QLCSs. These events exhibited higher concentrations over the lower Ohio River valley and middle Mississippi River valley southward to the northern Gulf coast states, but do occur with relative significant concentration across nearly the entire region east of the Rocky Mountains (Smith et al. 2012).

Smith et al. (2012) also noted a distinct tendency for a higher proportion of tornado events resulting from linear convective modes from the Ohio Valley southward to the lower Mississippi Valley (Fig. 2.25b). The kernel density estimate on linear convective mode tornado events as a percentage compared to all tornado events shows substantial percentages encompassing most of that region. The map in Figure 2.25b is comparable to that from Figure 2.18c, which showed the percentage of all tornado days as the result of lines of convective storms, or QLCSs. The distributions shown in that study (Trapp et al. 2005) are nearly identical to that shown in Smith et al. (2012).

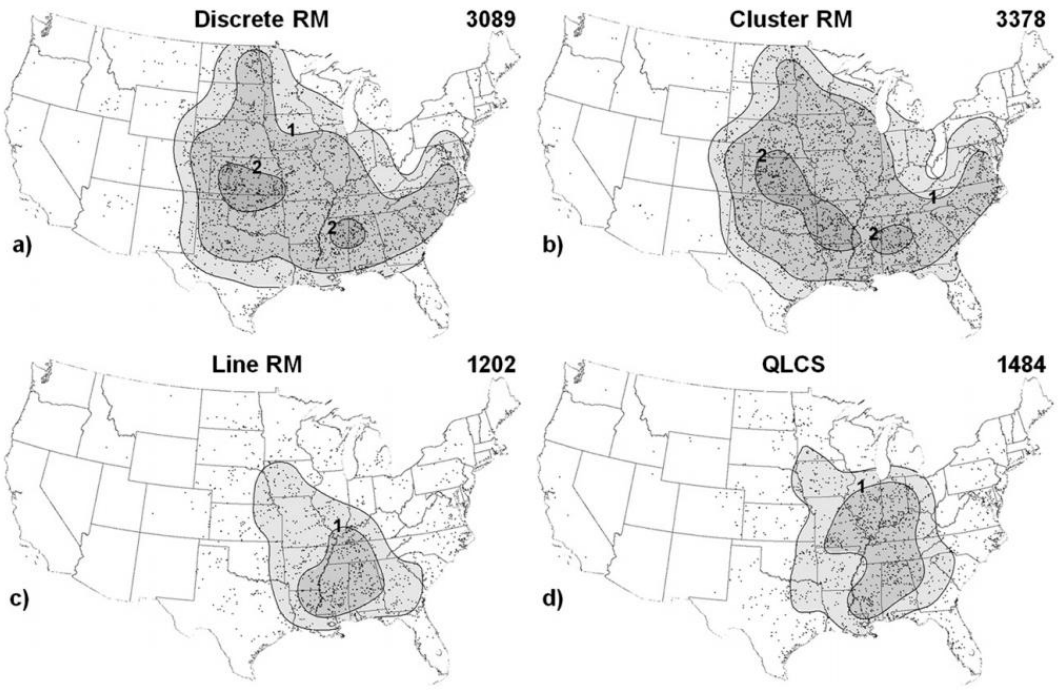

Figure 2.23 Fig. 7 from Smith et al. (2012) – As in Fig. 6 from Smith et al. (2012), but for (a) discrete RM, (b) cluster RM, (c) line RM, and (d) QLCS convective modes.

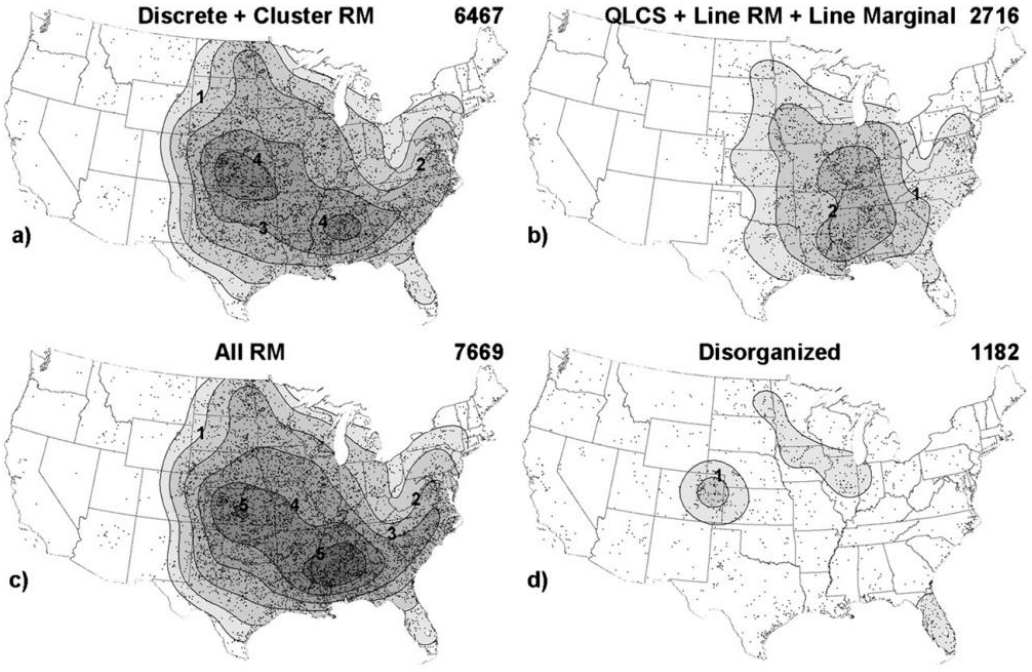

Figure 2.24 Fig. 8 from Smith et al. (2012) – As in Fig. 7 from Smith et al. (2012), but for (a) discrete RM + cluster RM, (b) QLCS + line RM + line marginal, (c) all RM, and (d) disorganized convective modes.

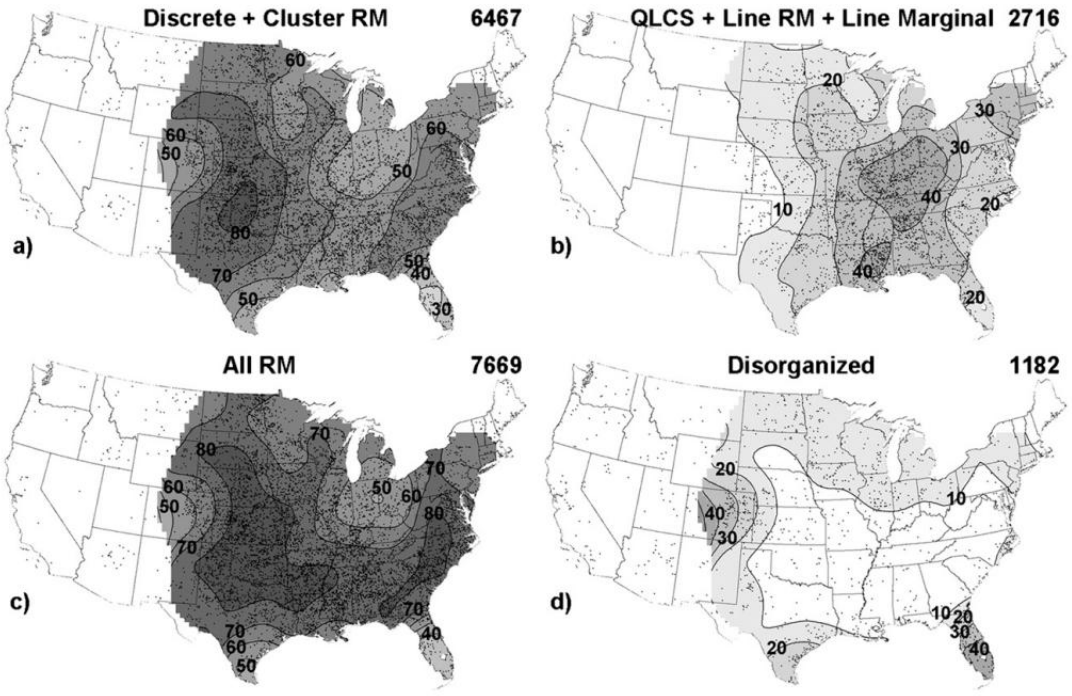

Figure 2.25 Fig. 10 from Smith et al. (2012) – Kernel density estimate on a 40 km x 40 km grid of (a) discrete RM + cluster RM, (b) QLCS + line RM + line marginal, (c) all RM, and (d) disorganized convective modes tornado event percentage compared to all tornado events (2003-11), with 10% contour intervals labeled (black lines). Other conventions are the same as in Fig. 6 from Smith et al. (2012).

2.8.2 Supercell and QLCS Tornado Environments

The work of Smith et al. (2012) was continued by Thompson et al. (2012) as Part II of III of research performed entitled "Convective Modes for Significant Severe Thunderstorms in the Contiguous United States." The focus of Thompson et al. (2012) was not on classification and climatology, but rather on the environments of Supercell and QLCS tornadoes. The same classifications for events were used for Thompson et al. (2012) as for Smith et al. (2012).

Within the sample, right-moving supercells dominated tornado production. Thompson et al. (2012) found that the Supercell Composite Parameter (SCP), as well as

its constituent components effective storm-relative helicity (ESRH) and effective bulk wind difference (EBWD), discriminated well between the disorganized tornadic storms and the three classes of supercells. EBWD and ESRH parameter values were similar between supercells and linear hybrid and QLCS cases. However, lesser vertical shear existed in the marginal supercell cases. Overall, as noted by Thompson et al. (2012), differences in the environments between supercells and linear modes of convection were relatively small. The small differences in the environments, according to Thompson et al. (2012), indicated that point measures of buoyancy and vertical wind shear, by themselves, are not able to clearly discriminate between storm modes.

Thompson et al. (2012) noted that large outliers exist within their dataset, especially when considering parameters such as MLCAPE and SBCAPE. Thompson et al. (2012) also noted that this could be due to the 40 km grid spacing utilized (RUC-40); RUC-40 grid points may be too far-spaced and could heavily impact the parameters' values. A very large sample size, however, should minimize the impact of outliers within the sample (Thompson et al. 2012).

Over the entire sample of tornado events within the study, most-unstable parcel CAPE (MUCAPE) exhibited a wide range of values; from less than 500 J kg^{-1} to greater than 3500 J kg^{-1}. Differences in mean MUCAPE values exceeded 600 J kg^{-1} between discrete RM and linear tornado events (Tables 2-2 and 2-3), and this result is statistically significant (for a two-tailed *t* test with unequal variances). However, while the tornadic linear convective modes exhibited somewhat lesser values of MUCAPE compared to discrete and cluster RM supercells, substantial overlap existed between the classifications. Therefore, the results of Thompson et al. (2012) suggest that CAPE itself

	Discrete RM	Line RM	QLCS	Disorg
MUCAPE ($J\ kg^{-1}$)	2167 (1980)	1559 (1343)	1381 (1130)	1643 (1502)
EBWD (kt)	50 (49)	50 (51)	42 (44)	25 (23)
ESRH ($m^2\ s^{-2}$)	261 (223)	295 (279)	230 (181)	68 (35)
SCP	10.7 (8.3)	9.2 (7.6)	6.2 (4.0)	1.9 (0.1)

Table 2-2 Table 1 from Thompson et al. (2012) – Mean (median) values of the effective-layer SCP and its three components across four tornadic convective mode subsets.

	Discrete RM − line RM	Discrete RM − QLCS	Line RM − QLCS	Discrete RM − disorg
MUCAPE	***607***	***786***	**178**	***523***
EBWD	−1	**7**	**8**	***25***
ESRH	**−34**	**30**	**65**	***192***
SCP	**1.4**	***4.5***	***3.1***	***8.7***

Table 2-3 Table 2 from Thompson et al. (2012) – Mean differences in the effective-layer SCP and its three components across four tornadic convective mode subsets. Parameter values are the same as for Table 1 from Thompson et al. (2012). Boldface differences are statistically significant at $\alpha < 0.001$, and boldface and italic differences are considered to be sufficiently large to be of operational significance.

is not a good discriminator between tornadic storm modes across all seasons combined. MLCAPE during the winter season, however, best differentiated between QLCS tornadoes and significant tornado right-moving supercell events. During other seasons, deeper-layer shear (0-6 km BWD and EBWD) and low-level vertical shear (0-1 km SRH and ESRH) tended to be smaller for QLCS tornadoes as compared to significant tornado right-moving supercell events.

Overall, Thompson et al. (2012) showed that environmental differences between the supercells and linear modes were relatively small. It is believed that the relatively small environmental differences indicate that point measures of buoyancy and vertical wind shear alone are not able to discriminate clearly between storm modes. Thus, Thompson et al. (2012) suggests that convective mode forecasts must instead rely on factors such as shear vector and mean wind orientation to the focus of storm initiation. Focus of storm initiation, in this instance, is meant to be features such as cold fronts or surface drylines. Other factors that the convective mode forecasts should rely on include the magnitude of ascent along the initiating boundary, as well as initial storm spacing and potential storm interactions.

2.9 Summary

QLCSs have been a subject of research for over a half-century. From work on MCS organization and observations (Leary and Houze 1979; Bluestein and Jain 1985; Johns and Hirt 1987; etc.), to the more recent work concerning the dynamics of QLCS environments with regards to tornadogenesis and other damaging effects (Trapp et al. 2005; Smith et al. 2012; Thompson et al. 2012), the topic continues to be at the forefront of severe storms research. The work of Smith et al. (2012) and Thompson et al. (2012) provided more insight into damaging severe storms, which included the likes of right-moving supercells and QLCSs, for the contiguous United States. It is the hope of this study to examine QLCSs with regards to tornadogenesis on a central US domain, and provide a more specific regional insight to the topic.

Chapter 3 Methodology

3.1 Event Selection

Thirty-two QLCS events were selected between 2005 and 2012, all from within the specified central U.S. domain (Fig. 1.1), and across all seasons (Table 3-1). Of these 32 events, 31 were deemed to successfully fulfill research criteria; 15 July 2007 LVX was not included in the analysis due to significant errors within the dataset. Events were chosen so that eight QLCS events existed in each of the following subsets: Tornado, Hybrid, Wind, and Marginal. In order to choose these events the SPC Severe Weather Events Archive was utilized, using their "Obs and Mesoanalysis" tab, which allowed for examination of the radar mosaic. Concurrently, SPC Storm Reports were used to classify the various events into the 4 aforementioned subsets.

Only 32 cases were used due to limitations of data processing. Originally, the time period was set to be from 2003 to 2011, and the goal was to utilize as many events as possible. The time period of 2003 and forward was chosen due to the entire data set being available as RUC-20 km data. However, due to a transitioning phase of data storage within the National Climatic Data Center's National Operational Model Archive and Distribution System (NOMADS), dates between August 2005 and October 2009 had been transferred to Atmospheric Radiation Measurement Climate Research Facility's website. One date outside of that time period (August 2005-October 2009), 26 June 2011, was also transferred to the Atmospheric Radiation Measurement Climate Research Facility's website. Data requested from the Atmospheric Radiation Measurement Climate

Research Facility was delivered in both a ".grb" format, and ".grib2" format. The ".grb" format was the only format that could be converted within the utilized version of WDSS-II, which therefore eliminated the cases that were delivered in the ".grib2" format. The elimination of cases due to this issue was random and did not affect any one season in particular, and did not preferentially affect the distribution of cases.

QLCS events were classified as tornado events if they were deemed to produce 3 or more tornado reports per radar location, while most events tallied more than 10 tornado reports. QLCS events were classified as hybrid events if they produced between 1 and 3 tornado reports, while also producing a reasonable amount of wind reports (in this instance, greater than 15). This subset is used to add a transition subset between tornado events and wind events, since there is ambiguity involved with classifying QLCS events. One case in particular, 26 Oct 10 LMK, was included in the hybrid subset even though it met the tornado threshold to be classified as a tornado event. The reason for this was that the first report was a brief touchdown, the second report was the result of a storm survey after the event that found EF-0 damage, and the third report didn't include any details. Therefore, it was found to be more fitting of the hybrid event type classification. QLCS events were classified as wind events if they produced 0 tornado reports, yet produced 15 or more wind reports; the most important aspect being that they produced 0 tornado reports. The marginal classification was used for QLCS events with 0 tornado reports and 6 or less wind reports. While classifying each event, radar observations were used to aid the process of choosing the most representative events of each subset. A complete list of events used in this study, which includes their representative time steps and associated storm reports, is provided in Table 3-1.

Event Date	Radar Location	Representative Time Step	Event Subset	Storm Reports (Tornado, Wind)
15 November 2005	IND	2000 UTC	Tornado	14, 27
15 November 2005	PAH	2100 UTC	Tornado	11, 17
29 February 2012	SGF	0600 UTC	Tornado	13, 37
29 February 2012	TWX	0300 UTC	Tornado	3, 13
31 December 2010	LSX	1700 UTC	Tornado	21, 17
26 May 2011	LVX	0200 UTC	Tornado	5, 34
25 May 2011	PAH	2300 UTC	Tornado	30, 58
20 April 2011	LVX	0400 UTC	Tornado	21, 90
10 August 2011	INX	0800 UTC	Hybrid	1, 23
16 November 2005	LMK	0000 UTC	Hybrid	1, 19
29 February 2012	ICT	0300 UTC	Hybrid	1, 31
26 October 2010	IND	1400 UTC	Hybrid	1, 29
26 October 2010	LVX	1500 UTC	Hybrid	3, 33
21 July 2006	LSX	1600 UTC	Hybrid	1, 31
19 June 2010	DVN	0000 UTC	Hybrid	1, 51
26 May 2011	IND	0300 UTC	Hybrid	1, 25**
29 February 2012	EAX	0400 UTC	Wind	0, 15
30 January 2008	LVX	0100 UTC	Wind	0, 66
09 June 2005	EAX	0200 UTC	Wind	0, 14
03 October 2006	LOT	0400 UTC	Wind	0, 39
06 November 2005	LSX	0400 UTC	Wind	0, 16
18 June 2010	LOT	2000 UTC	Wind	0, 63
18 July 2010	LSX	1400 UTC	Wind	0, 15
19 June 2010	EAX	1700 UTC	Wind	0, 32
*15 July 2007	LVX	2100 UTC	Marginal	0, 2
23 September 2006	PAH	1500 UTC	Marginal	0, 1
23 September 2006	LVX	1800 UTC	Marginal	0, 5
08 June 2010	LSX	1600 UTC	Marginal	0, 3
12 June 2010	EAX	1600 UTC	Marginal	0, 1
21 February 2012	SGF	0200 UTC	Marginal	0, 6
21 February 2012	EAX	0200 UTC	Marginal	0, 0
11 March 2010	PAH	0800 UTC	Marginal	0, 1

Table 3-1 Complete list of events, including their representative time step and associated storm reports, that was used in this study. *15 July 2007 LVX was not included in the analysis due to significant errors within the dataset. **Storm reports were modified to only include time step of QLCS, not the previous supercells that had earlier passed through the radar domain.

3.2 Data Downloading and Processing

NEXRAD Level II radar was obtained for this research through the National Climatic Data Center's Hierarchical Data Storage System (HDSS). Once the raw radar

data that was requested had been delivered, it was then processed through the second generation of the National Severe Storm Laboratory's Weather Decision Support System (WDSS-II), using the algorithm "ldm2netcdf," to be converted into a usable format (netCDF). Next, the algorithm "llsd" was used to process circulation data and obtain azimuthal shear, divergence, and rotation tracks (2h and 6h). Finally, the "w2merger" algorithm was used to convert the radar data from a multi-elevation polar grid to a Cartesian grid so that it could be more easily processed during future steps.

Rapid Update Cycle at 20-km resolution (RUC-20) analysis data was obtained through the National Climatic Data Center's National Operational Model Archive and Distribution System (NOMADS), while a few dates were obtained from the Atmospheric Radiation Measurement Climate Research Facility's website. The reason for a few dates being obtained from the Atmospheric Radiation Measurement Climate Research Facility's website was because data that was needed had been transferred to their server, as a result of their effort to convert data to a new format and compress it. Once the RUC-20 data was downloaded, the data was processed through the National Severe Storm Laboratory's Weather Decision Support System (WDSS-II), using the "gribToNetcdf" algorithm, to obtain a usable format (netCDF). Further processing was required to obtain the near storm environment (NSE) parameters, using the "nse" algorithm, which are the RUC-20 parameters used in this research. Also, in order to use only RUC-20 data within the specific radar ranges, a GPS Waypoint Registry was utilized (Williams 2013). This allowed for the calculation of the NW and SE corners latitude and longitude, which was entered into the "gribToNetcdf" algorithm to obtain a field which is effectively a 256 km × 256 km gridded data at a 1 km × 1 km resolution centered on the radar location.

3.3 QLCS Case Studies

The analysis process of this research will be broken up into smaller sections to aid in the describing of procedures. In Section 3.1, the process for choosing which 32 QLCS events to study was described, as well as how they would each be classified. Section 3.2 describes the downloading and processing of data. Each set of data, both radar and RUC-20, was processed to obtain fields that existed on a Cartesian grid, 256 km × 256 km, at a 1 km × 1 km resolution, centered on the radar location. This allowed for the data to be more readily examined, both observationally within WDSS-II, and statistically within MATLAB.

3.3.1 Domain of Events Chosen

As shown in Figure 1.1, the domain for this study is the central United States. Radar sites were chosen to maintain regional characteristics of QLCSs and to assure the researcher that other features, such as large bodies of water (Lake Michigan, specifically) and mountain ranges, would not affect the study. Therefore, the chosen domain exists as a box from Wichita, KS (ICT) to Indianapolis, IN (IND), and Tulsa, OK (INX) to Chicago, IL (LOT).

3.3.2 Analysis of Data from Chosen QLCS Events

For the analysis of the QLCS events, RUC-20 data (analysis times only) and NEXRAD Level-II radar data (from times closest to RUC-20 analysis times) were examined. For each event, a most representative time step was chosen. The choice of a

most representative time step was important, as it allowed for the analysis of the environment of interest for each event. The most representative time step was chosen to be the time step before, or nearest, the maximum storm reports of concern for a given event. If an equal number of maximum storm reports of concern occurred in two consecutive hours, the time step between the two was selected. For hybrid events, however, the time step prior to the tornado report was chosen because this was considered the environment of interest for that event type, especially considering the forecast problems to be answered. The use of the previously outlined methods allowed for the calculation of parameters without concern of averaging down (or up) atmospheric parameters for time steps that aren't necessarily the environment of interest. From this data set, a set of thirty NSE parameters from the RUC-20 data was selected for this research, based on the following literary works: Parker and Johnson (2000, 2004), Cohen et al. (2007), Johns and Hirt (1987), Evans and Doswell (2001), Coniglio et al. (2004), and Godfrey et al. (2004). Each NSE parameter was processed within MATLAB for each time step of each event to identify their maximum values within the storm's environment. The decision to use maximum values within the storm's area was made with the following thoughts in mind: 1) Averaging values across the length of the QLCS would "water down" the parameter values by incorporating data from locations not necessary to study, which would heavily influence the statistics and not do any favors as far as narrowing down the possible NSE parameter values for the various event types, and 2) Maximum values are where a forecaster's attention tends to focus, as it is safe to assume the minimum values of the parameters chosen exist in less intense regions of the QLCS. Also, it is important to note that Thompson et al. (2012) compared and analyzed the

environments of various events across multiple convective modes for the contiguous United States, whereas this study looks to compare the environments of various event types across one convective mode (QLCS) for a central United States domain.

3.3.3 Near Storm Environment (NSE) Parameters

The NSE parameters chosen for this study were selected based upon the literature read for Chapter 2. Although some parameters chosen were not explicitly stated in the text, their basis for being included still exists within the literature. The parameters utilized are listed in Appendix A, and their definitions are located in Appendix B.

3.4 MATLAB and ProStat Procedures

To begin the process of assessing different NSE parameters, each parameter was processed within MATLAB to convert the file from "netCDF" to an "M" file. This conversion allowed for each parameter to be examined within MATLAB, so that the maximum values could be determined within each storm cell. Storm cells were identified as contiguous pixels of reflectivity, using 35 dBZ as a threshold for reflectivity, similar to Smith et al. (2012), and a minimum size criterion of 200 km^2. This relatively large minimum size criterion was used to verify that the storms considered were QLCS events, and not simply supercell lines. After the storm cells for each event had been identified, the enclosed regions (cells) were then tagged, converted to a binary image, and given an identification (ID) code. The ID codes for the cells of interest were then used as the template field for the NSE parameters. Once the clusters of pixels had been identified and

ID codes assigned, values could then be derived for the selected NSE parameters for each cell in the domain. This was accomplished by overlaying matrices of NSE data to the matrix of identified cells. The NSE values could then be calculated for each individual storm cell within the given domain from all the pixels contained in the given cell. The NSE parameter values, for all storm cells within the QLCS events, returned from this method were formatted into an ".xlsx" file, allowing for statistical tests and graphical representation of the data within ProStat.

The data, once formatted into an ".xlsx" file, was then transferred into a data sheet within ProStat. From this main data sheet, more data sheets were created specifically for each NSE parameter. Each NSE parameter data sheet had 4 columns (one for each event type). Once within each individual data sheet, error values (produced by MATLAB to be -99900) and "NaN" error values (65855) were deleted from the data set. These errors were most likely caused by an error within the raw RUC-20 data. The errors were not a significant problem, as their appearance was relatively rare and were easily removed. Once that had been accomplished, a box and whiskers plot was generated for each NSE parameter, for all four event types (Appendix C). ProStat makes accomplishing this step very simple, as a menu option exists to create a box and whiskers plot for the data sheet. Chart/axis titles were then edited and added, producing the final box and whiskers plots shown in this research. Just as the box and whiskers plots were generated within ProStat, so were the statistical tests. For this research, it was decided that a non-parametric one-tail Mann-Whitney Test would be beneficial (Mann and Whitney 1947), especially considering the size of the data set, the non-normal distribution of the data set, and the questions that were to be answered.

The one-tail Mann-Whitney tests were performed within ProStat, as well, for each individual NSE parameter data sheet. It is important to note that every storm cell identified for each QLCS event was compared using the Mann-Whitney tests, which made the sample size larger for each QLCS event type. A test was performed multiple times for each data sheet, so that the following categories could be evaluated: Tornado vs. Hybrid, Hybrid vs. Wind, Wind vs. Marginal, and Tornado vs. Wind. Each Mann-Whitney Test produced a Z value, from which one can accept or reject the null hypothesis, and a one-tail probability, from which one could produce a confidence test to determine the confidence that the value is not only statistically different, but also greater-than or less-than the parameter value for the other compared event type. In each case, the null hypothesis was that there is not a statistical difference between the two compared event types for the given parameter. A rejection of this null hypothesis meant that there was a statistical difference between the two event types for the given parameter. Any Z value greater than 1.65 or less than -1.65 rejects the null hypothesis, and each one-tail probability must be less than, or equal to, 0.05 (95% probability level) to be considered statistically confident that the value for one event type is greater than, or less than, the value for the other compared event type. These data sets, both provided by the box and whiskers plots and the Mann-Whitney Test, were then used to begin the analysis of each storm type from which conclusions could be drawn.

3.5 Radar Observations

Radar observations were also described. This was done by choosing a representative event for each, and describing the event itself. The representative events

were selected by the researcher based upon which event most closely exhibited the median values of the statistically different parameters produced during event comparisons. The event that best portrayed those aforementioned values, for each event type, was selected. In section 5.1, the representative time step for the representative event was observed, just as for the statistical comparison. However, unlike for the NSE parameter comparisons, the time step for one-half hour and an hour ahead in time was also shown. This was done simply to show the evolution of the QLCS event over the next hour that was valid for the RUC-20 analysis time step selected. In section 5.2, for each selected representative event, a cross-sectional analysis of base velocity and base reflectivity was performed. Cross-sections were performed through a region that included >35 dBZ reflectivity values, on a radial from the radar site, as close to perpendicular to the line of convection as possible, in order to determine flow through the system using base velocity.

Chapter 4 Statistical Results for Event Comparisons

4.1 Tornado vs. Hybrid Events

4.1.1 Forecast Problems to be investigated with this Comparison

In order to understand why the comparison between “Tornado” and “Hybrid” QLCS events was performed, one must first know what classified an event as such. For a QLCS event to be classified as a tornado event, it must have produced 3 or more tornado reports per radar domain of interest. For a QLCS event to be classified as a hybrid event, it must have produced between 1 and 3 tornado reports, while also producing a 15 or more wind reports. The hybrid subset was used to add a transition subset between tornado and wind events, since there is ambiguity involved with the classification of QLCSs. One may notice that a single event with 3 tornado reports was included with the hybrid subset, rather than the tornado subset. The event, 26 Oct 10 LMK, was deemed to be a hybrid event because the first report was a brief touchdown, the second report was the result of a storm survey after the event that found EF-0 damage, and the third report didn't include any details. Therefore, it was found to be fitting of the hybrid event type classification. The rest of the hybrid events produced only one tornado report each.

The forecast problem to be investigated with this comparison is as follows: Is it possible to forecast between a QLCS event that will produce a single tornado vs. a QLCS event that will produce multiple tornadoes along the line of storms? By comparing the

values of the 30 NSE parameters chosen using the non-parametric Mann-Whitney Test, this study looked for differences between the NSE parameters that one could use when forecasting for such events.

4.1.2 NSE Parameters of Use

Through the utilization of the Mann-Whitney Test, there were eight NSE parameters that were identified to be statistically different between tornado and hybrid events. To be considered statistically different, the Z value produced by the Mann-Whitney Test for each parameter comparison must have been either less than -1.65, or greater than 1.65. Furthermore, not only were these eight parameters found to be statistically different, but they were also found to be greater than, or less than, their counterpart with a 95% probability level, or higher. This fact was identified through the utilization of a one-tail probability test. For a confidence level of 95% or higher, the one-tail probability must have a confidence test less than, or equal to, 0.05. These eight NSE parameters are broken into subsets of "Shear Parameters," "Instability Parameters," and "Moisture Parameters" for this particular comparison. Each will be listed in order of decreasing probability level, meaning the first to be noted within each subset will be the most statistically different between the two event types with the greatest probability level.

4.1.3 Shear Parameters, all Tornado > Hybrid

The four NSE shear parameters that were statistically different between the two event types are: *Shear Vector Magnitude: 0-3 km, Speed Shear: 0-3 km, Shear Vector*

NSE Parameter	Z value	Confidence Test	Probability Level
Shear Vector Magnitude: 0-3 km	-3.18953479	0.00071251	99.93%
Speed Shear: 0-3 km	-3.17166625	0.000757835	99.92%
Precipitable Water	-2.8142954	0.002444214	99.76%
Shear Vector Magnitude: 0-6 km	-2.63560998	0.00419931	99.58%
BRN Shear	-2.45692456	0.007006606	99.30%
DCAPE: 1 km	-2.24250205	0.012464471	98.75%
Lapse Rate at MULFC	-1.87312448	0.030525599	96.95%
Sfc Dew Point	-1.81365704	0.034865272	96.51%

Table 4-1 NSE parameters that were statistically different in comparison of tornado and hybrid events are shown.

Magnitude: 0-6 km, and *Bulk Richardson Number (BRN) Shear*. As shown in Table 4-1, all four NSE shear parameters were found to have probability levels greater than 99%, with *Shear Vector Magnitude: 0-3 km* found to be at 99.93%. The small value of the confidence test (0.00071251) provides confidence that this parameter, *Shear Vector Magnitude: 0-3 km*, can be used under the assumption that the parameter's value will be greater for tornado events than for hybrid events (Fig. 4.1a). This fact lends this study a first look at answering the aforementioned forecast problem. The other three NSE shear parameters of use, *Speed Shear: 0-3 km*, *Shear Vector Magnitude: 0-6 km*, and *Bulk Richardson Number (BRN) Shear*, all exhibited the same behavior of their values being greater for tornado events than for hybrid events (Fig. 4.1b-d). The results of the Mann-Whitney Test suggest that greater amounts of shear, along with other necessary ingredients, are more conducive to tornadic environments (similar to findings from Atkins et al. 2005). Interesting to note, as well, is that the greater values of shear seemingly point to a difference between QLCSs with multiple tornadoes along the line as compared to QLCSs with a single tornado and a more prevalent straight-line wind threat.

4.1.4 Instability Parameters, all Tornado < Hybrid

Two NSE parameters representing instability were found to be statistically different for the Tornado vs. Hybrid comparison; *DCAPE: 1 km*, and *Lapse Rate at MULFC* (Table 4-1). These instability parameters are opposite of the shear parameters previously mentioned in the fact that the values for each are greater for hybrid events than for tornado events (Fig. 4.2). This is noted by the high probability levels associated for each, with *DCAPE: 1 km* at 98.75% and *Lapse Rate at MULFC* at 96.95%. This result is reasonable: With steeper lapse rates for hybrid events (represented by the *Lapse Rate at MULFC*), more moist parcels are accelerated upward, and act to create a strong, mid-level warm pool thanks to latent heat release. As the greater values of DCAPE for hybrid events (represented by DCAPE: 1km) enhance downdrafts and precipitation falls, evaporational cooling takes place and strengthens the cold pool. A strong warm pool aloft coupled with a strong surface cold pool act to contribute to the development of a strong rear inflow jet; and the stronger the flow in the rear inflow jet, the greater the potential for damaging winds at the surface (Trapp and Weisman 2003; Wheatley et al. 2006) during hybrid events, as compared to tornado events.

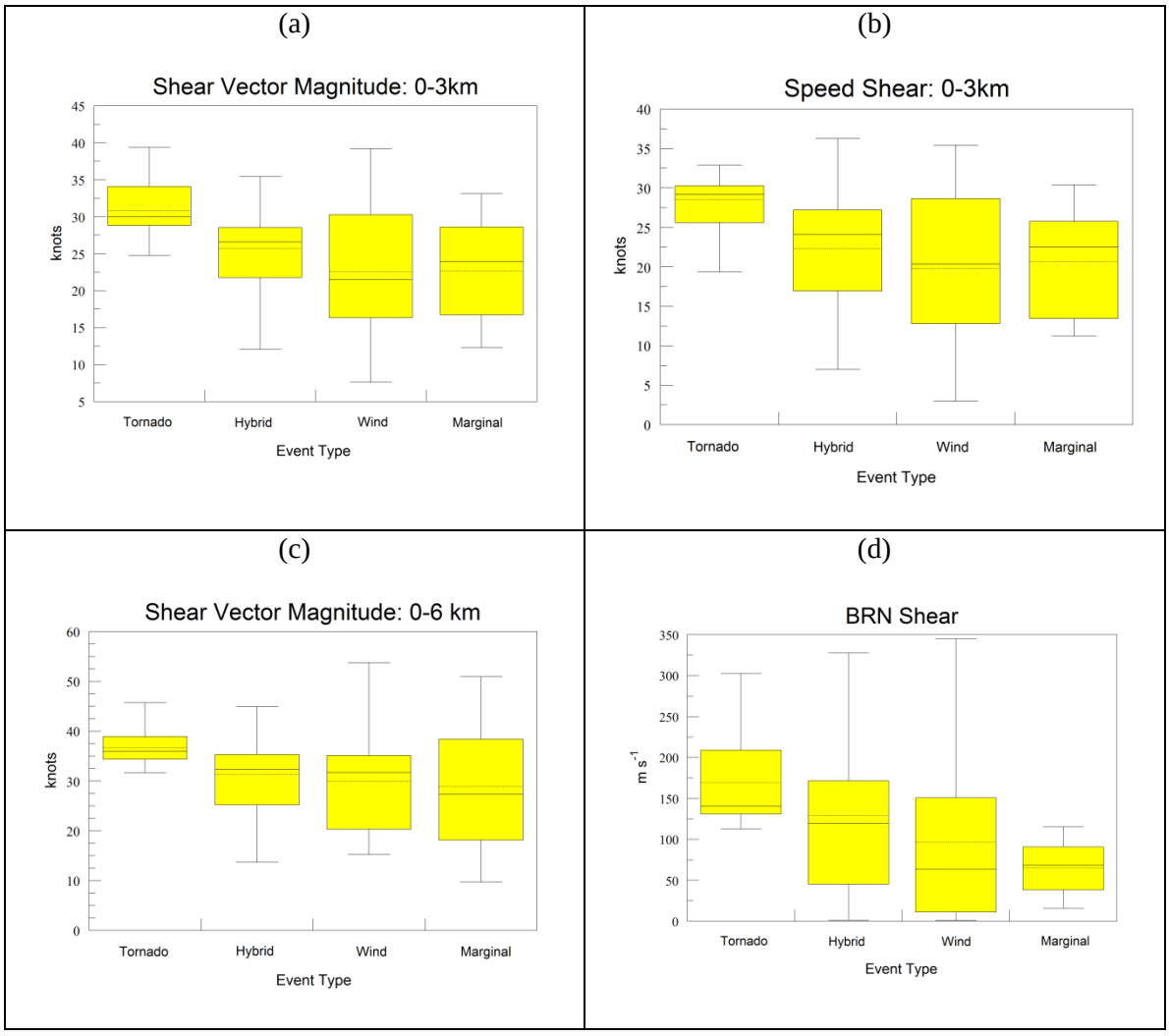

Figure 4.1 Box and whiskers plots for (a) Shear Vector Magnitude: 0-3 km, (b) Speed Shear: 0-3 km, (c) Shear Vector Magnitude: 0-6 km, and (d) BRN Shear for the comparison of tornado and hybrid events.

4.1.5 Moisture Parameters, all Tornado < Hybrid

The final two NSE parameters that were statistically different for this particular comparison are *Precipitable Water* and *Surface Dew Point*. Just as the instability parameters outlined above, these parameters representing moisture exhibited lower values for tornado events than for hybrid events (Fig. 4.3). This is once again noted by the

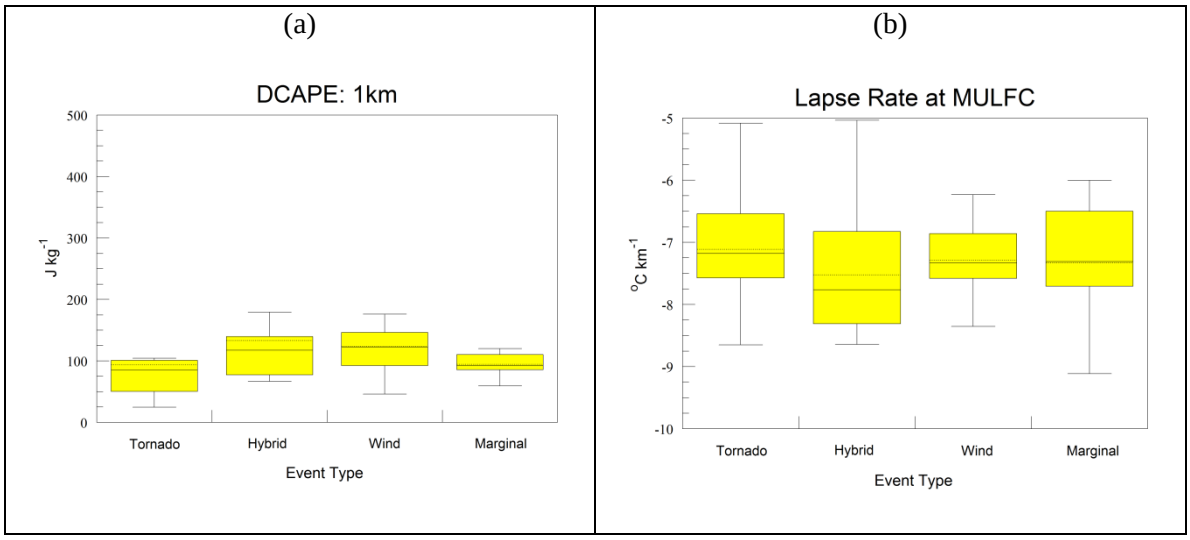

Figure 4.2 Box and whiskers plots for (a) DCAPE: 1 km and (b) Lapse Rate at MULFC for the comparison of tornado and hybrid events.

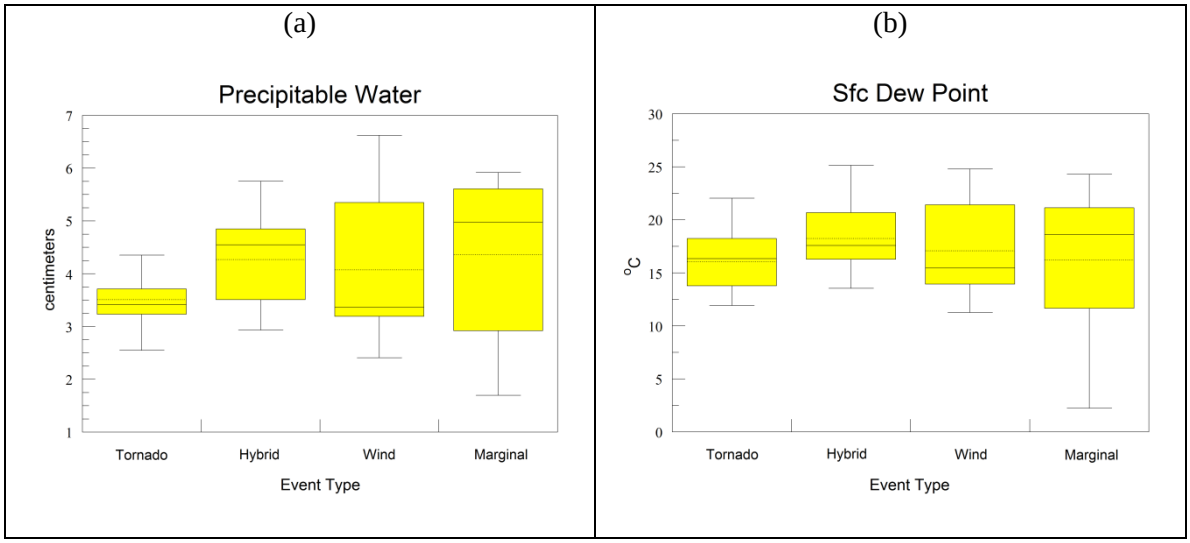

Figure 4.3 Box and whiskers plots for (a) Precipitable Water and (b) Sfc Dew Point for the comparison of tornado and hybrid events.

confidence test levels for each. The probability level for *Precipitable Water* is relatively high at 99.76%, and for *Surface Dew Point* is 96.51% (Table 4-1). As with the shear and instability parameters results, the results for the moisture parameters are also reasonable. The moister environment associated with the hybrid event environments would allow for more water loading and precipitation, and this increased precipitation would allow for more evaporational cooling as the drops fall to the surface. As the rain-cooled air becomes cooler, the more negatively buoyant it becomes. This will act to enhance the downdrafts, cold pool, and severe winds at the surface associated with the QLCS (Wakimoto 2001). Thus, this point strengthens the notion that a statistical difference exists between tornado events and hybrid events, thanks in large part to the fact that hybrid events seemingly more closely resemble wind events that just happen to produce a single tornado. More support of this thought exists in the upcoming comparisons.

4.1.6 Implications of Results

The results of the comparison between tornado events and hybrid events for the central US are revealing, as they show that significant statistical differences do exist between the two event types. Using the parameters set forth above, this research suggests that one may be able to distinguish during the forecasting stage the likelihood of an event being more or less a wind event with a singular tornado along the QLCS, or an event producing multiple tornadoes along the QLCS. This could have far reaching effects not only from a forecasting perspective, but also a nowcasting perspective. In places such as Columbia, MO the radar coverage is not ideal, and this information could allow a forecaster to be more judicial with the tornado warnings. The eight NSE parameters

outlined above could provide the support needed to make the often challenging decisions surrounding QLCS events.

4.2 Tornado vs. Wind

4.2.1 Forecast Problems to be investigated with this Comparison

Just as in the previous comparison, one must know what classified an event as a "Tornado" or "Wind" QLCS event to understand the reason for the upcoming comparison. Since it has already been described what classifies an event as a tornado event, this explanation will focus solely on what classifies an event as a wind event. A QLCS event was classified as a wind event if it produced 0 tornado reports, yet produced 15 or more wind reports per radar domain of interest. The utilized thresholds made certain that the event was only a straight-line wind threat. Wind events ranged from producing 15 wind reports (28 Feb 12 EAX) to 66 wind reports (29 Jan 08 LMK). It is noted that greater numbers of reports often come from more densely populated areas, so it was decided that 15 wind reports would be necessary to distinguish a wind event.

With this following comparison of tornado vs. wind events, the forecast problem to be investigated is this: Is it possible to distinguish a difference between QLCS events that produce tornadoes and QLCSs that don't produce a single tornado but pose a significant wind damage threat? Just as the previous comparison, all 30 NSE parameters were investigated and compared between event types, and the results for this are shown below.

4.2.2 NSE Parameters of Use

For the comparison of tornado vs. wind events, the use of the Mann-Whitney Test determined that there are eight NSE parameters that are statistically different between the two event types. Once again, to be considered statistically different, the Z value produced by the Mann-Whitney Test for each parameter comparison must have been either less than -1.65, or greater than 1.65. Also, every one of the eight parameters was found to not only be statistically different between event types, but the parameters also exhibited greater-than or less-than values as compared to their counterpart for the other event type at a 95% probability level or higher. This is noted by each parameter comparison exhibiting confidence test values of less than, or equal to, 0.05. Furthermore, the eight NSE parameters were broken down into subsets of "Shear/Rotation Parameters" and "Instability Parameters," for this comparison and each will be listed in order of decreasing probability level.

4.2.3 Shear/Rotation Parameters, all Tornado > Wind

The six NSE shear/rotation parameters that were statistically different between the two event types are: *Storm Relative (SR) Helicity: 0-3 km*, *Storm Relative (SR) Helicity: 0-1 km*, *Bulk Richardson Number (BRN) Shear*, *Speed Shear: 0-3 km*, *Shear Vector Magnitude: 0-3 km*, and *Shear Vector Magnitude: 0-6 km* (Table 4-2). As shown in Figure 4.4a-f, all six of the NSE shear/rotation parameters were found, statistically, to have values greater for tornado events than for wind events. The highest probability level exists for *Storm Relative (SR) Helicity: 0-3 km*, which is 99.87%, while the other five parameters listed above all maintain probability levels greater than 99%. The high

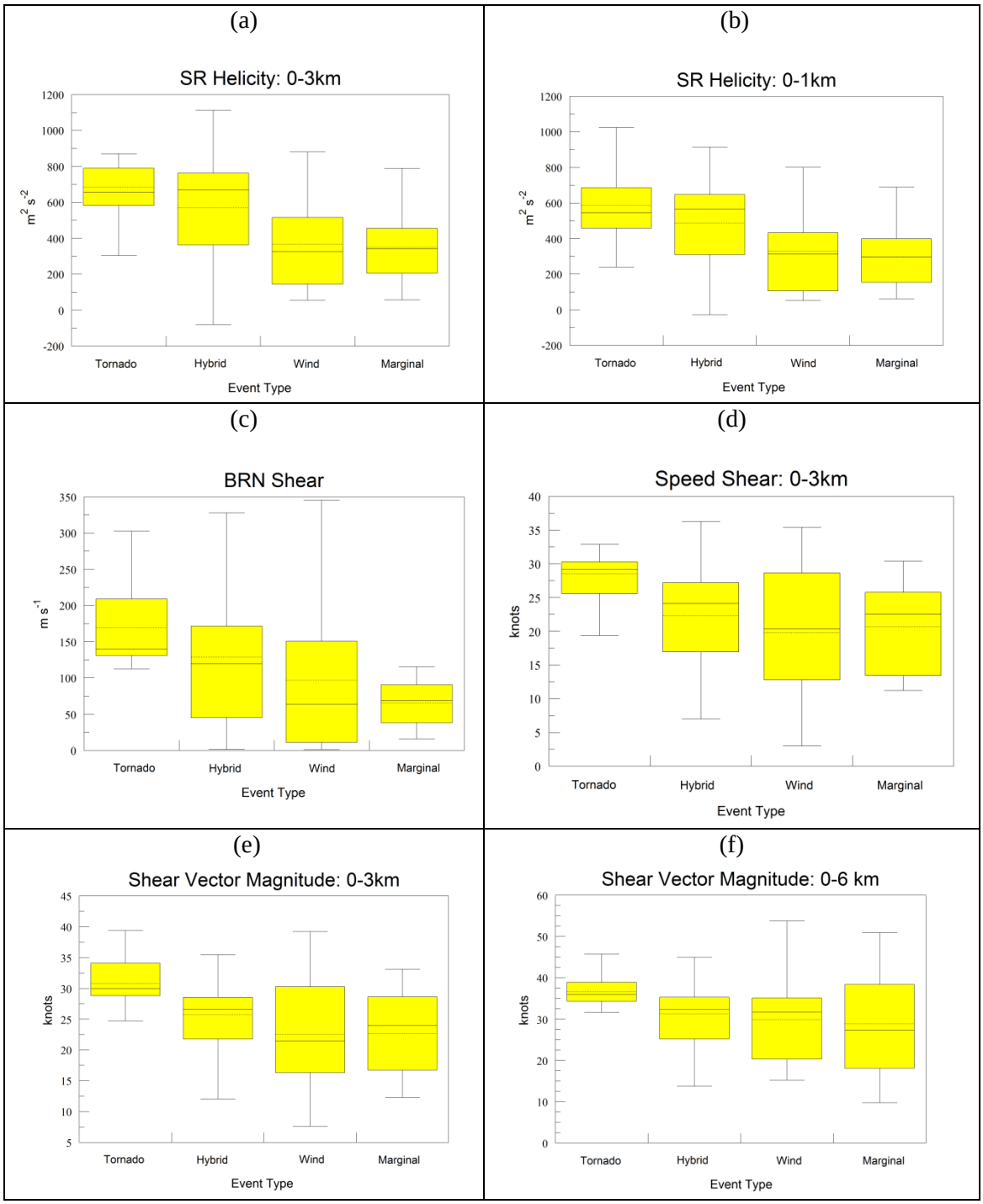

Figure 4.4 Box and whiskers plots for (a) SR Helicity: 0-3 km, (b) SR Helicity: 0-1 km, (c) BRN Shear, (d) Speed Shear: 0-3 km, (e) Shear Vector Magnitude: 0-3 km, and (f) Shear Vector Magnitude: 0-6 km for the comparison of tornado and wind events.

NSE Parameter	Z value	Confidence Test	Probability Level
SR Helicity: 0-3 km	-3.02999131	0.001222804	99.87%
SR Helicity: 0-1 km	-2.84475167	0.002222303	99.77%
BRN Shear	-2.73890044	0.003082252	99.69%
Speed Shear: 0-3 km	-2.68597483	0.003615927	99.64%
Shear Vector Magnitude: 0-3 km	-2.47427238	0.006675393	99.33%
Shear Vector Magnitude: 0-6 km	-2.34195835	0.009591428	99.04%
DCAPE: 1 km	-2.23610712	0.012672378	98.73%
Lapse Rate: 850 to 500 mb	-1.67027683	0.047432302	95.26%

Table 4-2 NSE parameters that were statistically different in comparison of tornado and wind events are shown.

probability levels for each of these six parameters lend confidence that they can each be used to distinguish between a tornadic environment and a non-tornadic, damaging wind environment. As with the first comparison between tornado and hybrid events, the results of this comparison between tornado and wind events suggest that, with all other ingredients (such as, but not limited to, CAPE and CIN) being equal, greater amounts of speed shear are conducive to tornadic events and lesser amounts of speed shear are conducive to wind events (similar to Atkins et al. 2005). Results of this comparison also suggest that environments with a greater potential for cyclonically rotating updrafts (*SR Helicity: 0-3 km and SR Helicity 0-1 km)* are more conducive to tornadic environments.

4.2.4 Instability Parameters, all Wind > Tornado

Two NSE instability parameters were found to be statistically different (i.e., had Z values less than, or equal to, -1.65) for the tornado event vs. wind event comparison; *DCAPE: 1 km*, and *Lapse Rate: 850 to 500 mb* (Table 4-2). Just as when comparing

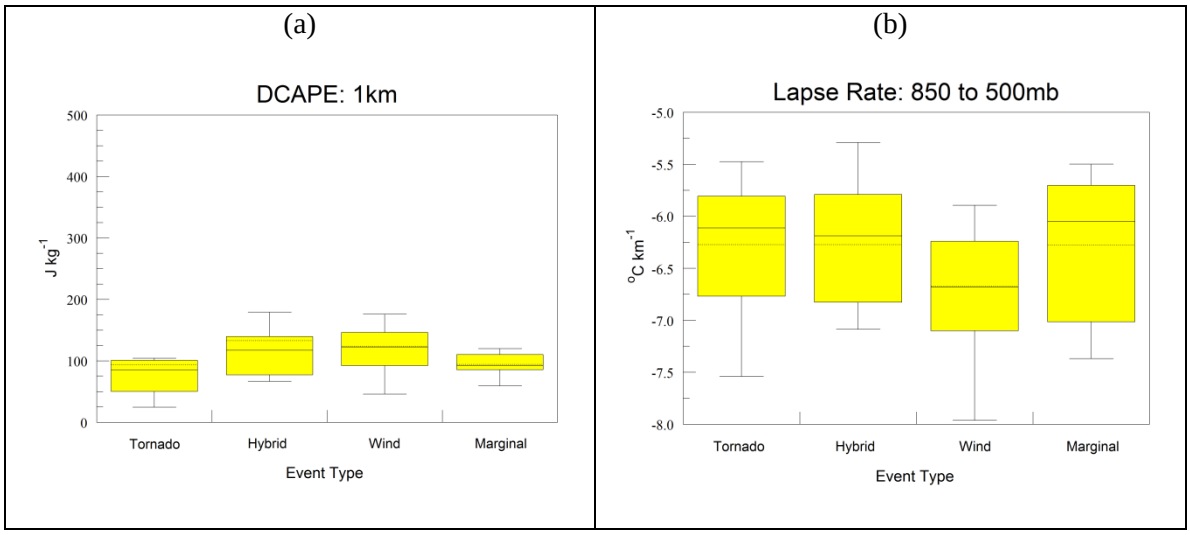

Figure 4.5 Box and whiskers plots for (a) DCAPE: 1 km and (b) Lapse Rate: 850 to 500 mb for the comparison of tornado and hybrid events.

tornado events to hybrid events, *DCAPE: 1* km appears in this comparison, as well. A different lapse rate parameter shows up as statistically different for this comparison, however; rather than the lapse rate at the most unstable LFC, this comparison finds a statistical difference in *Lapse Rate: 850 to 500 mb*. Furthermore, just as the previous comparison, the instability parameters' values are greater for wind events than for tornado events (Fig. 4.5a-b). These results are consistent with the previous results found for the comparison between tornado and hybrid events, and appear to support the conclusion that hybrid events seemingly more closely resemble wind events. As explained previously, with steeper lapse rates (this time represented by *Lapse Rate: 850 to 500 mb*) and greater values of DCAPE for wind events (represented by DCAPE: 1km), a greater potential exists for damaging winds at the surface during wind events as compared to tornado events. This is similar to findings from Cohen et al. (2007), where it was noted that mid-level environmental lapse rates were greatest for Derecho-producing

MCSs, and DCAPE increases with increasing MCS intensity (with respect to severe surface wind production).

4.2.5 Implications of Results

The results of the comparison between tornado events and wind events for the central US domain are revealing in the fact that one can draw conclusions based upon the data. The results found within this study indicate that there is a statistical difference, with high confidence, between QLCS tornadic events and QLCS wind events. This study suggests that the greater shear environments were most conducive to tornadic events, whereas the greater instability (both upward accelerations and downward) were more likely to be wind events (similar to findings from Cohen et al. 2007). The results of this comparison imply that there is a difference between QLCS tornadic environments and QLCS wind environments, and the NSE shear parameters (Fig. 4.4) will have values greater for tornadic environments than for wind environments. Furthermore, one can be confident, to a high degree, that the NSE instability parameters represented above (Fig. 4.5) will have greater values for QLCS wind events than for QLCS tornado events. These results alone can help in beginning to solve the difficult forecasting and nowcasting problem that QLCS events pose.

4.3 Hybrid vs. Wind

4.3.1 Forecast Problems to be investigated with this Comparison

Classifications for hybrid QLCS events and wind QLCS events have previously been discussed for the other event comparisons; therefore they will not be detailed within this section. The forecast problem to be addressed with the comparison of "Hybrid" events and "Wind" events is as follows: Is it possible to distinguish between a wind-only event and a hybrid event, which arguably holds more similarities to wind events than tornado events? Once again, all 30 NSE parameters were investigated and compared between event types, and the results are detailed below.

4.3.2 NSE Parameters of Use

For this comparison of hybrid vs. wind events, the Mann-Whitney Test was utilized. In doing so, it was determined that only one NSE parameter was statistically different between the two event types. Just as the other parameters listed above (Tables 4-1 and 4-2) for the other event comparisons, the parameter was not only found to be statistically different between the two event types, but it also exhibited a confidence test of less than 0.05 (95% probability level), meaning that a forecaster can be confident that the parameter value was greater for one event type than for the other event type.

NSE Parameter	Z value	Confidence Test	Probability Level
SR Helicity: 0-3 km	-1.84333069	0.032640372	96.74%

Table 4-3 NSE parameter that was statistically different in comparison of hybrid and wind events is shown.

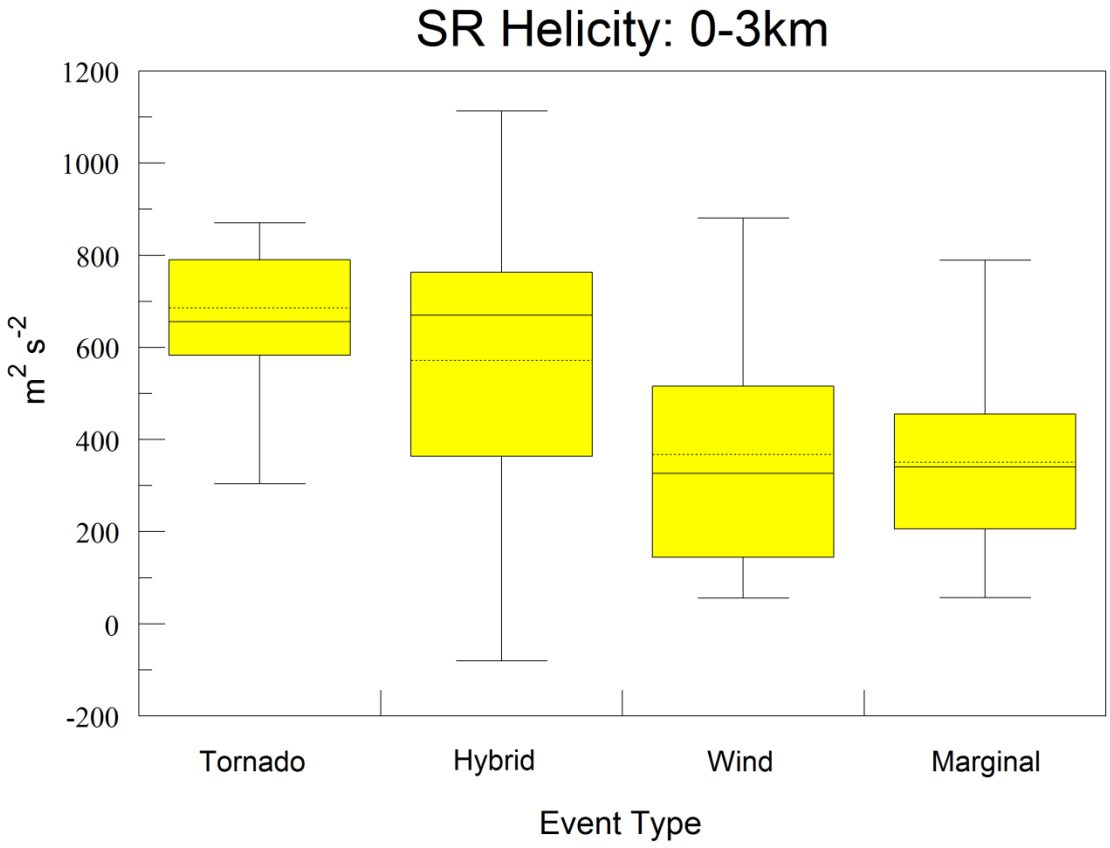

Figure 4.6 Box and whiskers plot for SR Helicity: 0-3 km for the comparison of hybrid and wind events.

4.3.3 Rotation Parameter, Hybrid > Wind

The only NSE parameter that was statistically different between these two event types is *Storm Relative (SR) Helicity: 0-3 km*. As shown in Figure 4.6, the value for *Storm Relative (SR) Helicity: 0-3 km* is greater for hybrid events than for wind events.

With the high probability level associated with this comparison, 96.74%, the forecaster can be confident that the value of this parameter will be larger for hybrid events than for wind events (Table 4-3). This result is reasonable, since the hybrid events do produce at least one tornado, they arguably would be associated with more potential for cyclonically rotating updrafts than the wind events, although not necessarily by much. The results of the comparison suggest this, as it only provided one statistically different parameter between the two event types.

4.3.4 Implications of Results

The results of the comparison between hybrid events and wind events for the central US domain are different than what has been previously shown for the other comparisons, in the fact that there were not multiple parameters (only one) shown to be statistically different (i.e., Z values less than, or equal to, -1.65). The results found within this study indicate that there may not be a reasonable way to distinguish between a hybrid event and a wind event; at least not with the 30 parameters utilized. Put another way, this amounts to not being able to distinguish between a wind event that produces a single tornado (hybrid) and an exclusively wind event. This result is discouraging, yet not disheartening. Perhaps the dataset is limiting, and there are other parameters that were not reviewed that would possibly show statistical differences between the two. For this study, however, it appears as though there may not be much of a difference, at all, between the two event types. In addition to similar NSE parameter values, the plan-view radar analysis performed (section 5.1) showed nearly identical base reflectivity structures between the representative hybrid and wind event. Both events exhibited a strong

reflectivity gradient at the leading edge, and a broad, trailing stratiform precipitation region. Altogether, this means that one may be able to, using the 30 parameters within this study, distinguish between a multiple tornado QLCS event and a singular tornado QLCS event, a multiple tornado QLCS event and an exclusively wind event, but not between a single tornado QLCS (hybrid) event and a solely wind QLCS event.

4.4 Wind vs. Marginal

4.4.1 Forecast Problems to be investigated with this Comparison

Just as in the previous three comparisons (Tornado vs. Hybrid, Tornado vs. Wind, and Hybrid vs. Wind), to fully understand why the comparison between "Wind" and "Marginal" events was performed, event classifications must be described. Since the classification of a QLCS event as a wind event has already been described (Section 3.1), the classification of a marginal QLCS event will be defined. An event was determined to be a marginal event if it produced 0 tornado reports and 6 or less wind reports per radar domain of interest. Simple enough, this maintained that the QLCS was not a significant damaging wind threat, thus a marginal event.

With this following comparison of wind vs. marginal events, the forecast problem to be investigated is this: What, if any, are the environmental differences that allow for a QLCS event to have a significant wind damage threat or, instead, be a marginal QLCS event with little-to-no damaging wind threat? Once again, all 30 NSE parameters were investigated and compared between event types, and the results for this are shown below.

4.4.2 NSE Parameters of Use

The Mann-Whitney Test was utilized, just as for the other comparisons within this study, to determine if any statistical differences exist between wind and marginal QLCS events. For this comparison, 5 NSE parameters were found to be statistically different between the event types, as well as scoring less than 0.05 for their respective confidence tests (95% probability level), so one can be confident in knowing that each parameter value was greater for one event type than for the other event type.

4.4.3 Shear/Rotation Parameters, all Wind > Marginal

The two NSE shear/rotation parameters that were found to be statistically different during this comparison were *Shear Vector Magnitude: 0-1 km*, and *ML 100 mb Avg EHI*; both of these parameters were found, statistically, to have greater values for wind events than for marginal events. The higher of the two probability levels exist for *Shear Vector Magnitude: 0-1 km*, at 96.46%, while the probability level for *ML 100 mb Avg EHI* was 95.68% (Table 4-4). Figure 4.7 shows a box and whiskers plot that displays the values for the specified parameters for each event type in the sample, and shows the difference in the values for each parameter. The results of the comparison between wind and marginal events suggest that greater shear values are important to maintain the rigorous and organized convection associated with the wind events and do not necessarily exist during marginal QLCS events. This can be supported by the fact that within stronger sheared environments, bows-shaped cells and systems are more apt to develop. These bow-shaped cells are known for producing damaging surface winds (Klimowski et al. 2000; Wheatley et al. 2006; Wakimoto et al. 2006). The results of this comparison

NSE Parameter	Z value	Confidence Test	Probability Level
DCAPE: 1 km	-2.21812767	0.013273064	98.67%
ML 100 mb Avg LFC	-2.16371594	0.015243079	98.48%
ML 100 mb Avg CIN	-2.01379187	0.022015695	97.79%
Shear Vector Magnitude: 0-1 km	-1.80618968	0.35444359	96.46%
ML 100 mb Avg EHI	-1.71421953	0.043244208	95.68%

Table 4-4 NSE parameters that were statistically different in comparison of wind and marginal events are shown.

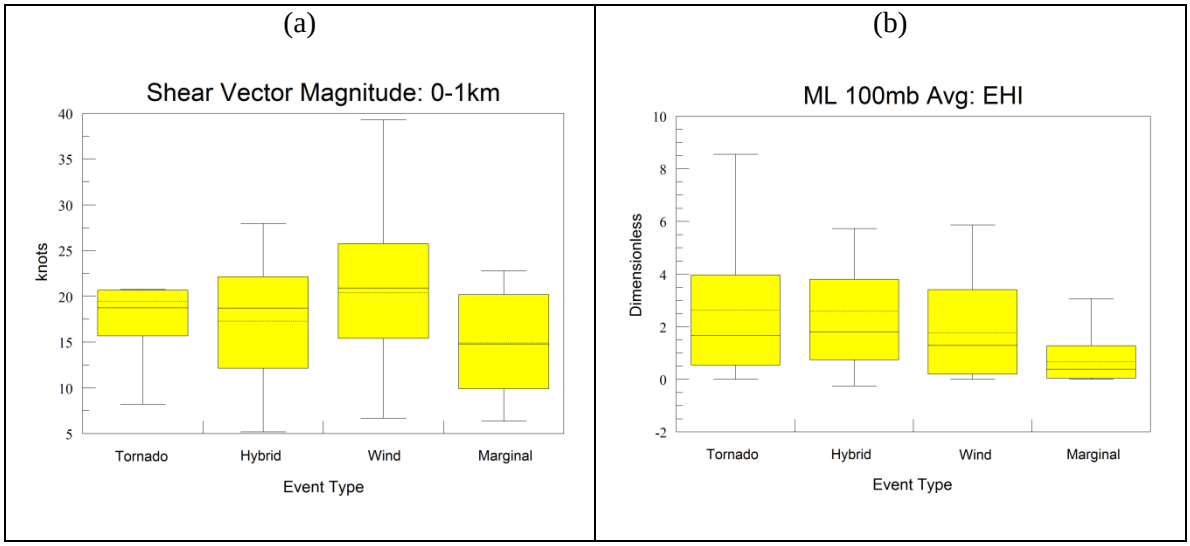

Figure 4.7 Box and whiskers plots for (a) Shear Vector Magnitude: 0-1 km and (b) ML 100 mb Avg EHI for the comparison of wind and marginal events.

also suggest that the potential for the environment to turn horizontal vorticity into vertical vorticity is greater for wind events than for marginal events. This implies a greater potential for mesovortices, of which can focus damaging wind effects. This is similar to findings from Atkins et al. (2005) and Wakimoto et al. (2006), from which it is suggested that a combination of both the RIJ and mesovortex flows may be important in creating strong local maxima in surface winds.

4.4.4 Various Parameters

There were three other NSE parameters found to be statistically different for wind events when compared to marginal events in this study. These three parameters are *DCAPE: 1 km*, *ML 100 mb Avg LFC*, and *ML 100 mb Avg CIN*. Just as all the other parameters of statistical significance in this study, the three various parameters in this comparison all exhibited confidence tests of less than 0.05 (95% probability levels), which lends high confidence that one parameter's values will be greater than the values for its counterpart of the compared event type (Table 4-4). The highest of the three probability levels exists for *DCAPE: 1 km* at 98.67%. The probability levels for the other two parameters are shown in Table 4-4.

Of these three particular parameters, *DCAPE: 1 km* is the only parameter whose value is greater for wind events than for marginal events (Fig. 4.8a). The other two parameters, *ML 100 mb Avg LFC* and *ML 100 mb Avg CIN*, both exhibit lesser values for wind events as compared to marginal events (Fig. 4.8b-c). This makes sense, as the level of free convection (LFC) should occur lower in height (above ground level) for more severe surface wind events. This would allow for, presumably, greater amounts of

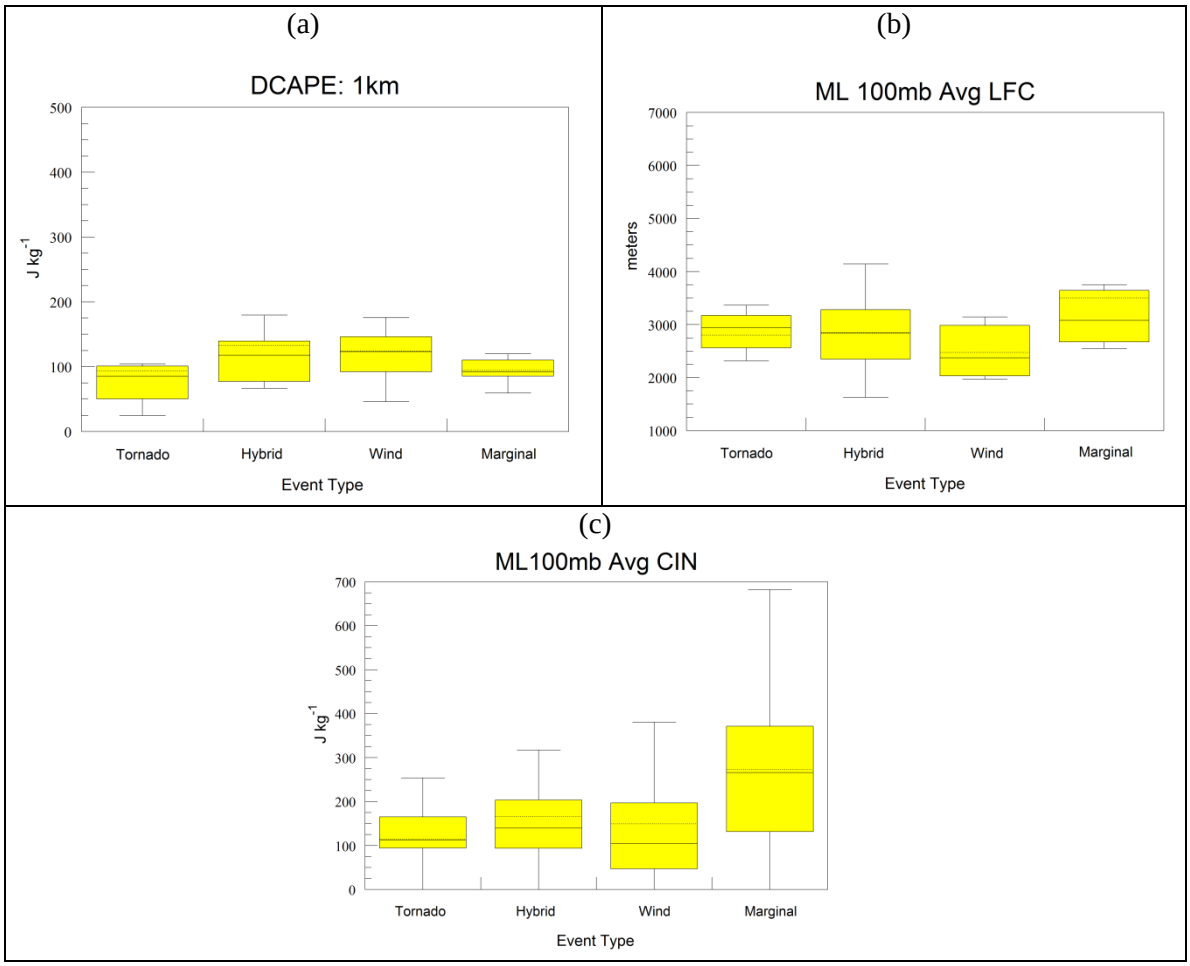

Figure 4.8 Box and whiskers plots for (a) DCAPE: 1 km, (b) ML 100 mb Avg LFC, and (c) ML 100 mb Avg CIN for the comparison of wind and marginal events.

positive area in the sounding, greater parcel accelerations and updrafts, and more intense convection than for marginal events, as well as decrease the convective inhibition that would limit convective potential. Furthermore, greater values of DCAPE in the lowest 1 km were found and should be expected for QLCS wind events (similar to findings from Cohen et al. 2007), as explained previously.

4.4.5 Implications of Results

The results of this comparison between wind events and marginal events for the central US domain have shown that 5 of the 30 parameters chosen for this study are, in fact, statistically different between the two event types. These 5 parameters (*Shear Vector Magnitude: 0-1 km*, *ML 100 mb Avg EHI*, *DCAPE: 1 km*, *ML 100 mb Avg LFC*, and *ML 100 mb Avg CIN*) have been shown, through the utilization of the Mann-Whitney Test on this sample, to be useful in determining whether an event will become a wind event or, instead, become a marginal QLCS event.

4.5 Seasonality of Events

The 31 QLCS events that fulfilled research criteria, and were used for this research, were not preferentially chosen from any season in particular, and were distributed nearly evenly across all seasons. Using the meteorological calendar, 5 QLCS events occurred in spring (March-May), 9 QLCS events during summer (June-August), 9 QLCS events during fall (September-November), and 8 during the winter season (December-February). Furthermore, if the year was split in half, with April through September constructing the warm season, and October through March constructing the cool season, the breakdown becomes nearly even; 15 events from warm season, and 16 from the cool season. The definition of warm season for this classification was expanded from Johns and Hirt (1987), who classified warm season as May-August, and was done simply to provide a breakdown of a year into two halves. The full list of events used, including dates and locations, can be found in Table 3-1.

Chapter 5 Radar Observations

A radar observational analysis was performed for this study. This radar observational study, however, was not inclusive of all 31 events within this research. Instead, a representative event was selected for each event type. In section 5.1, for each selected representative event, the radar reflectivity at lowest altitude was shown and analyzed. In section 5.2, for each selected representative event, a cross-sectional analysis of base velocity and base reflectivity was performed. An in-depth radar analysis including divergence, azimuthal shear, rotation tracks, etc. of all 31 events is beyond the scope of this research and, instead, could be performed at a later date.

5.1 Radar Reflectivity at Lowest Altitude Analysis

5.1.1 Tornado Event – 15 November 2005, PAH

The representative event selected for the tornado QLCS event type is 15 November 2005 from the radar site PAH (Paducah, KY). The methodology of representative event selection for the radar analysis is detailed in section 3.5. For this QLCS event, there were 14 tornado reports – well above the threshold for a tornado event set forth by this study. The most representative time step chosen from this event for this study is ~2100 UTC (Fig. 5.1), and therefore that will be the time step shown. The time steps of ~2130 UTC (Fig. 5.2) and ~2200 UTC (Fig. 5.3) are included for reference as to

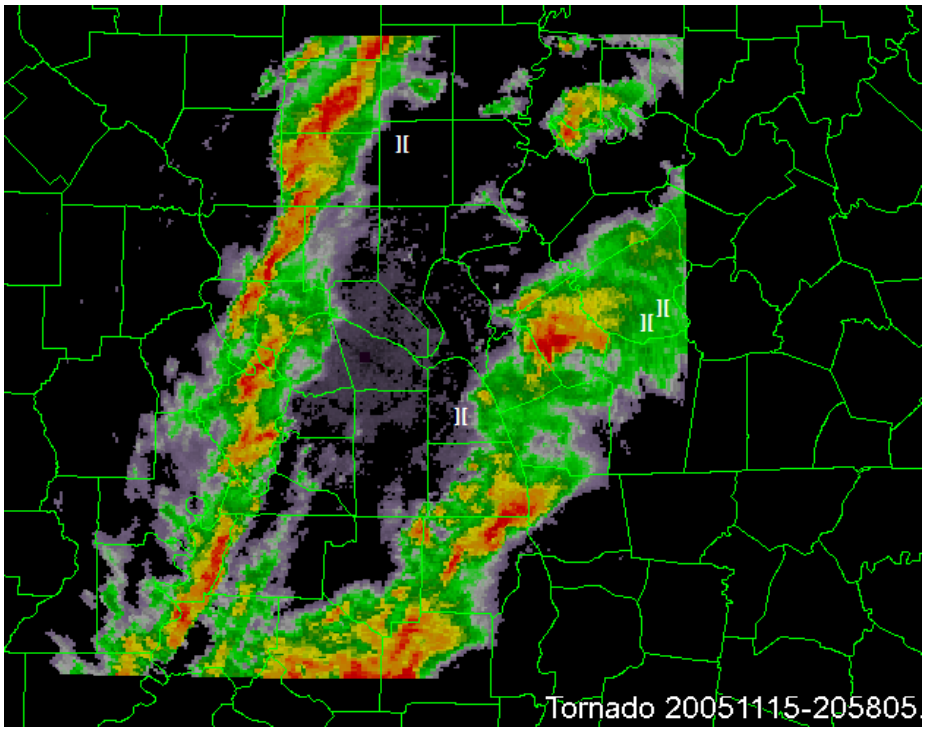

Figure 5.1 Merged Radar Reflectivity at Lowest Altitude for 15 November 2005 at 2058 UTC at PAH. Approximate location of tornado reports valid for 2100 UTC environment are marked with a white '|' symbol.

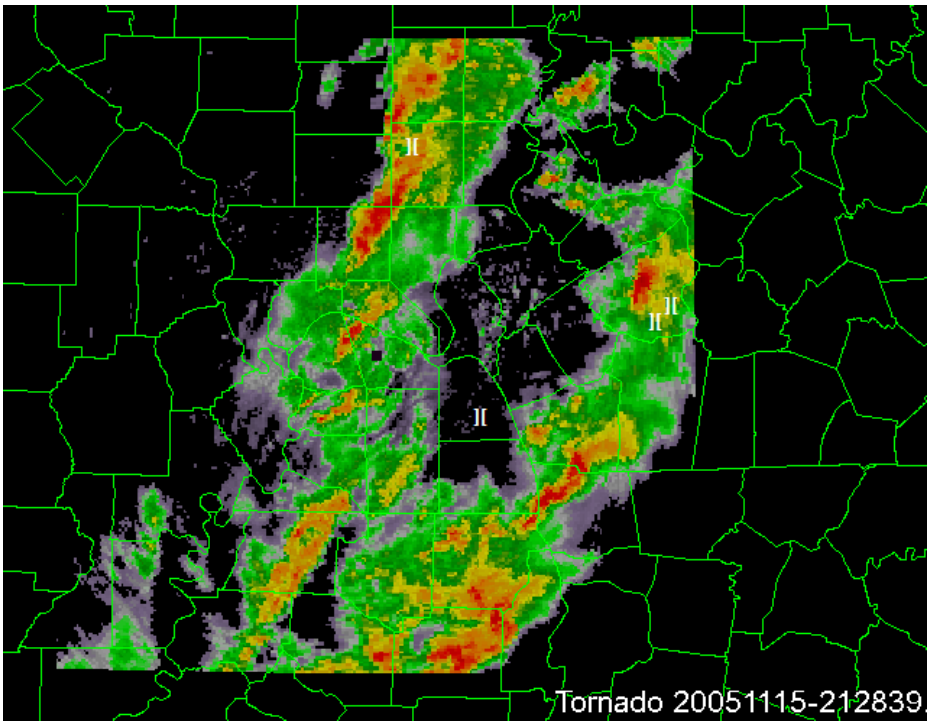

Figure 5.2 Merged Radar Reflectivity at Lowest Altitude for 15 November 2005 at 2128 UTC at PAH. Approximate location of tornado reports valid for 2100 UTC environment are marked with a white '|' symbol.

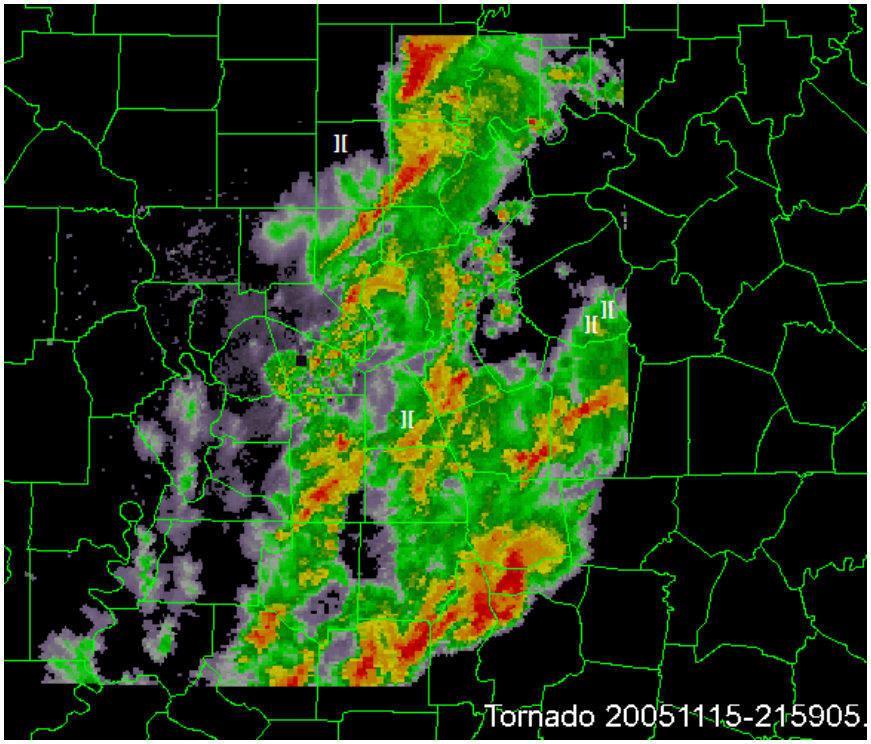

Figure 5.3 Merged Radar Reflectivity at Lowest Altitude for 15 November 2005 at 2159 UTC at PAH. Approximate location of tornado reports valid for 2100 UTC environment are marked with a white '|' symbol.

how the system propagated and evolved over the next hour. Initially, the QLCS appeared to be two separate and distinct lines, with the leading convective line exhibiting the characteristics of a supercell line, and the trailing convective line exhibiting leading stratiform (LS) QLCS characteristics (Parker and Johnson 2000).

Overall, tornado QLCS events were associated with more intense, discrete cells of convection embedded within the overall QLCS. This is not surprising, as the tornado events were associated with, statistically, greater amounts of shear; for example, *Shear Vector Magnitude: 0-3 km*, *Speed Shear: 0-3 km*, *Shear Vector Magnitude: 0-6 km*, and *Bulk Richardson Number (BRN) Shear* were found to have greater values for tornado events than for hybrid events.

5.1.2 Hybrid Event – 26 May 2011, IND

For the hybrid QLCS event type, the representative event selected is 26 May 2011 from IND (Indianapolis, IN). For this particular QLCS event, there was 1 tornado report and 25 wind reports – meeting the thresholds set forth by this study to be classified as such. Just as before, the most representative time step chosen for this event will be used; this time step is ~0300 UTC (Fig. 5.4). Once again, the time steps of ~0330 UTC (Fig. 5.5) and ~0400 UTC (Fig. 5.6) are included for reference as to how the system propagated and evolved over the next hour. The representative hybrid event shown exhibits a classic trailing stratiform (TS) precipitation structure (Parker and Johnson 2000), and notably, is very north-south oriented.

Overall, hybrid QLCS events were associated with strong, leading edge convection, typically followed by a broad region of stratiform precipitation (relative to tornado events). The strong, leading edge convection is often due to the lift created by the QLCS's cold pool. In Figures 5.4 through 5.6, one can see that the representative event chosen does exhibit this behavior. In fact, the gust front is visible in the radar imagery along the leading edge, nearest the strongest convection, in Figure 5.4 – usually a good indication of strong winds at the surface. Furthermore, the tornadic event was associated with more embedded discrete convection, and the hybrid event type was marked by a continuous band of convection along the leading edge, followed by a large stratiform region. Lesser amounts of shear available to the system appear to be responsible for this general lack of embedded discrete organization.

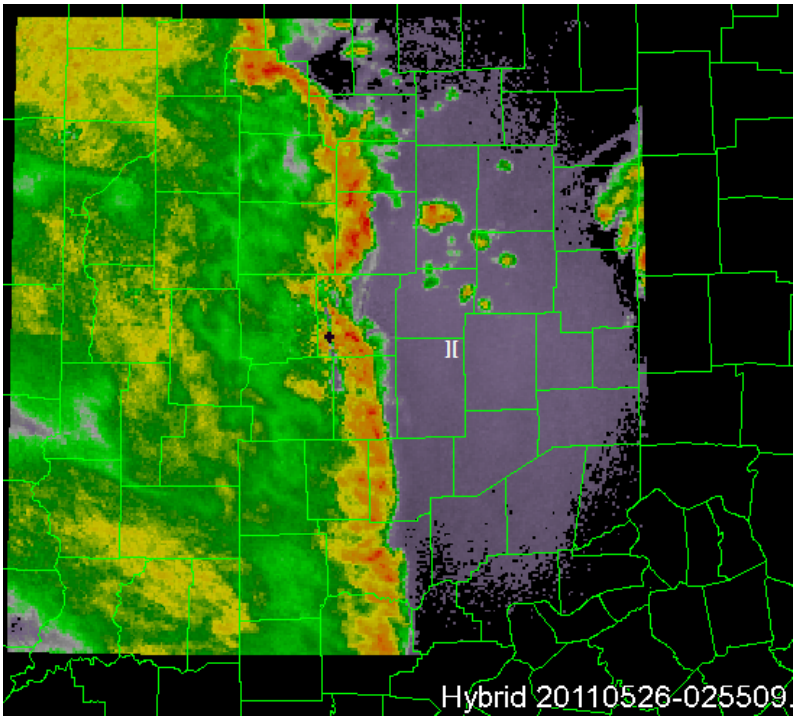

Figure 5.4 Merged Radar Reflectivity at Lowest Altitude for 26 May 2011 at 0255 UTC at IND. Approximate location of tornado report valid for 0300 UTC environment is marked with a white '||'.

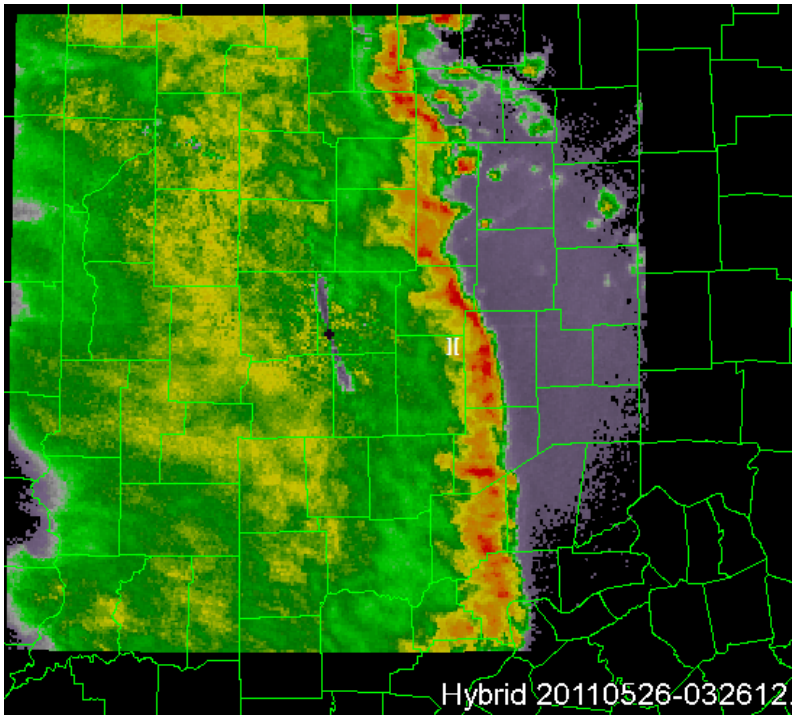

Figure 5.5 Merged Radar Reflectivity at Lowest Altitude for 26 May 2011 at 0326 UTC at IND. Approximate location of tornado report valid for 0300 UTC environment is marked with a white '||'.

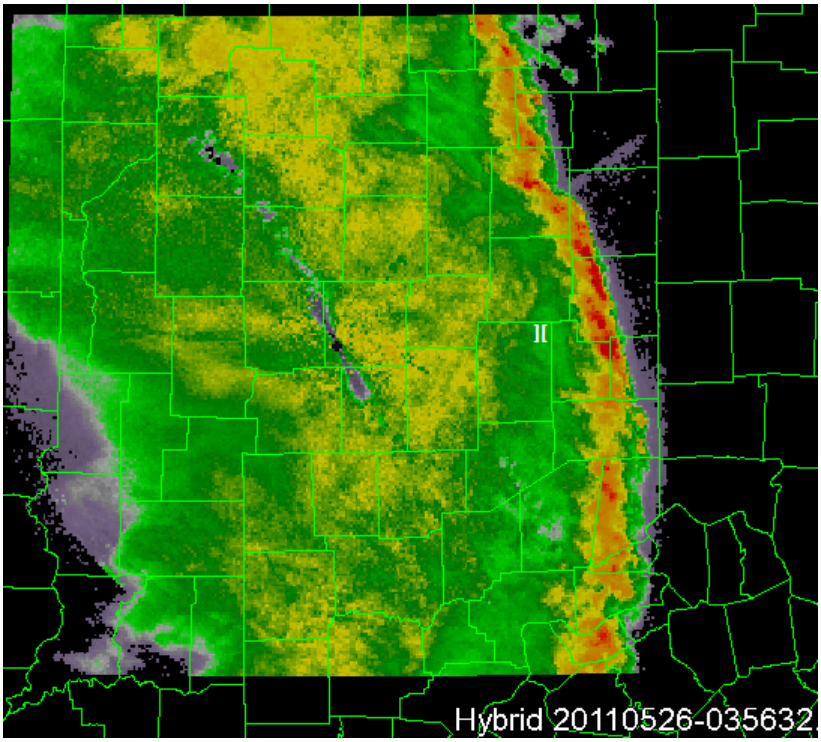

Figure 5.6 Merged Radar Reflectivity at Lowest Altitude for 26 May 2011 at 0356 UTC at IND. Approximate location of tornado report valid for 0300 UTC environment is marked with a white '||'.

5.1.3 Wind Event – 03 October 2006, LOT

The representative event selected for the wind event type was 03 October 2006 from LOT (Chicago, IL). For this QLCS event, there were 0 tornado reports and 39 wind reports – once again, meeting the thresholds set forth by this study. The most representative time step selected for this particular event is ~0400 UTC (Fig. 5.7). Just as before, the time steps of ~0430 UTC (Fig. 5.8) and ~0500 UTC (Fig. 5.9) are included for reference as to how the system propagated and evolved over the next hour. The wind event shown exhibits a trailing stratiform (TS) precipitation structure (Parker and Johnson 2000), but unlike the hybrid event, is oriented in an east-west fashion.

Overall, wind events and hybrid events are not too markedly different as far as

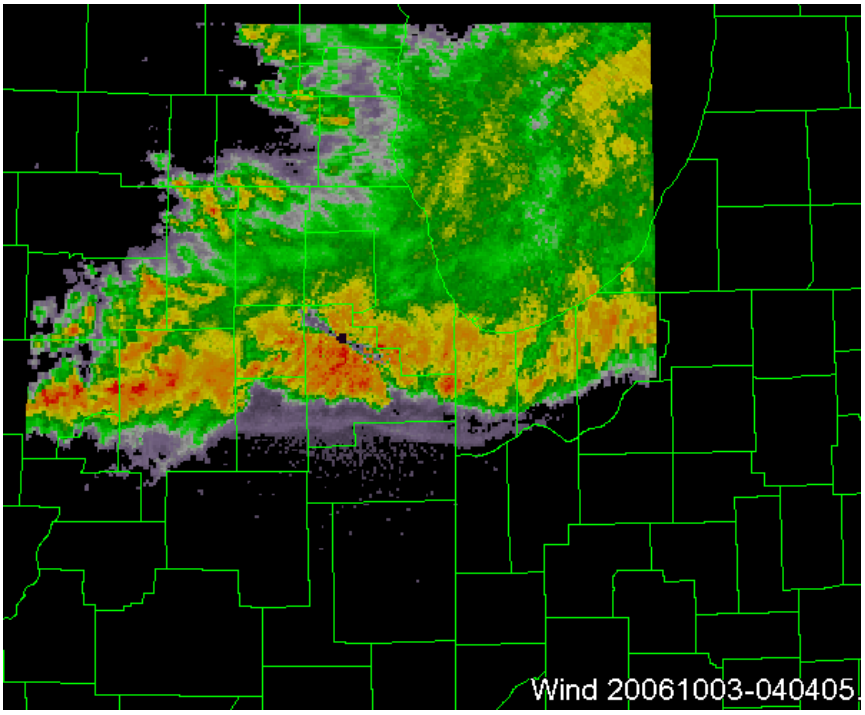

Figure 5.7 Merged Radar Reflectivity at Lowest Altitude for 03 October 2006 at 0404 UTC at LOT.

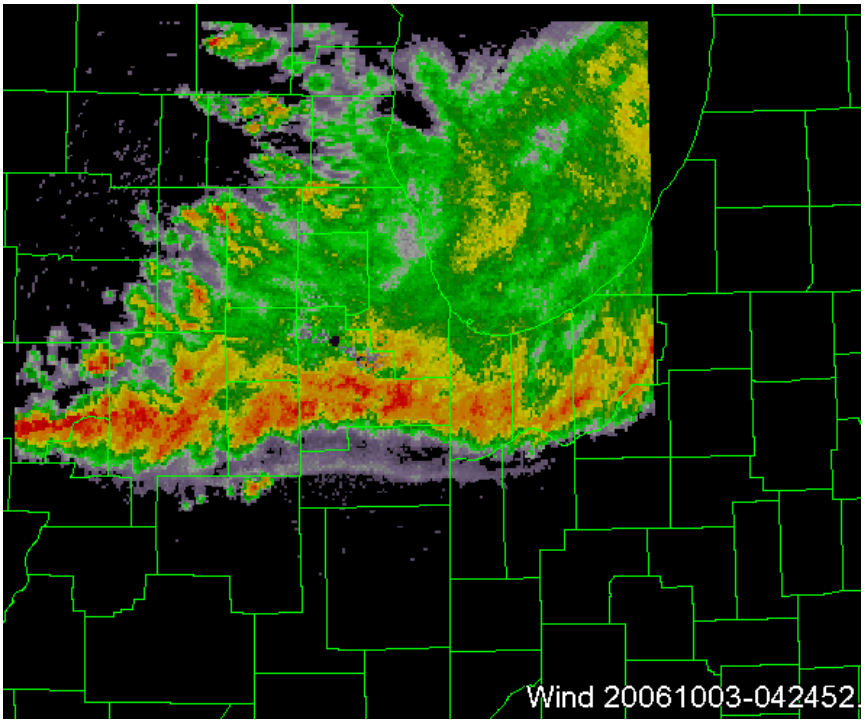

Figure 5.8 Merged Radar Reflectivity at Lowest Altitude for 03 October 2006 at 0424 UTC at LOT.

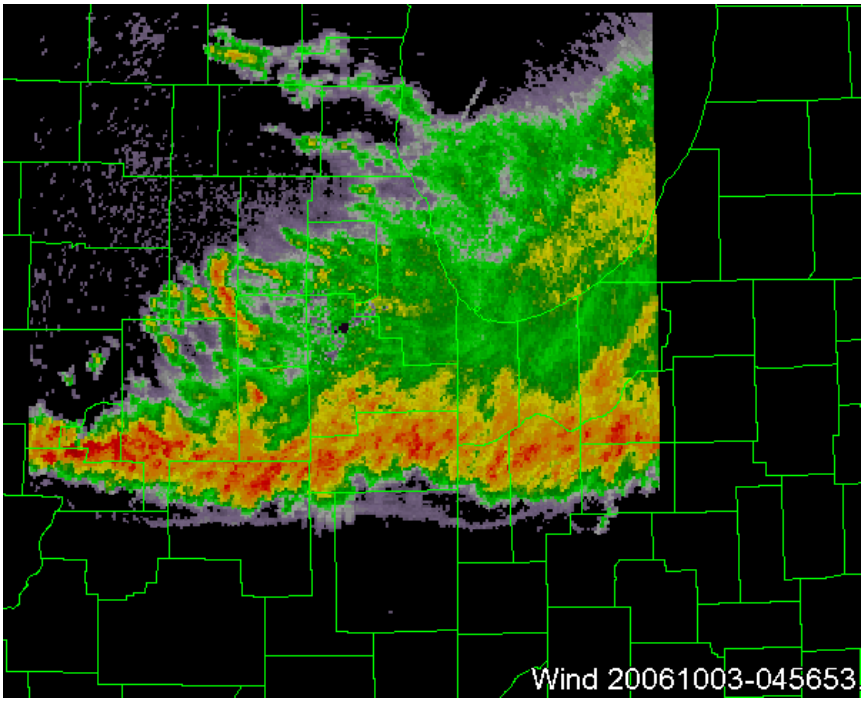

Figure 5.9 Merged Radar Reflectivity at Lowest Altitude for 03 October 2006 at 0456 UTC at LOT.

radar observations (Reflectivity at Lowest Altitude) are concerned. Just as with the representative hybrid event, the wind event exhibited strong, leading edge convection, with a relatively large stratiform precipitation region. What is more apparent, however, in the radar imagery is the appearance of the gust front. As one can see in the radar imagery shown (Fig. 5.7), the gust front is very apparent, especially as the time moves forward. In fact, by the final time step shown (Fig. 5.9), the gust front appears to be separated from the QLCS as it races ahead, out in front of the convection. This is evidence of a very strong cold pool; strong cold pools often exhibit propagation speeds that are much faster than the nearby QLCS. As a result of the strong cold pool and other processes outlined earlier, such as latent heat release, rear inflow jets (RIJ) are created. The RIJs increase the potential for damaging surface winds, and are often shown in radar imagery by a signature known as the rear-inflow notch (Przybylinski and Decaire 1985). Rear-inflow

notches, in the radar imagery shown above, can be seen in correlation with the gust front accelerations.

5.1.4 Marginal Event – 08 June 2010, LSX

For the final radar observational analysis, this time considering marginal events, the representative event selected is 08 June 2010 from LSX (St. Louis, MO). This marginal QLCS event produced 0 tornado reports and just 3 wind reports, which is well within the confines of the marginal event classification set forth by this study. Just as the rest of the radar observational analysis performed the most representative time step is used; which in this case is ~1600 UTC (Fig. 5.10). Following the procedure of the other three radar observations, the time steps of ~1630 UTC (Fig. 5.11) and ~1700 UTC (Fig. 5.12) are included for reference as to how the system propagated and evolved over the next hour.

Overall, marginal events were typically associated with less intense regions of convection and large stratiform regions. The event chosen represents what was typically seen from the marginal events in this study sample. Initially (~1600 UTC), the marginal event exhibits relatively deep convection in the reflectivity field along the leading edge of the QLCS. However, one will notice as time increases, the convective region weakens, and stratiform rain dominates. The persistent nature of the previous event types is not evident within this marginal event. Instead, the regions of greatest reflectivity diminish and give way to a more prevalent stratiform rain. Also, the marginal event doesn't exhibit the gust front feature on radar, at least not to the extent that hybrid and wind events do. In the first time step, ~1600 UTC, a gust front is detected on the radar as a result of, and

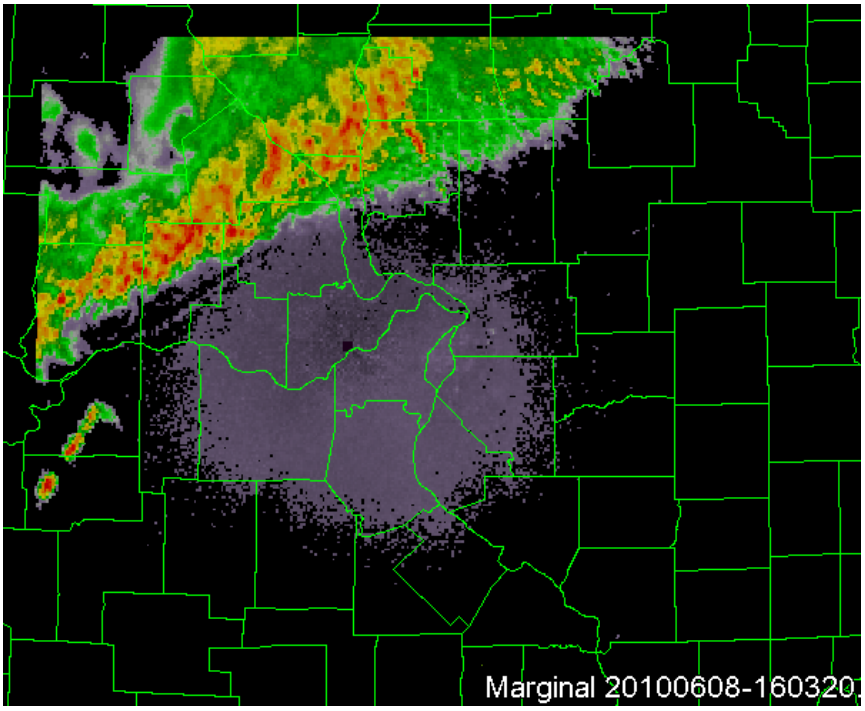

Figure 5.10 Merged Radar Reflectivity at Lowest Altitude for 08 June 2010 at 1603 UTC at LSX.

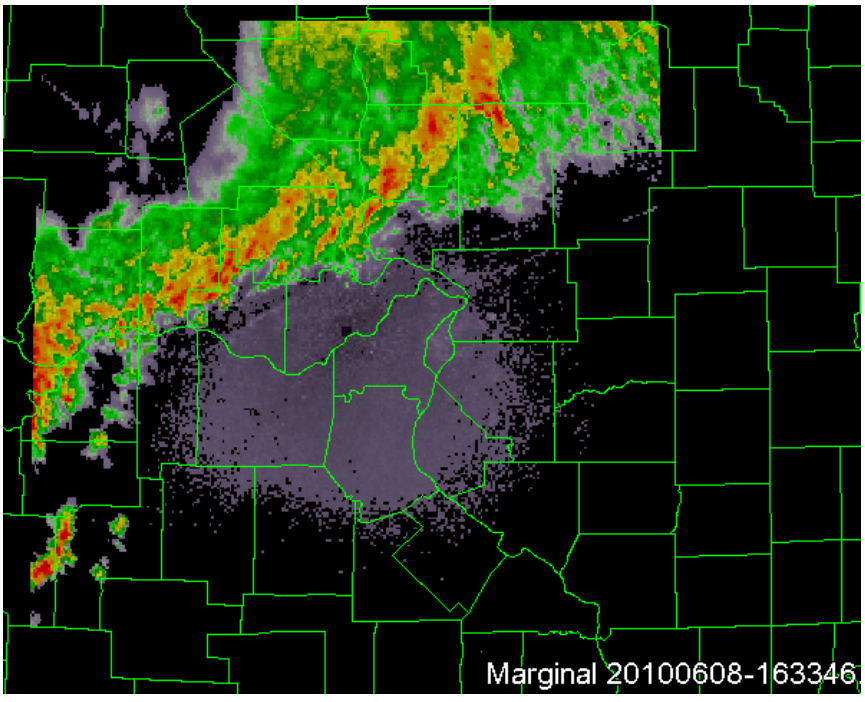

Figure 5.11 Merged Radar Reflectivity at Lowest Altitude for 08 June 2010 at 1633 UTC at LSX.

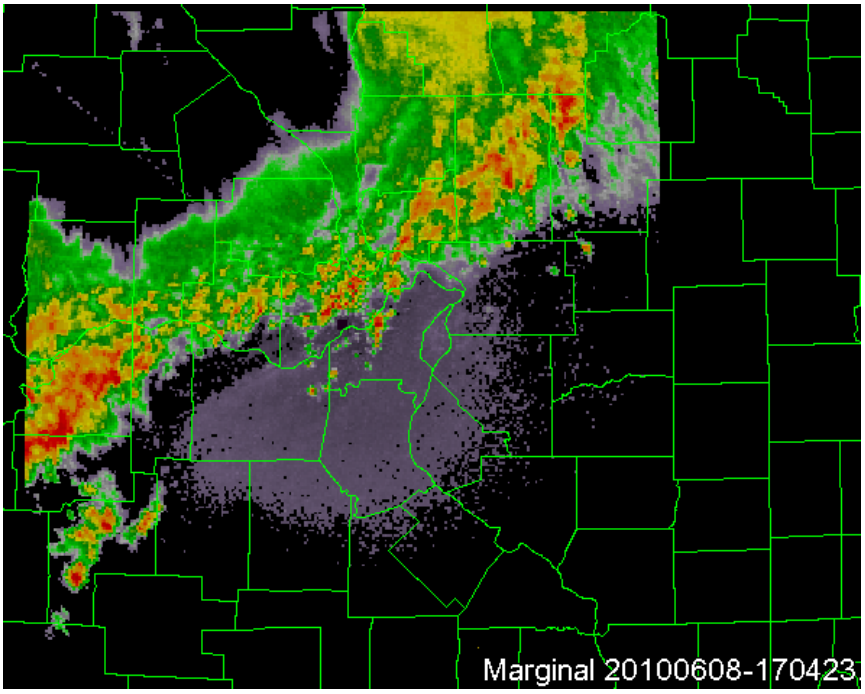

Figure 5.12 Merged Radar Reflectivity at Lowest Altitude for 08 June 2010 at 1704 UTC at LSX.

nearest, the most intense convection for the system. This feature does not appear for later time steps (~1630 UTC, ~1700 UTC) as the intense convection had been diminished, presumably marking the end of healthy convection within the QLCS, thus further diminishing the potential for damaging surface winds. Line orientation for this marginal event, much like the wind event, is oriented more east-west than the tornadic QLCS representative events (tornado and hybrid), which were oriented more north-south. A full radar analysis of all 31 events that also included a line orientation comparison could prove to be beneficial in determining if a correlation exists between line orientation and tornadic vs. non-tornadic QLCSs.

5.2 Cross-Sectional Radar Analysis

5.2.1 Tornado Event – 15 November 2005, PAH

The first set of cross-sections was for the tornado event from 15 November 2005 PAH at 2102 UTC. For this event, 3 different cross-sectional analyses were performed. The purpose of the cross-sectional radar analysis was to determine the flow and structure within the QLCS, especially as it pertained to the classifications set forth by Parker and Johnson (2000) and Parker and Johnson (2004). Cross-sections were performed through a region that included >35 dBZ reflectivity values, on a radial from the radar site, as close to perpendicular to the line of convection as possible, in order to determine flow through the system using base velocity.

In the first case, the cross-section shown (Fig. 5.13a) displayed outbound velocities in the lowest levels (< 5000 feet), and the outbound air flow ascended as it neared the trailing edge of the system to roughly 30,000 ft. In the same instance, inbound velocities were shown at the trailing edge of the system from 30,000 feet to the lowest height of the radar. It was within the convergence zone of the two air streams that the most intense convection occurred (Fig. 5.13b). Notably, within this cross-section, the overturning updraft shown in a theoretical model from Parker and Johnson (2000) could be deciphered (Fig. 2.1). As the outbound velocities ascended through the rear of the storm, inbound velocities existed towards the leading edge, which indicated a possible overturning updraft within this storm cell. The suggestion of an overturning updraft seemed to be the reason for the leading stratiform precipitation region, in this instance.

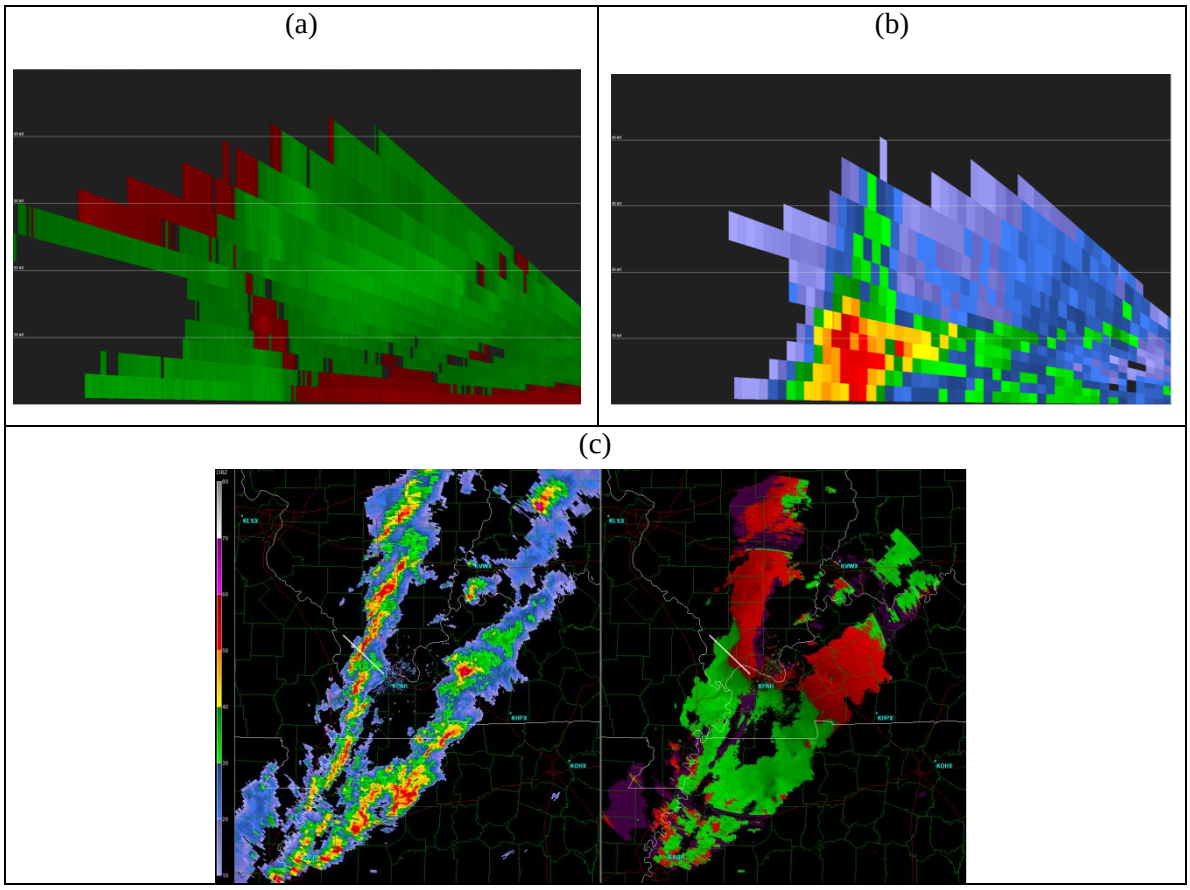

Figure 5.13 Radar imagery of (a) base velocity cross-section, and (b) base reflectivity cross-section, and (c) plan-view of both base reflectivity and base velocity is shown. The white line shown in image (c) is the location of the cross-section.

In the second cross-section, the cross-section (Fig. 5.14a) showed outbound velocities in the lowest levels from the edge nearest the radar to the edge furthest from the radar. This storm cell, in particular, was a storm cell that included significant rotation, most likely resulting in tornado production. The rotation was shown in Figure 5.14c by the couplet in which this particular cross-section dissected. The mix of inbound and outbound velocities that coincided with the intense convection (Fig. 5.14b) suggested a rotating updraft. The supercellular characteristics of this storm cell also appeared in both the base velocity and base reflectivity (Fig. 5.14c).

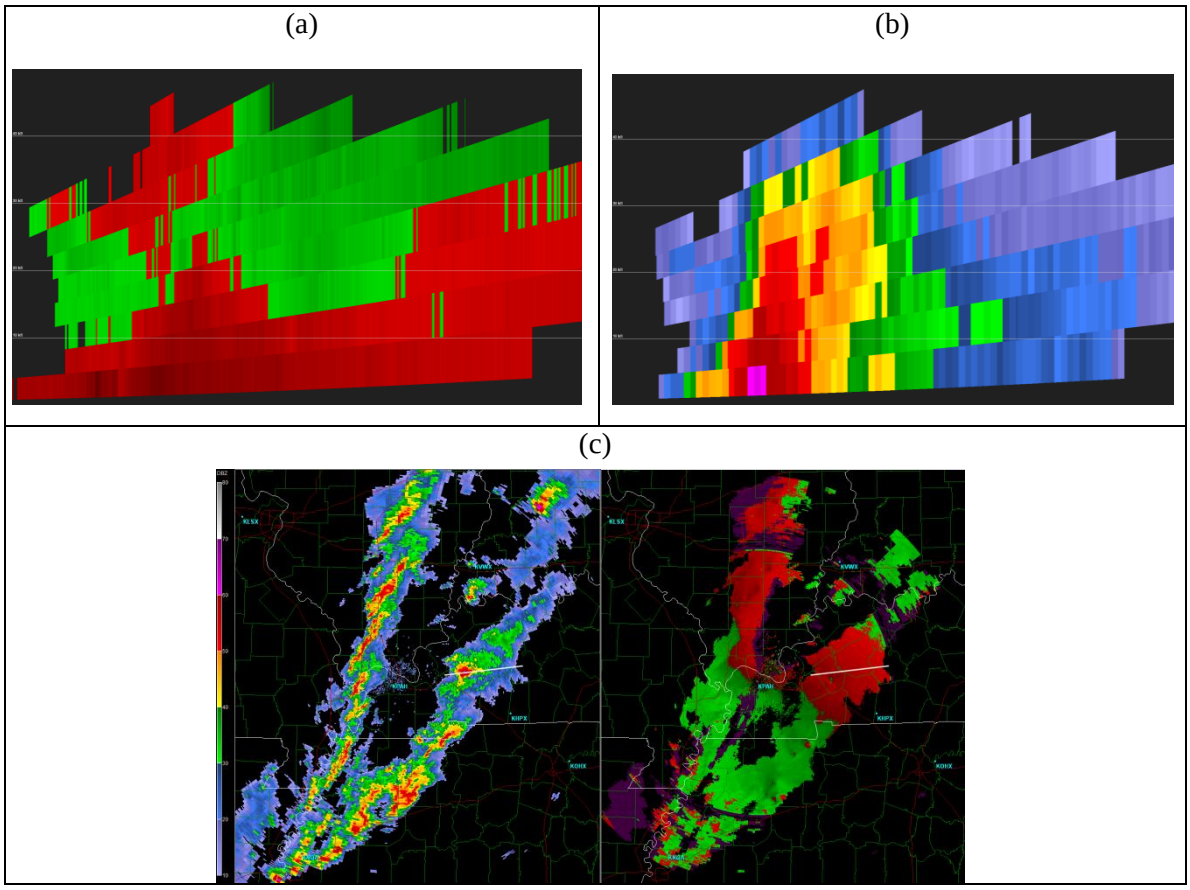

Figure 5.14 Radar imagery of (a) base velocity cross-section, and (b) base reflectivity cross-section, and (c) plan-view of both base reflectivity and base velocity is shown. The white line shown in image (c) is the location of the cross-section.

The third cross-section performed from the tornado event is shown in Figure 5.15. In this cross-section, inbound velocities were shown in the lowest levels, near the trailing edge of the system (Fig. 5.15a). Towards the leading edge of the system, however, rotation appeared once again, highlighted by the couplets shown in the cross-section (Fig. 5.15a) and the plan view base velocity (Fig. 5.15c). In the cross section, the rotation exhibited a vertical structure, which indicated a rotating updraft, much like the previous cross-section. However, in this instance, the rotating updraft was much shallower, shown especially well in the cross-section of base reflectivity (Fig. 5.15b). The velocities in the

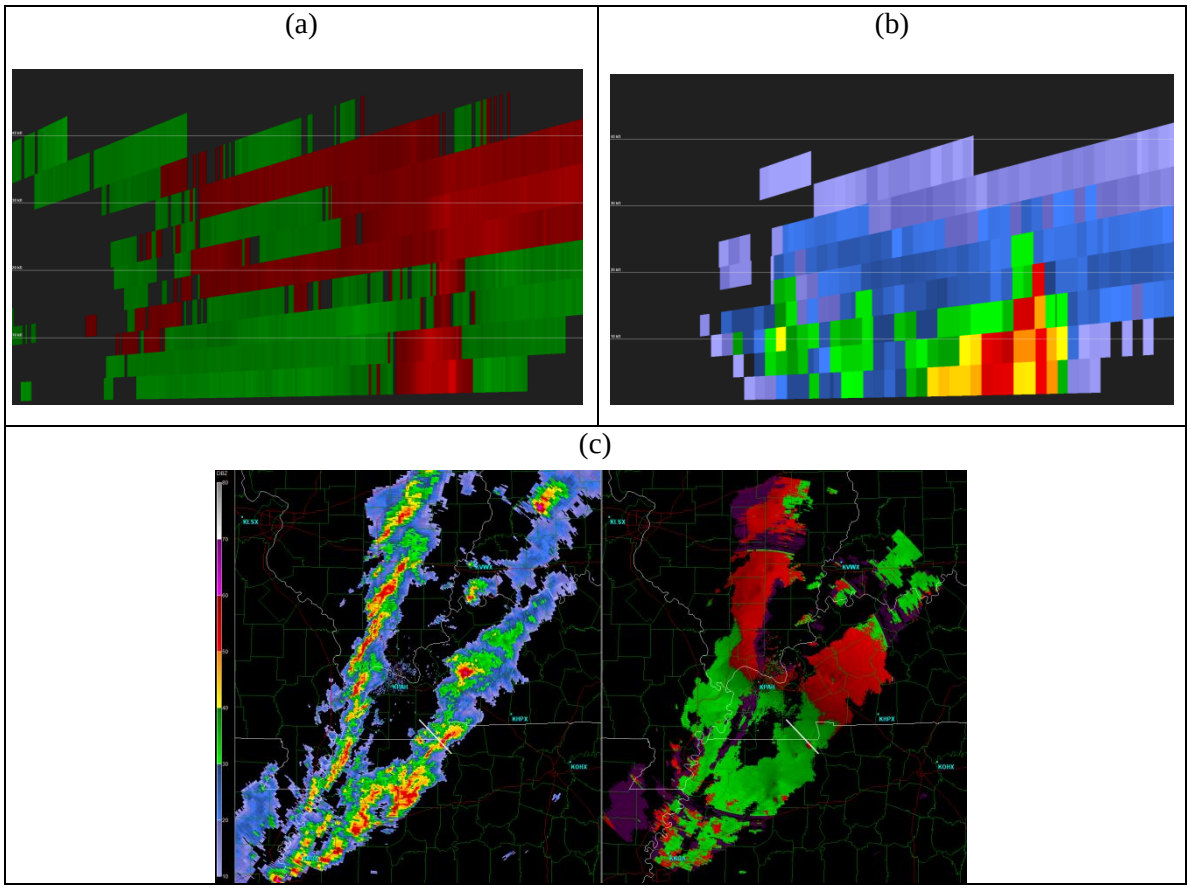

Figure 5.15 Radar imagery of (a) base velocity cross-section, and (b) base reflectivity cross-section, and (c) plan-view of both base reflectivity and base velocity is shown. The white line shown in image (c) is the location of the cross-section.

upper levels, nearest the edge closest to the radar site, showed numerous regions of inbound and outbound velocities. This was most likely slight changes in wind speed and direction manifesting itself as inbound and outbound, indicated by the low velocities for each.

5.2.2 Hybrid Event – 26 May 2011, IND

The second set of cross-sections was for the hybrid event from 26 May 2011 IND at 0356 UTC. The representative time step for this event was 0300 UTC, but at that time the QLCS was directly above the radar, not allowing for a useful cross-section of base velocities. Therefore, the radar scan from 0356 UTC was utilized, as this allowed the QLCS to travel away from the radar site but still remain within the time constraints of the valid representative environment (0300 UTC).

For this event, 2 different cross-sectional analyses were performed. The purpose of the cross-sectional radar analysis was to determine the flow and structure within the QLCS, especially as it pertained to the classifications set forth by Parker and Johnson (2000) and Parker and Johnson (2004). Once again, cross-sections were performed through a region that included >35 dBZ reflectivity values, on a radial from the radar site, as close to perpendicular to the line of convection as possible, in order to determine flow through the system using base velocity.

The first cross-section is shown in Figure 5.16. In this cross-section, outbound velocities were shown throughout the region except for a horizontal region of inbound velocities just under 10,000 feet above ground-level (AGL). This region of horizontal inbound velocities was most likely the result of velocity folding within the radar. Velocity folding occurs when a particle's radial velocity is outside the range of the Nyquist interval, resulting in the radial velocity being folded. In this case, the Nyquist velocity was 70 knots, and the outbound velocities were roughly 90 knots, resulting in the radar depicting inbound velocities at roughly 50 knots. In the region where the maximum outbound velocities met with a region of slower outbound velocities (near the QLCS's

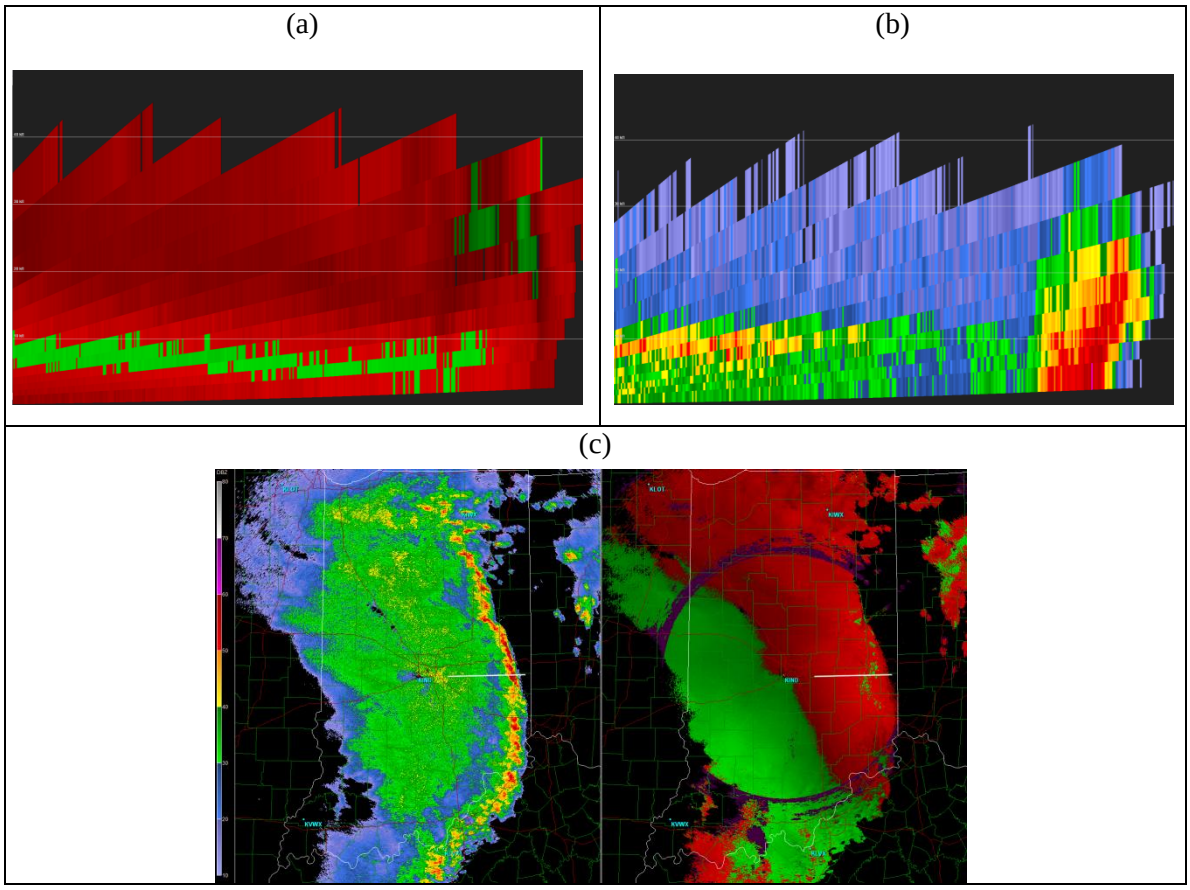

Figure 5.16 Radar imagery of (a) base velocity cross-section, and (b) base reflectivity cross-section, and (c) plan-view of both base reflectivity and base velocity is shown. The white line shown in image (c) is the location of the cross-section.

leading edge) there is convergence (Fig. 5.16a). The convergence zone coincided with the region of convection at the leading edge of the QLCS, and is shown in Figure 5.16b. From the plan-view of the radar reflectivity field, the QLCS appeared to be a trailing stratiform QLCS (Fig. 2.4a), as presented by Parker and Johnson (2000). However, the cross-section did not depict flow in the base velocities that would result in a trailing stratiform region (Fig. 5.16a). Inbound velocities were shown at the leading edge, near the top of the QLCS, which suggests that the radar beam may have been too low to analyze the air flow that created the trailing stratiform region, in this instance. However,

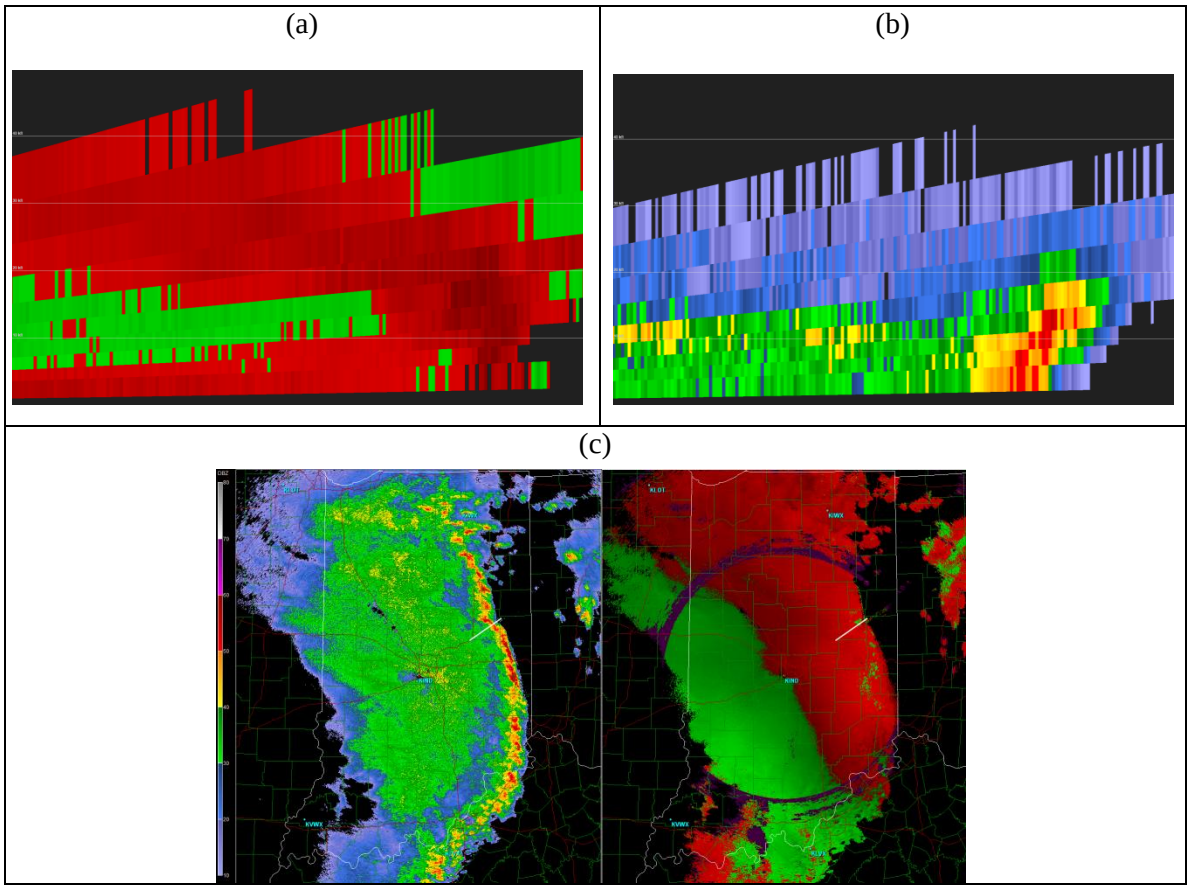

Figure 5.17 Radar imagery of (a) base velocity cross-section, and (b) base reflectivity cross-section, and (c) plan-view of both base reflectivity and base velocity is shown. The white line shown in image (c) is the location of the cross-section.

by using storm-relative velocity instead, the flow that led to the trailing stratiform region was apparent. The issue with base velocities, specifically for the hybrid event, is that the outbound velocities generated by the QLCS's overall motion generally masked the internal flow patterns. The hybrid QLCS moved across nearly half the width of Indiana in about an hour.

The second cross-section is shown in Figure 5.17. In this cross-section, outbound velocities were shown nearly throughout the region, except for a horizontal region of inbound velocities between about 6,000 feet and 19,000 feet AGL, and another region at

the leading edge of the QLCS, in the upper-levels of the system (Fig. 5.17a). The horizontal region of inbound velocities was most likely the result of velocity folding within the radar. The velocity folding in this region was very similar to the velocity folding in the region of the first cross-section. Just as in the other cross-section for this event (Fig. 5.16), convergence existed in the region where the maximum outbound velocities (shown as inbound velocities due to velocity folding) met with a region of slower outbound velocities (Fig. 5.17a). Coinciding with the convergence zone was the region of convection at the leading edge of the QLCS, as shown in Figure 5.17b. The plan-view of the radar reflectivity field (Fig. 5.17c) depicted a trailing stratiform QLCS, much like what is presented in Figure 2.4 by Parker and Johnson (2000).

Moreover, the plan-view of base reflectivity (Fig. 5.17c) nearly duplicated the definition of a trailing stratiform MCS from Parker and Johnson (2000): the hybrid event was “convex toward the leading edge”, had a “series of intense reflectivity cells solidly connected by echo of more moderate intensity”, a strong reflectivity gradient at the leading edge, and exhibited a secondary reflectivity maximum that was separated from the convective line by a narrow corridor of reflectivity (Fig. 5.17c).

The cross-section, in this instance, depicted front-to-rear flow in the base velocities at the leading edge of the QLCS. The inbound velocities in this region were important in the creation of the trailing stratiform region. Where the first cross-section did not depict the front-to-rear flow, the second cross-section did (Fig. 5.17a).

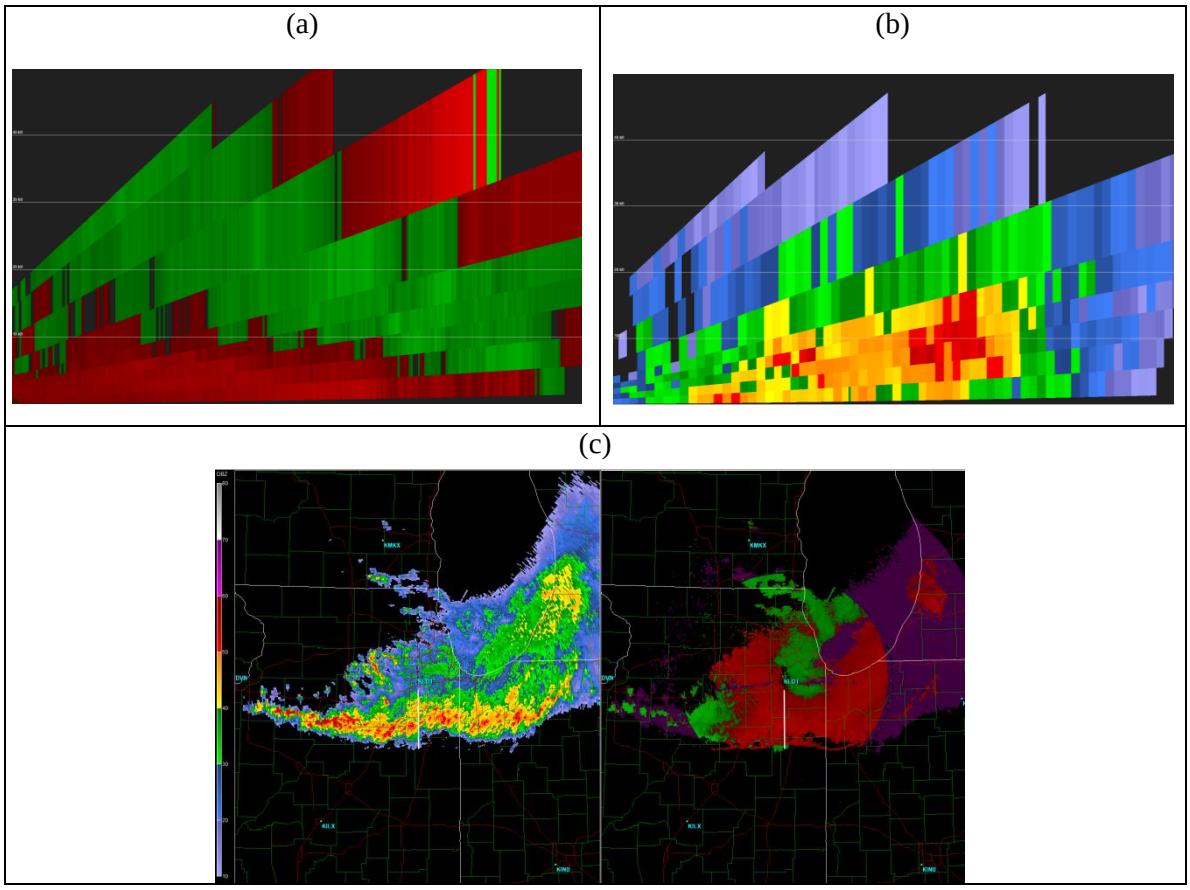

Figure 5.18 Radar imagery of (a) base velocity cross-section, and (b) base reflectivity cross-section, and (c) plan-view of both base reflectivity and base velocity is shown. The white line shown in image (c) is the location of the cross-section.

5.2.3 Wind Event – 03 October 2006, LOT

The third cross-section analysis was for the wind event from 3 Oct 2006 LOT at 0455 UTC. The representative time step for this event was 0400 UTC, but at that time the QLCS was directly above the radar, not allowing for a useful cross-section of base velocities. Therefore, the radar scan from 0455 UTC was utilized, as it allowed the QLCS to travel away from the radar site but still remain within the time constraints of the valid representative environment (0400 UTC).

For this event, one cross-section analysis was performed, and the purpose of the cross-sectional radar analysis was to determine the flow and structure within the QLCS, especially as it pertained to the classifications set forth by Parker and Johnson (2000) and Parker and Johnson (2004). Once again, cross-sections were performed through a region that included >35 dBZ reflectivity values, on a radial from the radar site, as close to perpendicular to the line of convection as possible, in order to determine flow through the system using base velocity.

The base velocities shown in this cross section provided an ideal view of ascending front-to-rear flow within the QLCS. The ascending front-to-rear flow was shown by the inbound velocities in Figure 5.18a. The outbound velocities in the lowest-levels of the QLCS showed a descending rear inflow, while the inbound velocities ascended above this inflow and acted to transport hydrometeors rearward. The cross-section, in this instance, was nearly identical to the conceptual model of a front-fed convective line with trailing stratiform precipitation (Fig. 2.9) from Houze et al. (1989), which was presented in Parker and Johnson (2004). Furthermore, an overturning updraft was depicted by the outbound velocities at the leading edge of the system, near the upper boundary of the QLCS (Fig. 5.18a).

5.2.4 Marginal Event – 08 June 2010, LSX

The fourth cross-section analysis was for the marginal event from 8 June 2010 at 1601 UTC. For this event, 2 different cross-sectional analyses were performed. The purpose of the cross-sectional radar analysis was to determine the flow and structure

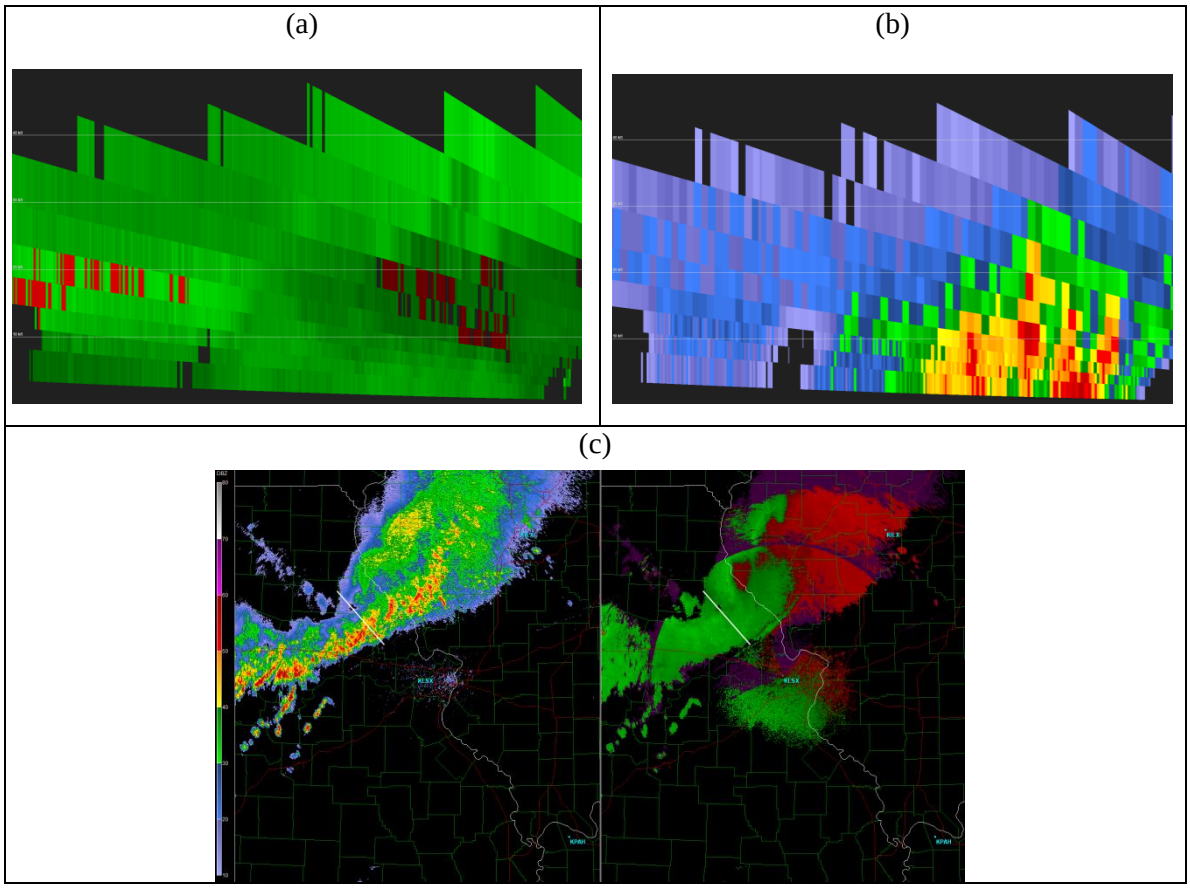

Figure 5.19 Radar imagery of (a) base velocity cross-section, and (b) base reflectivity cross-section, and (c) plan-view of both base reflectivity and base velocity is shown. The white line shown in image (c) is the location of the cross-section.

within the QLCS, especially as it pertained to the classifications set forth by Parker and Johnson (2000) and Parker and Johnson (2004). Cross-sections were again performed through a region that included >35 dBZ reflectivity values, on a radial from the radar site, as close to perpendicular to the line of convection as possible, in order to determine flow through the system using base velocity.

The first cross-section, shown in Figure 5.19a, depicted base velocities that were inbound throughout nearly the entire QLCS. Overall, the velocities shown were relatively low, and the cluster of inbound and outbound velocities was likely small variations in

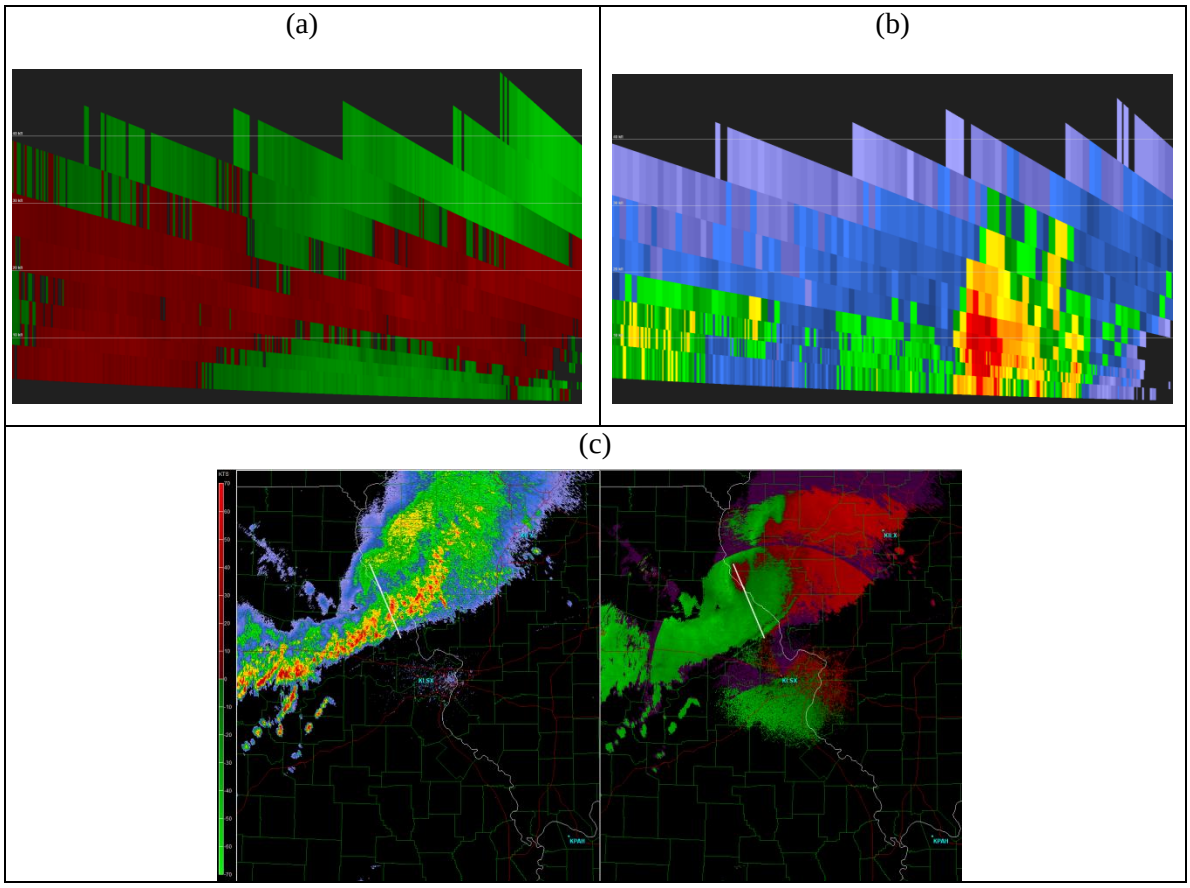

Figure 5.20 Radar imagery of (a) base velocity cross-section, and (b) base reflectivity cross-section, and (c) plan-view of both base reflectivity and base velocity is shown. The white line shown in image (c) is the location of the cross-section.

wind speed and direction. The small variations presented themselves in the same region as the convection (Fig. 5.19b), and were most likely the wind shear needed to organize the convection.

The second cross-section, shown in Figure 5.20a, had notable differences than the previous cross section for the marginal event. Where the previous cross-section showed nearly all inbound velocities (Fig. 5.19a) this cross-section depicted flow as both inbound and outbound (Fig. 5.20a). A slight descending rear-to-front air stream was shown in the lowest levels of the QLCS, along with a modest ascending front-to-rear flow above the

rear-to-front airstream. Coinciding with the modest ascension was the convective region (Fig. 5.20b). The convection, as a result of the modest ascension, was relatively shallow. The inbound and outbound velocities in the upper levels of QLCS led to both a trailing stratiform region, and a slight leading stratiform precipitation region (Fig. 5.20c).

From the marginal event, the inbound and outbound velocities shown made it difficult to determine the classification of the marginal QLCS event as it pertained to the archetypes presented by Parker and Johnson (2000, 2004). Using the plan-view base reflectivity (Fig. 5.19a, Fig. 5.20a), however, this QLCS appeared to be an example of a parallel stratiform precipitation QLCS (Parker and Johnson 2000). The reflectivity field exhibited a "paddle" shape, with the stratiform precipitation region mainly displaced to the northeast of the convection. This paddle shape was shown as an archetypal example for a parallel stratiform precipitation QLCS from Parker and Johnson (2000) (FIG. 2.6).

Chapter 6 Conclusions & Future Work

6.1 Summary and Conclusions

In this research, 30 NSE parameters were compared between four QLCS event types; tornado, hybrid, wind, and marginal. The comparison was performed through the use of the non-parametric Mann-Whitney Test, as well as displayed through the use of box and whiskers plots. After the analysis of the event type comparisons, a few conclusions were then drawn for each and will now be detailed in this section as a whole.

Overall, through the four comparisons performed, the results of this study are revealing in nature. For the central US domain, using the parameters outlined in this study, it may be reasonable to distinguish a difference, during the forecast (and nowcast) process, between a multiple tornado QLCS event and a single tornado QLCS event, a multiple tornado QLCS event vs. a solely wind event, and a QLCS wind event vs. a marginal QLCS event. Results shown through the Mann-Whitney Test provide confidence that there are parameters that can be used to determine what type of QLCS event can be expected. This can have a positive impact as it relates to forecasting and warning issuance on these often difficult-to-discern storm types. As mentioned previously, areas such as Columbia, MO have radar coverage that is far from ideal. With radar beams often too high in altitude in this area, as with many other locations, it is not possible to gather timely information about low-level rotation. Therefore, knowing what type of QLCS that one can expect to occur can be both vastly helpful and important. The fact that discernible differences exist (with regards to NSE parameters) between these

different QLCS event types should be a cause for encouragement. Where previously the forecasting community has relied almost solely on radar nowcasting and often "too-high" altitude radar beams to determine the QLCS event unfolding, there now exists a chance to not only forecast for a multiple tornado event vs. a single tornado event or wind event, but also a chance to be more judicial and confident in warning issuance. This study, however, does not address threshold values for the certain parameters for these events, but rather establishes that statistical differences, and "greater than"/"less than" values, exist between the event types. Additional work will need to be done to establish such thresholds. This work is replicable, and the methods allow for expansion of the entire data set to the extent of which can be determined by future researchers. For now, though, one can be encouraged that it may be possible to establish thresholds. With that being said, box and whisker plots do exist within this study (Fig. 4.1-4.8), and can give a reasonable expectation of values for the specified parameters for the various event types. The box and whiskers plots could make this research of immediate utilization by giving forecasters a reasonable idea of what values coincide with what type of event. Furthermore, this research presents a hypothetical forecaster's chart based on the values from this study, which is presented in section 6.2.

With the use of the same parameters, however, the results suggest it is not possible to determine a statistical difference between hybrid events and wind events. Unfortunately, that means that there is not a discernible statistical difference between the two event types; at least not within the confines of the 30 NSE parameters used for this research. Reasons for this may include the fact that the hybrid events, while producing one tornado report, were primarily a wind event. This seemingly made the differences in

these event types subtle. Optimistically, it could be possible that there are parameters that exist to showcase differences between these two types of events, but those were not included in this study. Further work including the full spectrum of parameters, a larger sample (in terms of the number of QLCS events studied), or both, may prove to find additional statistical differences. Within the scope of this study, however, statistical differences do not exist to a confident degree to distinguish between hybrid events and wind events. Consequently, that leaves this study with more questions to answer. These questions will be discussed in Section 6.3.

A radar observational analysis, for both plan-view imagery and cross-sections, was also performed for this study. One representative event was selected for each event type. The representative events were selected by the researcher based upon which event most closely exhibited the median values of the statistically different parameters produced during event comparisons. The event that best portrayed those aforementioned values, for each event type, was selected. The representative events selected were as follows: 15 November 2005 PAH (tornado), 26 November 2011 IND (hybrid), 03 October 2006 LOT (wind), and 08 June 2010 LSX (marginal).

With regards to the plan-view observational analysis, it was noted that the tornadic QLCS event was associated with more intense, discrete embedded convective cells within the overall QLCS, with a relatively narrow stratiform precipitation region. The hybrid event, on the other hand, was associated with strong, leading edge convection followed by a broad region of stratiform precipitation (relative to tornado events). Also, during the hybrid event, a gust front could be detected on radar. During the analysis of the representative wind event, it was noted that wind events and hybrid events aren't too

markedly different as far as radar observations (Reflectivity at Lowest Altitude) are concerned. The biggest difference, observationally, is that the leading edge convection is broader and the gust front is more apparent during the wind event. Finally, it was noted during the analysis of the representative marginal event, that there were much less intense regions of convection and a broad stratiform precipitation region.

The goal of the cross-sectional analysis was to examine base velocity and base reflectivity for each of the representative events, in order to determine the flow and structure of the QLCS, especially as it pertained to the classifications set forth by Parker and Johnson (2000) and Parker and Johnson (2004). Notably, the tornado event exhibited supercellular characteristics, especially in the second (Fig. 5.14) and third (Fig. 5.15) cross-sections. Both cross-sections from the hybrid event, shown in Figure 5.16a and Figure 5.17a, exhibited velocity folding along a horizontal strip between about 6,000 and 19,000 feet AGL. The velocity folding depicted very high outbound velocities, and the location in which the high outbound velocities converged with lower outbound velocities coincided with the location of the relatively intense, leading edge convection (Fig. 5.16b and Fig. 5.17b). Furthermore, the second hybrid event cross-section (Fig. 5.17a) depicted front-to-rear flow in the base velocities at the leading edge of the QLCS. The inbound velocities in that region were important in the creation of the trailing stratiform region (Parker and Johnson 2000).

The wind event cross-section was nearly identical to the conceptual model of a front-fed convective line with trailing stratiform precipitation (Fig. 2.9) from Houze et al. (1989), which was presented in Parker and Johnson (2004). The base velocities shown in this cross section provided an ideal view of ascending front-to-rear flow within the QLCS

(Fig. 5.18a); the outbound velocities in the lowest-levels of the QLCS showed a descending rear inflow, while the inbound velocities ascended above this inflow and acted to transport hydrometeors rearward, which created the trailing stratiform precipitation region. Finally, the marginal event cross-section appeared to be an example of a parallel stratiform precipitation QLCS (Parker and Johnson 2000). The cross-sections performed showed inbound and outbound velocities that made it difficult to determine the classification of the marginal QLCS event as it pertained to the archetypes presented by Parker and Johnson (2000, 2004). However, the plan-view of base reflectivity at the lowest altitude exhibited a "paddle" shape, with the stratiform precipitation region mainly displaced to the northeast of the convection. This paddle shape was shown as an archetypal example for a parallel stratiform precipitation QLCS from Parker and Johnson (2000) (Fig. 2.6).

6.2 Hypothetical Forecaster's Chart

For the hypothetical forecaster's chart (Table 6-1), the comparison of tornado events and wind events was used to determine which near storm environment parameters (NSE) were to be included. The comparison of tornado and wind events was used due to it being arguably the most valuable comparison performed: it provided that statistical differences do exist between environmental parameters of QLCSs that produce multiple tornadoes and those that pose strictly a straight-line wind damage threat. Only parameters that exhibited greater than 99% probability levels were used, as this was a very high confidence threshold for specific tornado event parameter values to be greater than the wind event values. Thresholds were decided on based upon the median values for the

NSE Parameter	Tornado Event Values	Wind Event Values
SR Helicity: 0-3 km	>655 m2s-2	>326 m2s-2
SR Helicity: 0-1 km	>544 m2s-2	>313 m2s-2
BRN Shear	>140 ms-1	>63 ms-1
Speed Shear: 0-3 km	>29 knots	>20 knots
Shear Vector Magnitude: 0-3 km	>30 knots	>21 knots
Shear Vector Magnitude: 0-6 km	>36 knots	>32 knots

Table 6-1 Hypothetical forecaster's chart based on median values, rounded to the nearest whole number, for NSE parameters that were statistically different on a 99% probability level for the tornado vs. wind event comparison.

different QLCS event types, and were rounded to the nearest whole number. The forecaster's chart presented here could be of immediate use by providing decision support for forecasting QLCS events within the domain (Fig. 1.1). It is important to note that the following values are relevant values for this domain only. The most statistically different NSE parameter was listed first, and then the next most statistically different NSE parameter, and so on and so forth. Box plots that display the median values used can be found in Figure 4.4.

6.3 Synthesis and Future Work

There is a great deal of work yet to be undertaken within regard to QLCS studies, especially as it relates to associated tornadogenesis. In this study, it was shown that NSE parameters do exist that distinguish between different event types. This work showed that statistical differences exist between event types, and for which event type the parameter values are greater than, or less than, the parameter values for the compared event type.

Specifically, eight NSE parameters were found to be statistically different between tornado events and wind events, and also between tornado events and hybrid events. The results between those comparisons suggested that it is possible to distinguish environmental differences between QLCSs that produce multiple tornadoes and QLCS that pose a strictly straight-line wind damage threat (tornado vs. wind comparison), and between QLCS events that produce multiple tornadoes and QLCSs that only produce a single tornado (tornado vs. hybrid comparison). Furthermore, only one NSE parameter was found to be statistically different between hybrid events and wind events, which may suggest that hybrid events and wind events are very similar within the constraints of the 30 NSE parameters utilized. Furthermore, it may not be possible to distinguish environmental differences between QLCS events that produce a single tornado and QLCSs that pose only a straight-line wind damage threat (hybrid vs. wind comparison). A larger data set that also incorporates additional NSE parameters may highlight differences that were not revealed in this research, thus providing impetus for future research. However, the results of this research suggested that it may not be possible to distinguish between QLCS hybrid events and QLCS wind events.

To continue work on this particular subject, the first step should be to incorporate more cases. 31 events were considered for this study, and there is the possibility to extend this to incorporate many more cases, of which the variety of event types can still be maintained and examined. This would be important not only for the statistical analysis of the events, but also for a more in-depth radar analysis.

It may also be useful to apply more than the 30 NSE parameters chosen. In this research, it was difficult to distinguish between QLCS wind and hybrid events. It may

therefore be possible that other NSE parameters exist that would perform better for this comparison. The 30 parameters selected for this research were based on the literature, but a study which investigates the full spectrum of parameters may prove to be worthwhile. From the information collected by including more cases and more NSE parameters, a flowchart could be derived for forecaster use. A hypothetical forecaster's chart was created (Table 6-1), based on median values, to provide decision support for forecasting tornado vs. wind events. The hypothetical forecaster's chart and research, as a whole, should be of immediate utilization as it stands, but a more robust analysis that includes a flowchart and greater statistical significance may prove effective for better forecasting of these often difficult-to-forecast QLCS events.

Given the results of this work, it is reasonable to assume that one day in the not-so-distant future, forecasters will have the tools necessary to forecast with a high degree of confidence between multiple tornado QLCS events and strictly straight-line wind damage events. Simply put, the better that the meteorological community understands the environmental differences between these types of events, the forecasting will also become better. Through increased confidence in the forecasts, forecasters could also be more confident in warning issuance for QLCS events. Currently, the meteorological community is seeking methods to reduce frequency of "false alarms" and "missed" events. Improved confidence in the forecast could help to immediately alleviate some of the issues with warning issuance. The results presented within this research provide insight into better forecasting QLCS events, especially as it pertains to tornadogenesis.

Appendix A

The following is the complete list of Near Storm Environment Parameters selected for investigation within this research. They are listed as their variable names within WDSS-II.

BRNShear, DCAPE_1km, DCAPE_3km, DCAPE_SfcLCL, HodographCurvature_6km, LapseRate_850-500mb, LapseRateAtMULFC, MeanRH_SfcTo1km, MeanRH_SfcToMULCL, MeanShear_0-6km, ML100mbAvgCAPE_Normalized, ML100mbAvgCIN, ML100mbAvgEHI, ML100mbAvgLCLHeight, ML100mbAvgLFC, ML100mbAvgLI, ML100mbAvgVGP, *MUBRNumber, PrecipitableWater, *SfcBRNumber, SfcDewPoint, SfcVGP, ShearVectorMag_0-1km, ShearVectorMag_0-3km, ShearVectorMag_0-6km, SpeedShear_0-3km, SRHelicity0-1km, SRHelicity0-3km, SWEAT, ThetaEDiffSfcToThetaEMin

*MUBRNumber and SfcBRNumber were downloaded and attempted to be utilized, but they were not included in the final results of this study; the data included too many errors and non-sensible numbers for inclusion.

Appendix B

The following are the definitions of the NSE parameters used in this research:

BRNShear – Bulk Richardson Number shear term (the denominator of the Bulk Richardson Number). BRN shear is similar to the Boundary Layer - 6 km shear, except that BRN shear uses a difference between the low level wind and a density-weighted mean wind through the mid levels.

DCAPE_1km, DCAPE_3km, DCAPE_SfcLCL – Downdraft CAPE for the lowest 1 km, lowest 3 km, and from the surface to LCL. DCAPE can be used to estimate the potential strength of rain-cooled downdrafts with thunderstorms convection, and is similar to CAPE. Larger DCAPE values are associated with stronger downdrafts.

HodographCurvature_6km – Curvature of a hodograph, in the lowest 6 km, which represents the wind profile present. 0 = straight line, > 0 is cyclonic, < 0 is anticyclonic curvature.

LapseRate_850-500mb, LapseRateAtMULFC – The lapse rate is the rate of change of temperature in the vertical of the atmosphere; represented both for the 850mb-500mb layer and the lapse rate present at the most unstable LFC. Represented in units of °C km^{-1}.

MeanRH_SfcTo1km, MeanRH_SfcToMULCL – Defined as the ratio of water vapor density to the saturation water vapor density, usually expressed as a percent. RH can also be defined as the ratio of actual vapor pressure to the saturation vapor pressure, expressed

as a percent. In this research, the mean for the layer between the surface and 1 km, and the layer from the surface to the most unstable LCL, is used.

MeanShear_0-6km – Wind shear expressed as an average over the 0-6 km layer. Represented in units of m s^{-1} km^{-1}.

ML100mbAvgCAPE_Normalized – Mean Layer 100 mb Average Normalized CAPE. It is CAPE that is divided by the depth of the buoyancy layer (units of m s^{-2}). Values near or less than .1 suggest a "tall, skinny" CAPE profile with relatively weak parcel accelerations, while values closer to .3 to .4 suggest a "fat" CAPE profile with large parcel accelerations possible.

ML100mbAvgCIN – Mean Layer 100 mb Average Convective Inhibition. A numerical measure of the strength of "capping," typically used to assess thunderstorm potential. Low level parcel ascent is often inhibited by such stable layers near the surface.

ML100mbAvgEHI – Mean Layer 100 mb Average Energy Helicity Index. EHI is designed to convey the ability of the atmosphere to turn horizontal vorticity into vertical vorticity.

ML100mbAvgLCLHeight – Mean Layer 100 mb Average Lifting Condensation Level. This is the level at which a lifted parcel becomes saturated, and is a reasonable estimate of cloud base height when air parcels experience forced ascent.

ML100mbAvgLFC – Mean Layer 100 mb Average Level of Free Convection. The LFC is the level at which a lifted parcel begins a free acceleration upward to the equilibrium level.

ML100mbAvgLI – Mean Layer 100 mb Average Lifted Index. The lifted index is the temperature difference between the 500 mb temperature and the temperature of a parcel lifted to 500 mb. Negative values denote unstable conditions.

ML100mbAvgVGP – Mean Layer 100 mb Average Vorticity Generation Parameter. The VGP is meant to estimate the rate of tilting and stretching of horizontal vorticity by a thunderstorm updraft.

MUBRNumber – Most Unstable Bulk Richardson Number. The BRN is a ratio of buoyancy to vertical shear. U = the wind speed difference between the density weighted 0-6 km mean wind and the lowest 500 m mean wind.

$$BRN = \frac{CAPE}{\frac{1}{2} * U^2}$$

PrecipitableWater - Measure of the depth of liquid water at the surface that would result after precipitating all of the water vapor in a vertical column over a given location, usually extending from the surface to 300 mb. Represented in units of cm for this research.

SfcBRNumber – Surface Bulk Richardson Number. See definition and equation of Bulk Richardson Number within the definition for MUBRNumber.

SfcDewPoint – The temperature at which saturation is achieved if air is cooled while holding pressure and water vapor mixing ratio constant.

SfcVGP – Surface Vorticity Generation Parameter. The VGP is meant to estimate the rate of tilting and stretching of horizontal vorticity by a thunderstorm updraft.

ShearVectorMag_0-1km, ShearVectorMag_0-3km, ShearVectorMag_0-6km – The magnitude of the vector representing wind shear changes with height through a given layer; most commonly 0-1 km, 0-3 km, and 0-6 km. Units expressed in knots.

SpeedShear_0-3km – Parameter that represents wind shear; this time as a change in wind speed with height. Units expressed in knots.

SRHelicity0-1km, SRHelicity0-3km – SRH is a measure of the potential for cyclonic updraft rotation in right-moving supercells, and is calculated for the lowest 1 and 3 km layers above ground level.

SWEAT – SWEAT is a stability index. SWEAT values +250 indicate a potential for strong convection, values +300 indicate the threshold for severe thunderstorms, and values +400 indicate the threshold for tornadoes.

In the following equation: $T_{d\,850}$ is the dewpoint temperature at the 850 mb level, TT is the Total Totals index, f_{850} and f_{500} are the wind speed (in knots) for the 850 mb and 500 mb levels, respectively, and s = sin(500 mb wind direction – 850 mb wind direction).

$$SWEAT = 12T_{d850} + 20(TT - 49) + 2f_{850} + f_{500} + 125(s + 0.2)$$

ThetaEDiffSfcToThetaEMin – Difference between Theta-e at the surface and the minimum Theta-e. Theta-e (θ_e), or Equivalent Potential Temperature, is the temperature a parcel of air would have if: a) it was lifted until it became saturated, b) all water vapor was condensed out, and c) it was returned adiabatically (i.e., without transfer of heat or

mass) to a pressure of 1000 millibars. Theta-e, which typically is expressed in degrees Kelvin, is directly related to the amount of heat present in an air parcel. Thus, it is useful in diagnosing atmospheric instability.

Appendix C

The following is the entire set of box and whiskers plots generated of the NSE parameters for each event type:

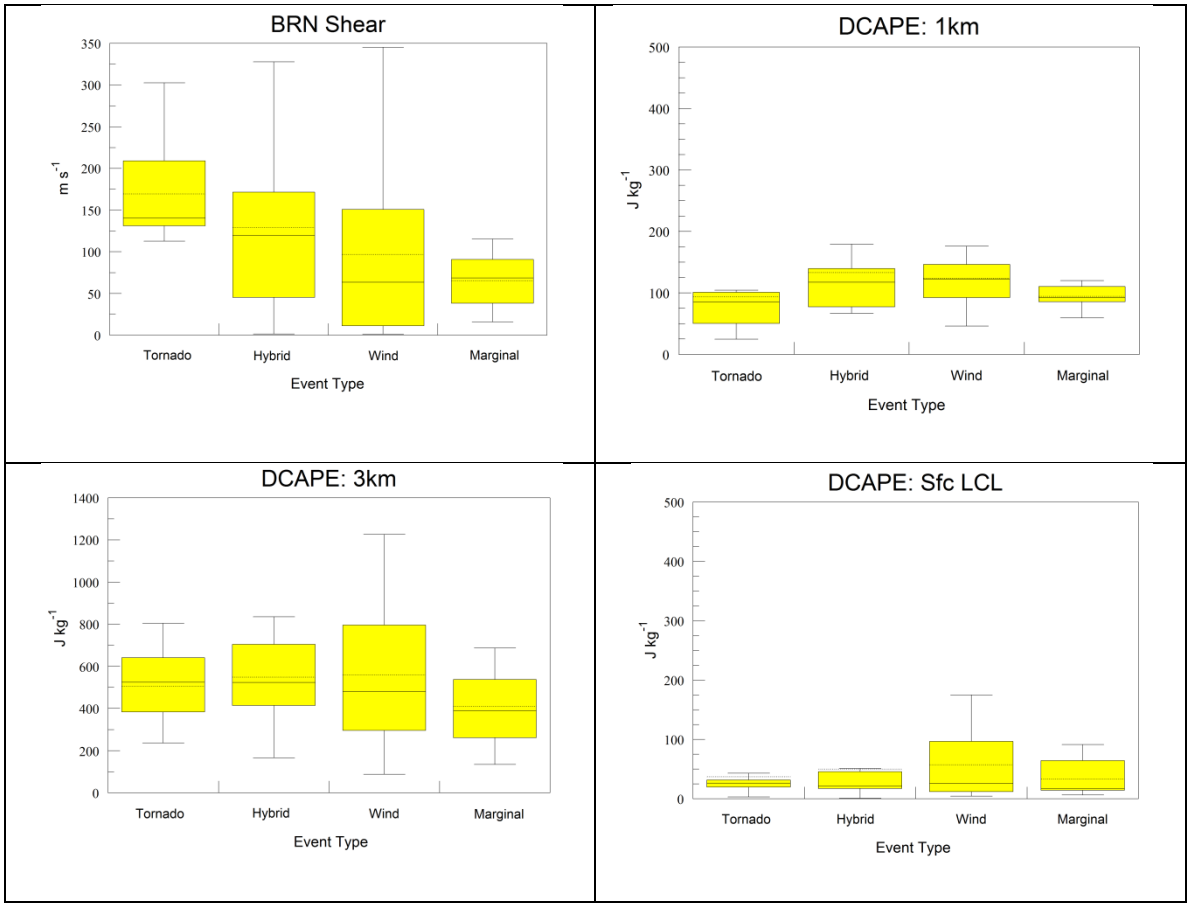

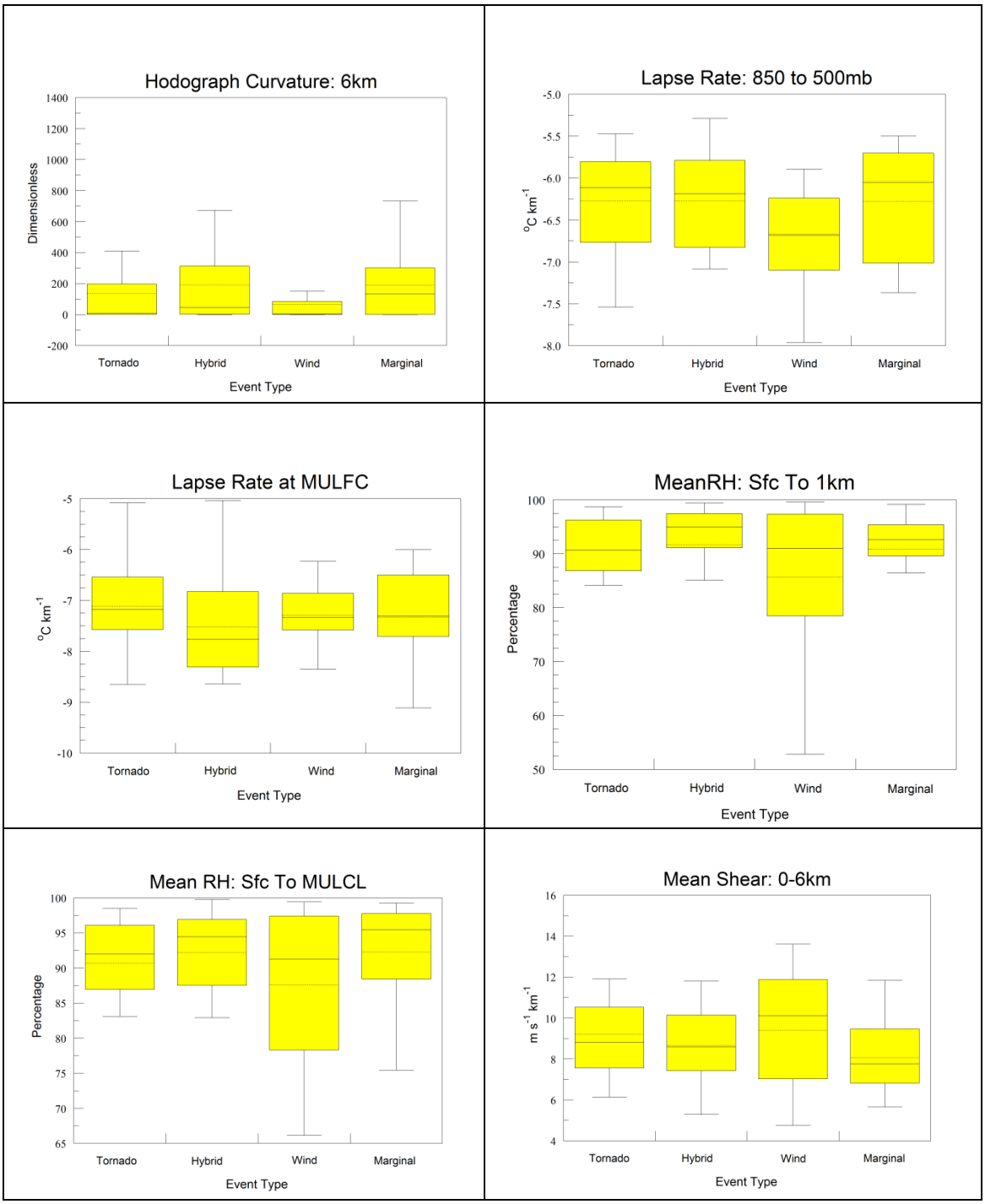
Hodograph Curvature: 6km
Dimensionless
1400
1200
1000
800
600
400
200
0
-200
Tornado
Hybrid
Wind
Marginal
Event Type
Lapse Rate: 850 to 500mb
°C km-1
-5.0
-5.5
-6.0
-6.5
-7.0
-7.5
-8.0
Tornado
Hybrid
Wind
Marginal
Event Type
Lapse Rate at MULFC
°C km-1
-5
-6
-7
-8
-9
-10
Tornado
Hybrid
Wind
Marginal
Event Type
MeanRH: Sfc To 1km
Percentage
100
90
80
70
60
50
Tornado
Hybrid
Wind
Marginal
Event Type
Mean RH: Sfc To MULCL
Percentage
100
95
90
85
80
75
70
65
Tornado
Hybrid
Wind
Marginal
Event Type
Mean Shear: 0-6km
m s-1 km-1
16
14
12
10
8
6
4
Tornado
Hybrid
Wind
Marginal
Event Type

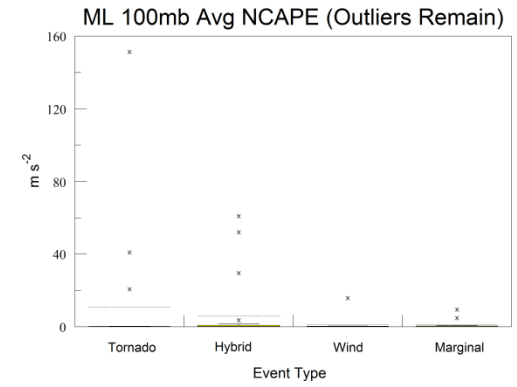
ML 100mb Avg NCAPE (Outliers Remain)
m s-2
160
120
80
40
0
Tornado
Hybrid
Wind
Marginal
Event Type

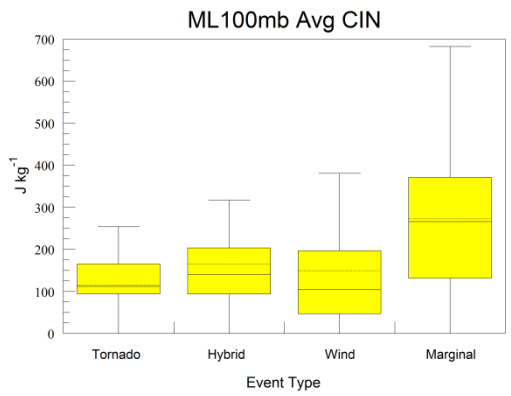
ML100mb Avg CIN
J kg-1
700
600
500
400
300
200
100
0
Tornado
Hybrid
Wind
Marginal
Event Type

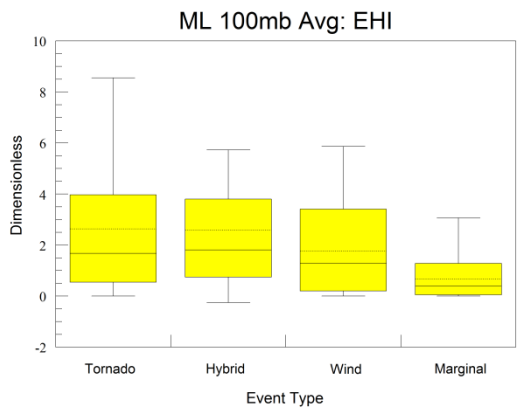
ML 100mb Avg: EHI
Dimensionless
10
8
6
4
2
0
-2
Tornado
Hybrid
Wind
Marginal
Event Type

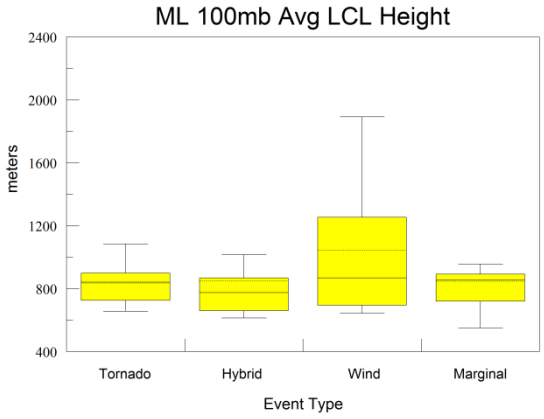
ML 100mb Avg LCL Height
meters
2400
2000
1600
1200
800
400
Tornado
Hybrid
Wind
Marginal
Event Type

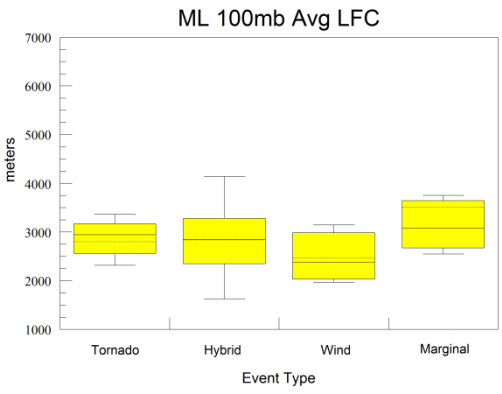
ML 100mb Avg LFC
meters
7000
6000
5000
4000
3000
2000
1000
Tornado
Hybrid
Wind
Marginal
Event Type

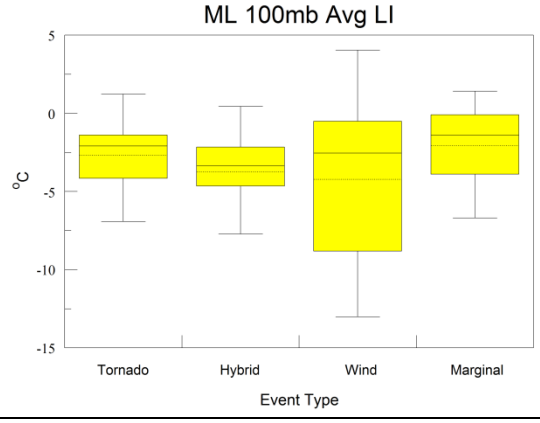
ML 100mb Avg LI
°C
5
0
-5
-10
-15
Tornado
Hybrid
Wind
Marginal
Event Type

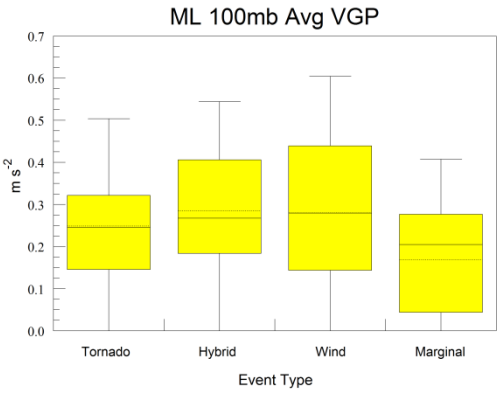
ML 100mb Avg VGP
m s-2
0.0
0.1
0.2
0.3
0.4
0.5
0.6
0.7
Tornado
Hybrid
Wind
Marginal
Event Type

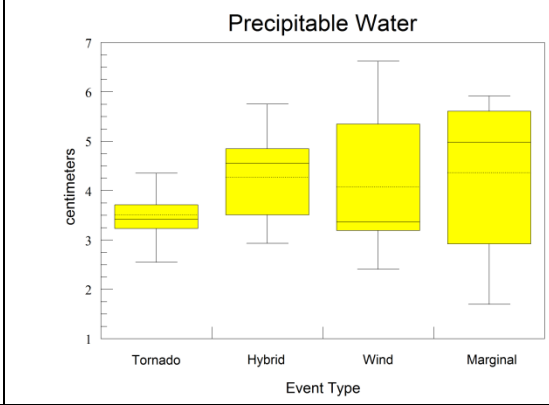
Precipitable Water
centimeters
1
2
3
4
5
6
7
Tornado
Hybrid
Wind
Marginal
Event Type

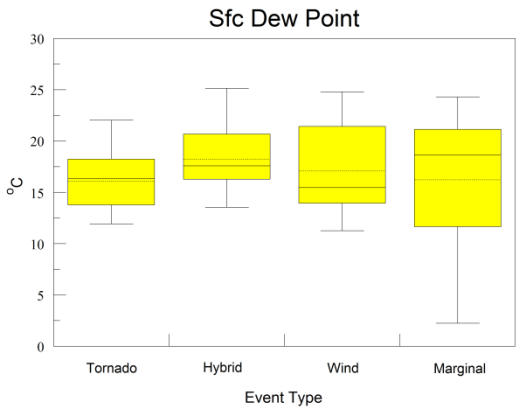
Sfc Dew Point
°C
0
5
10
15
20
25
30
Tornado
Hybrid
Wind
Marginal
Event Type

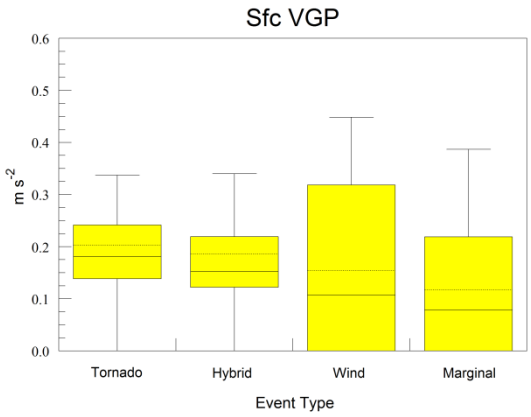
Sfc VGP
m s-2
0.0
0.1
0.2
0.3
0.4
0.5
0.6
Tornado
Hybrid
Wind
Marginal
Event Type

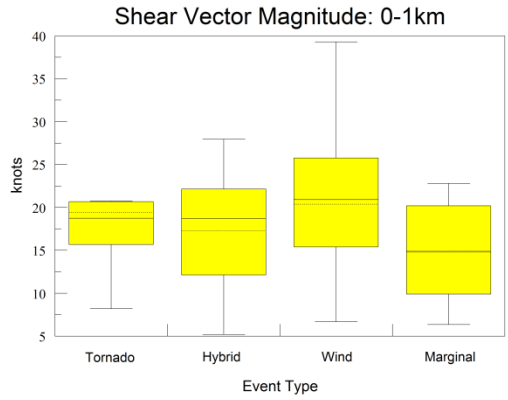
Shear Vector Magnitude: 0-1km
knots
5
10
15
20
25
30
35
40
Tornado
Hybrid
Wind
Marginal
Event Type

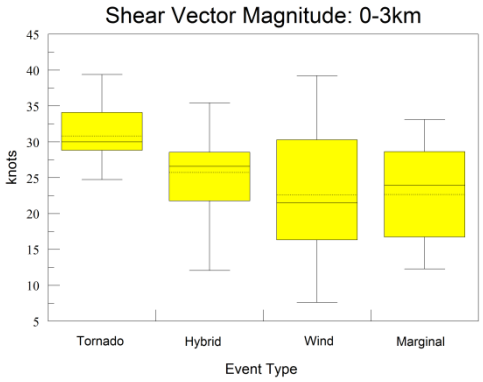
Shear Vector Magnitude: 0-3km
knots
5
10
15
20
25
30
35
40
45
Tornado
Hybrid
Wind
Marginal
Event Type

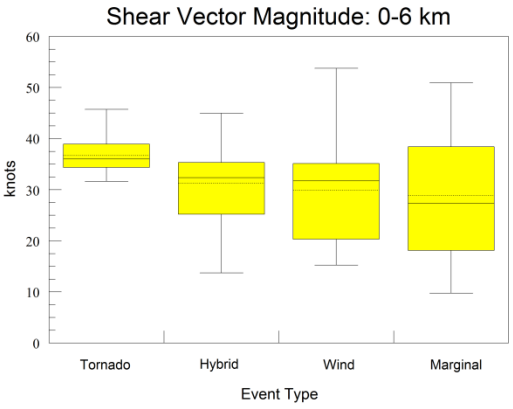
Shear Vector Magnitude: 0-6 km
knots
0
10
20
30
40
50
60
Tornado
Hybrid
Wind
Marginal
Event Type

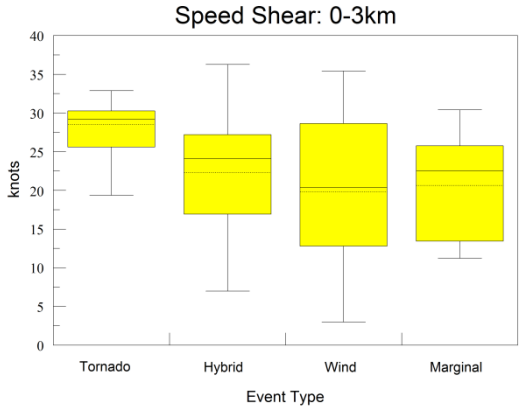
Speed Shear: 0-3km
knots
0
5
10
15
20
25
30
35
40
Tornado
Hybrid
Wind
Marginal
Event Type

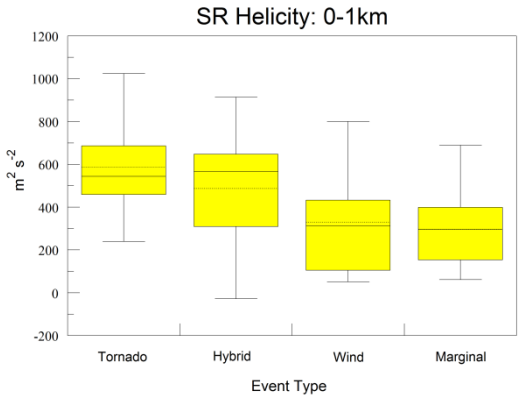
SR Helicity: 0-1km
m^2 s^-2
-200
0
200
400
600
800
1000
1200
Tornado
Hybrid
Wind
Marginal
Event Type

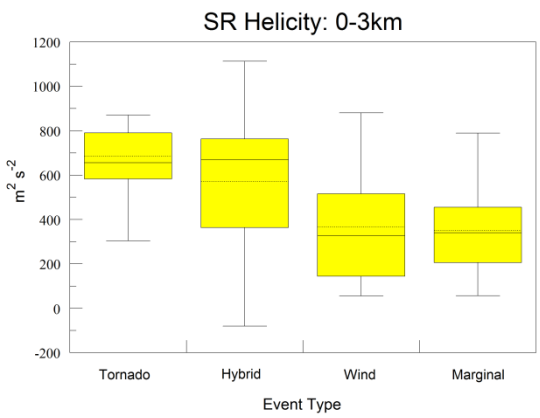
SR Helicity: 0-3km
m^2 s^-2
-200
0
200
400
600
800
1000
1200
Tornado
Hybrid
Wind
Marginal
Event Type

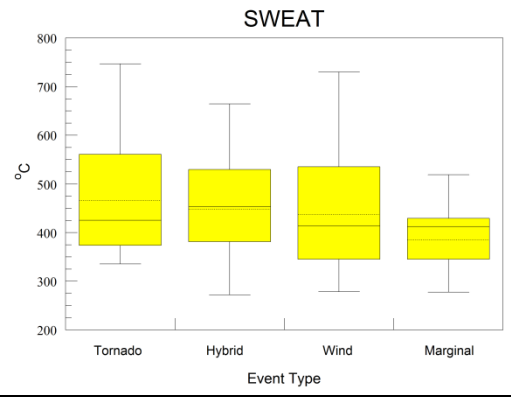
SWEAT
°C
200
300
400
500
600
700
800
Tornado
Hybrid
Wind
Marginal
Event Type

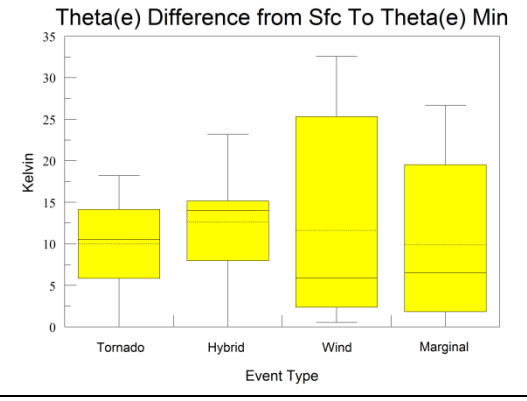
Theta(e) Difference from Sfc To Theta(e) Min
Kelvin
0
5
10
15
20
25
30
35
Tornado
Hybrid
Wind
Marginal
Event Type

References

Alfonso, A. P., and L. R. Naranjo, 1996: The 13 March 1993 severe squall line over western Cuba. *Wea. Forecasting*, **11**, 98-102.

Atkins, N. T., C. S. Bouchard, R. W. Przybylinski, R. J. Trapp, and G. Schmocker, 2005: Damaging surface wind mechanism within the 10 June 2003 Saint Louis bow echo during BAMEX. *Mon. Wea. Rev.*, **133**, 2275–2296.

Atkins, N. T., J. M. Arnott, R. W. Przybylinski, R. A. Wolf, and B. D. Ketcham, 2004: Vortex structure and evolution within bow echoes. Part I: Single-Doppler and damage analysis of the 29 June 1998 derecho. *Mon. Wea. Rev.*, **132**, 2224–2242.

Atkins, N. T., and M. St. Laurent, 2009: Bow echo mesovortices. Part II: Their genesis. *Mon. Wea. Rev.*, **137**, 1514-1532.

Bluestein, H. B., and M. H. Jain, 1985: Formation of mesoscale lines of precipitation: Severe squall lines in Oklahoma during the spring. *J. Atmos. Sci*., **42**, 1711–1732.

Browning, K. A., 1964: Airflow and precipitation trajectories within severe local storms which travel to the right of the winds. *J. Atmos. Sci*., **21**, 634–639.

Cohen, A. E., M. C. Coniglio, S. F. Corfidi, and S. J. Corfidi, 2007: Discrimination of mesoscale convective system environments using sounding observations. *Wea. Forecasting*, **22**, 1045–1062.

Coniglio, M. C., and D. J. Stensrud, and M. B. Richman, 2004: An observational study of derecho-producing convective systems. *Wea. Forecasting*, **19**, 320–337.

Emanuel, K. A., 1986: Overview and definition of mesoscale meteorology. Mesoscale meteorology and Forecasting, P. S. Ray, Ed., *Amer. Meteor. Soc*., 1–17.

Evans, J. S., and C. A. Doswell III, 2001: Examination of derecho environments using proximity soundings. *Wea. Forecasting*, **16**, 329–342.

Fankhauser, J. C., G. M. Barnes, and M. A. LeMone, 1992: Structure of a midlatitude squall line formed in strong unidirectional shear. *Mon. Wea. Rev*., **120**, 237–260.

Forbes, G. S., and R. M. Wakimoto, 1983: A concentrated outbreak of tornadoes, downbursts and mircobursts, and implications regarding vortex classification. *Mon. Wea. Rev*., **111**, 220–235.

Fovell, R. G., and P. S. Dailey, 1995: The temporal behavior of numerically simulated multicell-type storms. Part I: Modes of behavior. *J. Atmos. Sci*., **52**, 2073–2095.

Fujita, T. T., 1978: Manual of downburst identification for Project Nimrod. Department of Geophysical Sciences, University of Chicago Satellite and Mesometeorology Research Paper No. 156, 104 pp.

Funk, T. W., K. E. Darmofal, J. D. Kirkpatrick, V. L. DeWald, R. W. Przybylinski, G. K. Schmocker, and Y.-J. Lin, 1999: Storm reflectivity and mesocyclone evolution associated with the 15 April 1994 squall line over Kentucky and southern Indiana. *Wea. Forecasting*, **14**, 976–993.

Godfrey, E. S., R. J. Trapp, and H. E. Brooks, 2004: A study of the pre-storm environment of tornadic quasi-linear convective systems. Preprints, 22nd Conference on Severe Local Storms, Hyannis, MA, *Amer. Meteor. Soc*. 3A.5.

Houze, R. A., Jr., 1993: Cloud Dynamics. Academic Press, 573 pp.

Houze, R. A., Jr.: Mesoscale convective systems, *Rev. Geophys*., **42**, RG4003.

Houze, R. A., Jr., B. F. Smull, and P. Dodge, 1990: Mesoscale organization of springtime rainstorms in Oklahoma. *Mon. Wea. Rev*., **118**, 613–654.

Houze, R. A., Jr., S. A. Rutledge, M. I. Biggerstaff, and B. F. Smull, 1989: Interpretation of Doppler weather radar displays of midlatitude mesoscale convective systems. *Bull. Amer. Meteor. Soc*., **70**, 608–619.

James, R. P., P. M. Markowski, and J. M. Fritsch, 2006: Bow echo sensitivity to ambient moisture and cold pool strength. *Mon. Wea. Rev*., **134**, 950–964.

Johns, R. H., and W. D. Hirt, 1987: Derechos: Widespread convectively induced windstorms. *Wea. Forecasting*, **2**, 32–48.

Klimowski, B. A., M. J. Bunkers, M. R. Hjelmfelt, and J. N. Covert, 2003: Severe convective windstorms over the northern high plains of the United States. *Wea. Forecasting*, **18**, 502–519.

Klimowski, B. A., R. Przyblinski, G. Schmocker, and M. R. Hjelmfelt, 2000: Observations of the formation and early evolution of bow echoes. Preprints, 20th Conf. on Severe Local Storms, Orlando, FL, *Amer. Meteor. Soc*., 44–47.

Leary, C. A., and R. A. Houze, Jr., 1979: The structure and evolution of convection in a tropical cloud cluster. *J. Atmos. Sci*., **36**, 437-457.

Lee, W.-C., R. E. Carbone, and R. M. Wakimoto, 1992: The evolution and structure of a "bow-echo–microburst" event. Part II: The bow echo. *Mon. Wea. Rev*., **120**, 2211–2225.

Mann, H. B. and Whitney, D. R. 1947: On a test of whether one of two random variables is stochastically larger than the other. *Analysis of Math. Sci.*, **18**, 50-60.

Miller, D. J., and R. H. Johns, 2000: A detailed look at extreme wind damage in derecho events. Preprints, 20th Conf. on Severe Local Storms, Orlando, FL, *Amer. Meteor. Soc*., 52–55.

Moncrieff, M. W., 1992: Organized convective systems: Archetypal dynamical models, mass and momentum flux theory, and parameterization. *Quart. J. Roy. Meteor. Soc*., **118**, 819–850.

Newton, C. W., and J. C. Fankhauser, 1964: On the movements of convective storms, with emphasis on size discrimination in relation to water budget requirements. *J. Appl. Meteor*., **3**, 651–668.

Nolen, R. H., 1959: A radar pattern associated with tornadoes. *Bull. Amer. Meteor. Soc.*, **40**, 277-279.

"NWS Louisville: Squall Line/Bow Echo Characteristics." *National Weather Service – Central Region Headquarters Home Page*. Web. 05 May 2011. <http://www.crh.noaa.gov/lmk/soo/docu/bowecho.php>.

Orlanski, I., 1975: A rational subdivision of scales for atmospheric processes. *Bull. Amer. Meteor. Soc*., **56**, 527–530.

Parker, M. D., 1999: May 1996 and May 1997 linear mesoscale convective systems of the Central Plains: Synoptic meteorology and a reflectivity-based taxonomy. Dept. of Atmospheric Science Paper No. 675, Colorado State University, Fort Collins, CO, 185 pp. [Available from Dept. of Atmospheric Science, Colorado State University, Fort Collins, CO 80523.]

Parker, M. D., and R. H. Johnson, 2000: Organizational modes of midlatitude mesoscale convective systems. *Mon. Wea. Rev*., **128**, 3413–3436.

Parker, M. D., and R. H. Johnson, 2004: Structures and dynamics of quasi-2D mesoscale convective systems. *J. Atmos. Sci*., **61**, 545–567.

Pettet, C. R., and R. H. Johnson, 2003: Airflow and precipitation structure of two leading stratiform mesoscale convective systems determined from operational datasets. *Wea. Forecasting*, **18**, 685–699.

Przybylinski, R. W., 1995: The bow echo: Observations, numerical simulations, and severe weather detection methods. *Wea. Forecasting*, **10**, 203–217.

Przybylinski, R. W., and D. M. DeCaire, 1985: Radar signatures associated with the derecho. One type of mesoscale convective system. Preprints, 14th Conf. on Severe Local Storms, Indianapolis, IN, *Amer. Meteor. Soc*., 228–231.

Rasmussen, E. N. and S. A. Rutledge, 1993: Squall line evolution. Part 1: Kinematic and reflectivity structure. *J. Atmos. Sci.*, **50**, 2584-2606.

Rutledge, S. A., and R. A. Houze Jr., 1987: Diagnostic modeling study of the trailing stratiform region of a midlatitude squall line. *J. Atmos. Sci*., **44**, 2640–2656.

Schiesser, H. H., R. A. Houze Jr., and H. Huntrieser, 1995: The mesoscale structure of severe precipitation systems in Switzerland. *Mon. Wea. Rev*., **123**, 2070–2097.

Smith, B. T., R. L. Thompson, J. S. Grams, C. Broyles, and H. E. Brooks, 2012: Convective modes for significant thunderstorms in the contiguous United States. Part I: Storm classification and climatology. *Wea. Forecasting*, **27**, 1114-1135.

StatisticsLectures.com, cited 2013: z-Table. [Available online at http://www.statisticslectures.com/tables/ztable/.]

Storm Prediction Center, cited 2013: Explanation of SPC Severe Weather Parameters. [Available online at http://www.spc.noaa.gov/exper/mesoanalysis/help/begin.html.]

Storm Prediction Center, cited 2013: Mesoanalysis Help. [Available online at http://www.spc.noaa.gov/exper/mesoanalysis/help/help_brn.html.]

Thompson, R. L., B. T. Smith, J. S. Grams, A. R. Dean, and C. Broyles, 2012: Convective modes for significant severe thunderstorms in the contiguous United States. Part II: Supercell and QLCS tornado environments. *Wea. Forecasting*, **27**, 1136-1154.

Trapp, R. J., and M. L. Weisman, 2003: Low-level mesovortices within squall lines and bow echoes. Part II: Their genesis and implications. *Mon. Wea. Rev*., **131**, 2804–2823.

Trapp, R. J., S. A. Tessendorf, E. S. Godfrey, and H. E. Brooks, 2005: Tornadoes from squall lines and bow echoes. Part I: Climatological distribution. *Wea. Forecasting*, **20**, 23–34.

Wakimoto, R. M., 1983: The West Bend, Wisconsin storm of 4 April 1981: A problem in operational meteorology. *J. Climate Appl. Meteor*., **22**, 181–189.

Wakimoto, R. M., 2001: Convectively driven high wind events. Severe Convective Storms, Meteor. Monogr., No. 50, *Amer. Meteor. Soc*., 255–298.

Wakimoto, R. M., C. A. Davis, and N. T. Atkins, 2006: High winds generated by bow echoes. Part II: The relationship between the mesovortices and damaging straight-line winds. *Mon. Wea. Rev*., **134**, 2813–2829.

Wallace, J. M., 1975: Diurnal variations in precipitation and thunderstorm frequency over the conterminous United States. *Mon. Wea. Rev*., **103**, 406–419.

Wheatley, D. M., R. J. Trapp, and N. T. Atkins, 2006: Radar and damage analysis of severe bow echoes observed during BAMEX. *Mon. Wea. Rev*., **134**, 791–806.

Williams, Ed, cited 2013: GPS Waypoint Registry: Great Circle Calculator. [Available online at http://www.waypoint.org/gps1-calc.html.]